NASA CR 137732
LSI ER 170E-4

ELECTROCHEMICAL CARBON DIOXIDE CONCENTRATOR ADVANCED TECHNOLOGY TASKS

FINAL REPORT

by

J. J. Schneider, F. H. Schubert,
T. M. Hallick and R. R. Woods

October, 1975

(NASA-CR-137732) ELECTROCHEMICAL CARBON DIOXIDE CONCENTRATOR ADVANCED TECHNOLOGY TASKS Final Report, 1 Jul. 1973 - 25 Aug. 1975 (Life Systems, Inc., Cleveland, Ohio.) 137 p HC $6.00
N76-14809
Unclas
CSCL 06K G3/54 07735

Prepared Under Contract No. NAS 2 - 6478

by

Life Systems, Inc.
Cleveland, Ohio 44122

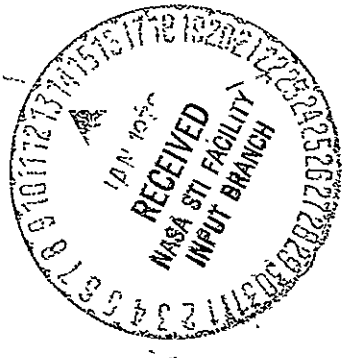

for

AMES RESEARCH CENTER

National Aeronautics & Space Administration

ER-170E-4

ELECTROCHEMICAL CARBON DIOXIDE CONCENTRATOR ADVANCED TECHNOLOGY TASKS

FINAL REPORT

by

J. J. Schneider, F. H. Schubert,
T. M. Hallick, and R. R. Woods

October, 1975

Distribution of this report is provided in the interest of information exchange. Responsibility for the contents resides in the authors or organization that prepared it.

Prepared Under Contract No. NAS2-6478

by

LIFE SYSTEMS, INC.
Cleveland, Ohio 44122

for

AMES RESEARCH CENTER

NATIONAL AERONAUTICS AND SPACE ADMINISTRATION

FOREWORD

The development work described herein was conducted by Life Systems, Inc. during the period of July 1, 1973 to August 25, 1975, under NASA Contract NAS26478. The Program Manager was F. H. Schubert. Technical support was provided as follows:

Personnel	Area(s) of Responsibility
Timothy M. Hallick	Advanced module testing
Fred C. Jensen	Honeycomb endplate design
Richard D. Marshall	Advanced module design
James J. Palagyi	Module assembly and data acquisition
Jon J. Schneider	Technology development testing utilization studies
Gary G. See	Advanced module design
Richard R. Woods, Jr.	Technology development testing

The contract's Technical Monitor was P. O. Quattrone, Chief, Environmental Control Research Branch, NASA Ames Research Center, Moffett Field, California.

TABLE OF CONTENTS

continued-

Table of Contents - continued

continued-

Table of Contents - continued

LIST OF FIGURES

continued-

PRECEDING PAGE BLANK NOT FILMED

List of Figures - continued

LIST OF TABLES

LIST OF ACRONYMS

AEDCM	Advanced Electrochemical Depolarized Concentrator Module
ARG	Air Revitalization Group.
BRS	Bosch CO_2 Reduction Subsystem
CS-6	Six-Man, Self-Contained, Electrochemical Carbon Dioxide Concentrating Subsystem
CX-1	One-Man, Experimental Carbon Dioxide Concentrator Subsystem
CX-6	Six-Man, Experimental Carbon Dioxide Concentrator Subsystem
EC/LSS	Environmental Control/Life Support Systems
EDC	Electrochemical Depolarized Concentrator
GSA	Ground Support Accessories
LSS	Life Support Systems
SEORS	Solid Electrolyte Oxygen Regeneration Subsystem
SSP	Space Station Prototype
WES	Water Electrolysis Subsystem

SUMMARY

Regenerative carbon dioxide (CO_2) removal concepts are needed to sustain man in space for extended periods of time. A program to develop an electrochemical CO_2 concentration technique has been underway at NASA and Life Systems, Inc. (LSI) for the past several years. The work reported herein, Electrochemical CO_2 Concentrator Advanced Technology Tasks, is a portion of the overall program.

Activities in four major areas were successfully completed:

1. Technology advancement studies of the basic electrochemical CO_2 removal process to provide a basis for the design of the next generation cell, module and subsystem hardware.

2. Development of an Advanced Electrochemical Depolarized Concentrator Module (AEDCM) having the characteristics of low weight, low volume, high CO_2 removal, good electrical performance and low process air pressure drop.

3. Component weight and noise reduction for the hardware of the six-man capacity CO_2 Collection Subsystem developed for the Air Revitalization Group (ARG) of the Space Station Prototype (SSP).

4. Electrochemical Depolarized Concentrator (EDC) concept application and integration studies to investigate increased utilization of the electrochemical CO_2 removal technique within spacecraft Environmental Control/Life Support Systems (EC/LSS)

The technology advancement studies included investigations into six specific areas relating to the EDC process. These areas were:

1. Mass transfer and process air pressure drop as related to the process air cavity configuration

2. Determination of gradients within a single cell air cavity of temperature, dew point, relative humidity (RH), CO_2 partial pressure (pCO_2) and static pressure

3. Cell moisture tolerance as related to performance, cell configuration and determination of operational limits

4. Investigation and testing of internally liquid-cooled EDC cells

5. Analysis of EDC exhaust gases to determine possible contaminants (none were found)

6. Operation of EDC cells and modules at elevated hydrogen-(H_2) to-process air pressure differentials

Based on the results of the technology advancement studies, the projected needs for spacecraft air revitalization and past EDC developments, an advanced EDC

module was designed, fabricated, assembled and tested. The new generation design allowed for an increased number of cells per module (up to 30) at an increased active electrode area per cell (twice that of previous baseline cells) to provide for multi-man scale-up without excessive increase in the number of modules. Also, cells could be either internally air- or liquid-cooled for decreased thermal gradients and increased application flexibility. The new design enabled the use of variable electrode-matrix-electrode thickness ratios to increase humidity tolerance while still maintaining the characteristics of low weight, volume and process air pressure drop without sacrificing electrical or CO_2 removal efficiencies.

The AEDCM was designed to remove the metabolic CO_2 generated by a crew of four men. It required 20 cells, each having an active area of 0.045 m^2 (0.488 ft^2). The advanced cells showed a decrease of 52% and 26% in weight and volume, respectively, compared to baseline cells used for the six-man capacity CO_2 Collection Subsystem for the SSP. Similarly, on a four man basis, the advanced module showed a 64% and 57% decrease in weight and volume, respectively, when compared to four previous baseline modules. A major portion of the weight and volume reductions were achieved through internal air cooling and plated anode current collectors as opposed to separate, externally air-cooled, finned anode current collectors. The four-man capacity advanced module was experimentally characterized as a function of process air pCO_2 process air flow rate, current density and anode gas flow rate. The CO_2 removal efficiency, as well as the cell voltage, were equal to or better than those achieved with previous generation air-cooled cells and modules. This performance was achieved at a substantial reduction (90%) in the process air pressure drop through the cathode compartments of the module.

Studies to reduce both the noise and weight of the CO_2 Collection Subsystem for SSP application were completed. A single blower was identified having sufficient capacity to replace the two process air blowers presently used. The new blower had a noise level reading of 71 dB versus 92 dB of the old blowers. In addition, a 210W power savings, as well as weight and volume savings, were realized. A lightweight module for application to the CO_2 Collection Subsystem of the SSP was designed, fabricated, and tested. The module used reduced thickness in the anode current collectors as well as the cell isolation spacers. As a result, a 26% and 21% reduction in weight and volume were achieved. To reduce the weight of the endplates used on the six modules of the SSP CO_2 Collection Subsystem, lightweight honeycomb endplates were designed and fabricated. The new endplates yielded a weight savings of 68% while achieving increased resistance to endplate deflection. The total weight reduction projected for the six-man capacity SSP CO_2 Collection Subsystem, due to blower, module and module endplate redesigns, was 70 kg (153 lb) out of a total subsystem weight of 368 kg (809 lb) or a 19% reduction.

Five areas of application of the EDC as part of an overall spacecraft EC/LSS were investigated. Included were integration studies and studies relating to increased utilization of the EDC concept aboard manned spacecraft. The five areas were:

1. Integration of the EDC with the Bosch CO_2 Reduction Subsystem (BRS) and the Solid Electrolyte Oxygen Regeneration Subsystem (SEORS)

2. Use of the EDC as an atmosphere contaminant removal subsystem

3. Use of the EDC module as a combined CO_2 and cabin humidity control component

4. Evaluation of the EDC as a CO_2 removal concept aboard the Shuttle Orbiter

5. Investigation of the feasibility of using the EDC with pre- and post-sorbers to increase CO_2 removal effectiveness at very low cabin pCO_2 levels

The integration studies showed that operation of the EDC with either of the two CO_2 reduction subsystems is feasible using a state-of-the-art hardware. The results of the contaminant removal studies showed that the electrolyte contained within the EDC cells has a capacity to move trace contaminants from the cabin atmosphere total control through the EDC alone is not feasible for long-term missions. However, the results showed that during downtime of a trace contaminant subsystem an EDC can provide short-term protection against those trace contaminants that would build up quickly to the maximum allowable concentration.

A concept to combine the CO_2 removal function and a water vapor removal function within a single EDC module was derived and its feasibility demonstrated at a single cell level. The results showed that the water removal function is governing with a 40% increase in cell area required over that needed to perform the CO_2 removal function.

An equivalent weight comparison was performed to identify the point (in man-days) at which the regenerative EDC CO_2 removal method becomes advantageous for use aboard the Space Shuttle Orbiter. The comparison was made with a presently envisioned baseline lithium hydroxide (LiOH) CO_2 removal system. The results showed that the break-even point between the EDC and the LiOH system occurred after 24 man-days with EDC power utilization and after 31 man-days without EDC power use. At the end of a 120 man-day mission, the total equivalent weight of the EDC is lower by 163 kg (358.5 lb).

The feasibility of a composite CO_2 removal system for application at low cabin pCO_2 levels was investigated. The concept consisted of a standard EDC combined with pre- and post- CO_2 sorbers. The post-sorber would adsorb the CO_2 exiting from the EDC and, following a reversal of flow direction of the process air, add the absorbed CO_2 to the air stream to increase the pCO_2 level entering the EDC. The process can be repeated by cycling the flow direction of the air. The results of the study showed that while the pCO_2 to the EDC can be successfully increased, allowing a smaller EDC to be used based on the higher inlet pCO_2, the power and heat load penalties associated with operation of the pre- and post-sorbers were excessive and did not result in a savings compared to using an EDC only.

INTRODUCTION

Regenerative processes for the revitalization of spacecraft atmospheres are essential toward making long-term manned missions in space a reality. An

important step in this overall air revitalization process is the collection and concentration of the metabolically produced carbon dioxide (CO_2) for oxygen (O_2) recovery. The Skylab program marked the beginning of the use of regenerative techniques for CO_2 collection by using cyclic adsorption/desorption beds containing commercial zeolite. The emerging requirements for maintaining the partial pressure of CO_2 (pCO_2) below 400 N/m^2 (3 mm Hg) made the zeolite systems unattractive due to their resulting weight and volume penalties.[1] An electrochemical technique of concentrating CO_2 from an air environment has evolved over the past nine years.[2] In this time, the concept has progressed from single cell operation to fabrication and testing of one- and multi-man systems. Under Contract NAS2-6478, Life Systems, Inc., under the sponsorship of NASA Ames Research Center, Moffett Field, California, has completed a variety of activities directed toward furthering the electrochemical concept of CO_2 removal.

The total contract program performed under NAS2-6478 was divided into two phases: (1) development of two six-man capacity subsystems (CX-6 and CS-6) and (2) performance of advanced technology activities. Results of the development of the two six-man subsystems have been reported previously.[3-7] The present report focuses on the advanced technology activities. These activities conducted in parallel with the development of the two subsystems, were divided into four basic areas of investigation:

1. Technology advancement studies
2. Advanced Electrochemical Depolarized Concentrator Module (AEDCM) development
3. Space Station Prototype (SSP) CO_2 Collection Subsystem, component weight and noise reduction studies
4. Increased Electrochemical Depolarized Concentrator (EDC) utilization studies

The objective of these four areas of investigation were:

1. To increase the understanding of the basic electrochemical CO_2 removal process and to provide a basis upon which the design of the next generation cell, module and system hardware could be based

2. To develop advanced EDC cell and module hardware having the characteristics of low weight, low volume, high CO2 removal, high electrical efficiency and low process air pressure drop

3. To demonstrate, with hardware, reduction in weight and noise possible for the six-man capacity CO_2 Collection Subsystem for the Air Revitalization Group (ARG) of the SSP

4. To perform EDC concept application and integration studies to investigate increased utilization of the electrochemical CO_2 removal technique within Spacecraft Environmental Control/Life Support Systems (EC/LSS)

The objectives of the program were met. The following sections summarize the results of the work completed and the conclusions and recommendations made.

(1) References cited are listed on Page 127.

TECHNOLOGY ADVANCEMENT STUDIES

To increase the understanding of the electrochemical CO_2 removal process and to provide a basis for the development of an advanced EDC, investigations into six areas of the EDC process were conducted.

The areas of investigation were:

1. Mass transfer and process air pressure drop as related to the process air cavity configuration (expanded metal spacers versus parallel slots)

2. Temperature, dew point, relative humidity (RH), pCO_2 and pressure drop gradients within the process air cavity

3. Cell moisture as related to performance, cell configuration, and operational limits

4. Internal liquid cooling of EDC cells

5. Composition of EDC exhaust gases as related to possible contaminants or contaminant transfer (air-to-hydrogen (H_2) side)

6. Operation with elevated H_2-to-process air pressure differentials (35.5 kN/m^2 (5 psid)) and resulting effects on operational limits and cell performance

Effect of Expanded Metal Air Cavity Spacer

At low process air pCO_2 levels CO_2 transfer is limited by the diffusion of CO_2 to the hydroxyl ion (OH^-) generation sites.[3] To enhance the transfer of CO_2 to the electrode-matrix sandwich, turbulators such as expanded metal (Exmet) screens are used as gas cavity spacers in baseline cell constructions. Normally, gains achieved in mass transfer due to turbulators result in increased process air pressure drop through the cathode compartment of a cell. Analytical and/or empirical expressions to determine this pressure drop as a function of air flow rate for various Exmet heights were not available in literature, making performance predictions, trade studies, and advanced cell hardware sizing extremely difficult.

In an effort to derive a model for predicting process air pressure drops for Exmet cavity spacers, both analytical and experimental activities were completed. Also, to quantify the impact of cathode compartment Exmet spacers on CO_2 removal efficiency and process air pressure drop, experimental comparisons between flow-through plain, rectangular cross section channels and flow-over Exmet spacers were made.

Analytical Process Air Pressure Drop Model

The model derived for predicting process air pressure drops over Exmet was one of approximating the Exmet by a series of triangular openings within a series of

imaginary rectangular slots. The openings at any one point in the slots were represented by two different size isosceles triangles (designated as triangle R and triangle S). The slots were assumed to travel diagonally to the direction of process air flow and therefore required a length correction. Only the entrance and slot frictional flow effects were considered, while the effects of the slant of the openings, current collector and/or electrode surface interfaces (roughness factor) and the exit effects of the openings were assumed negligible.

The model was expressed as:

$$\Delta P = \frac{N\rho}{2}\left(K_R\bar{V}_R^{\,2} + K_S\bar{V}_S^{\,2}\right) + \frac{2fL_C\bar{V}_t^{\,2}\rho}{De} \qquad (1)$$

since

$$Re = \frac{De\bar{V}_t}{\nu_{air}} \qquad (2)$$

$$\Delta P = \frac{N\rho}{2}\left(K_R\bar{V}_R^{\,2} + K_S\bar{V}_S^{\,2}\right) + \frac{2(fRe)L_C\rho\nu_{air}}{De^2} \qquad (3)$$

where

ΔP = pressure drop through the Exmet

N = number of triangles per path length

ρ = density of process air

K_R, K_S = entrance pressure drop coefficient for triangle R and triangle S

$\bar{V}_R, \bar{V}_S$ = average process air velocity through triangle R and triangle S

f = friction factor

Re = Reynold's Number

L_C = corrected process air flow path length

$\bar{V}_t$ = average process air velocity through the slot

ν_{air} = viscosity of process air

De = equivalent diameter of slot

For an 80-mil Exmet (CS-6 and CX-6 baseline), equation (3) reduces to:

$$P = 3.165V^2 + 0.273V \quad (4)$$

where

P = pressure drop, inches of water

V = process air flow rate, scfm

Figure 1 compares the measured with the calculated pressure drops for both 0.15 and 0.20 cm (0.06 and 0.08 in) thick Exmet as a function of process air flow.

Exmet Versus Rectangular Slots Evaluation

A single cell was constructed using the CS-6 baseline 0.20 cm (0.008 in) (80 mil) Exmet spacer in the cathode compartment. The cell was operated at CS-6 baseline conditions, 373.3 N/m^2 (2.8 mm Hg) pCO_2 and 15.86 dm^3/min (0.56 scfm) per cell for 160 hours, attaining an average Transfer Index (TI) of 2.12, where TI is defined as the mass of CO_2 removed per mass of O_2 consumed. The cell was then disassembled and the Exmet and cathode current collector was replaced by a current collector having machined channels. This current collector had 11 slots, each 0.20 cm (0.08 in) deep and 0.64 cm (0.25 in) wide, running parallel to the air flow. The width between each pair of slots was 0.32 cm (0.125 in). The cell was restarted keeping the same operating parameters as before.

The CO_2 removal performance rapidly fell to a TI of 1.15. Over a 160-hour test the cell performance remained between a TI of 0.90 and 1.20 for a 1.10 average. The cell was again disassembled and rebuilt with the original Exmet current collector. Upon restarting, the average TI with the Exmet spacer was 2.20.

A pressure drop versus air flow test was also conducted for both the Exmet and the slotted current collector cell. Figure 2 shows the result of the test. As expected, the pressure drop for the slotted collector was less than that for a cell having the Exmet cavity spacer. For example, a pressure drop of 0.522 kN/m^2 (2.1 in of water) and 0.973 kN/m^2 (3.9 in of water) was obtained at 14.16 dm^3/min (0.5 scfm) per cell for the slotted and Exmet spacers, respectively.

The results showed that the change from slotted channels to Exmet spacers increased the CO_2 transfer efficiency by approximately 100% at equal process air flow rates.[2] The lower efficiency for the slots is a direct result of the laminar flow pattern caused by the plain channel spacer. It can be concluded that the Exmet spacer creates a turbulent flow pattern which, while increasing the process air pressure drop, also increases the CO_2 transfer efficiency.

An analytical comparison of the two concepts was made using the test results but based on equal process air blower power. The process air flow through the Exmet cell was analytically reduced until equal blower power (based on air flow and the pressure drop data of Figure 2) resulted. The decrease in TI due to air flow reduction was determined from previous data[3] and the net TI of the Exmet cell compared to the slotted cell at baseline air flow rate. The results indicated that the Exmet cell still showed an 87% increase in TI over the slotted cell.

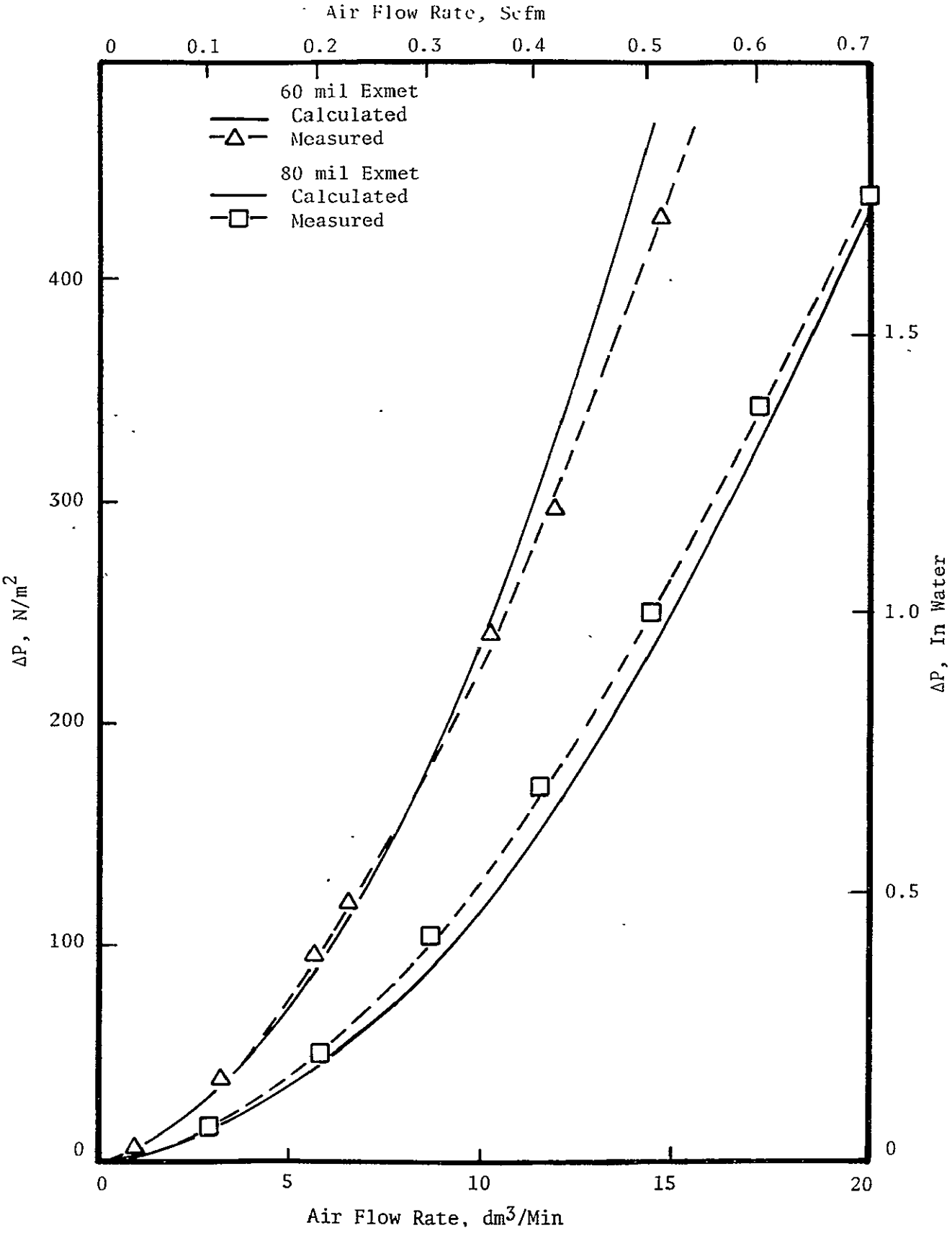

FIGURE 1 COMPARISON OF CALCULATED WITH MEASURED PRESSURE DROP ACROSS EXMET SPACERS

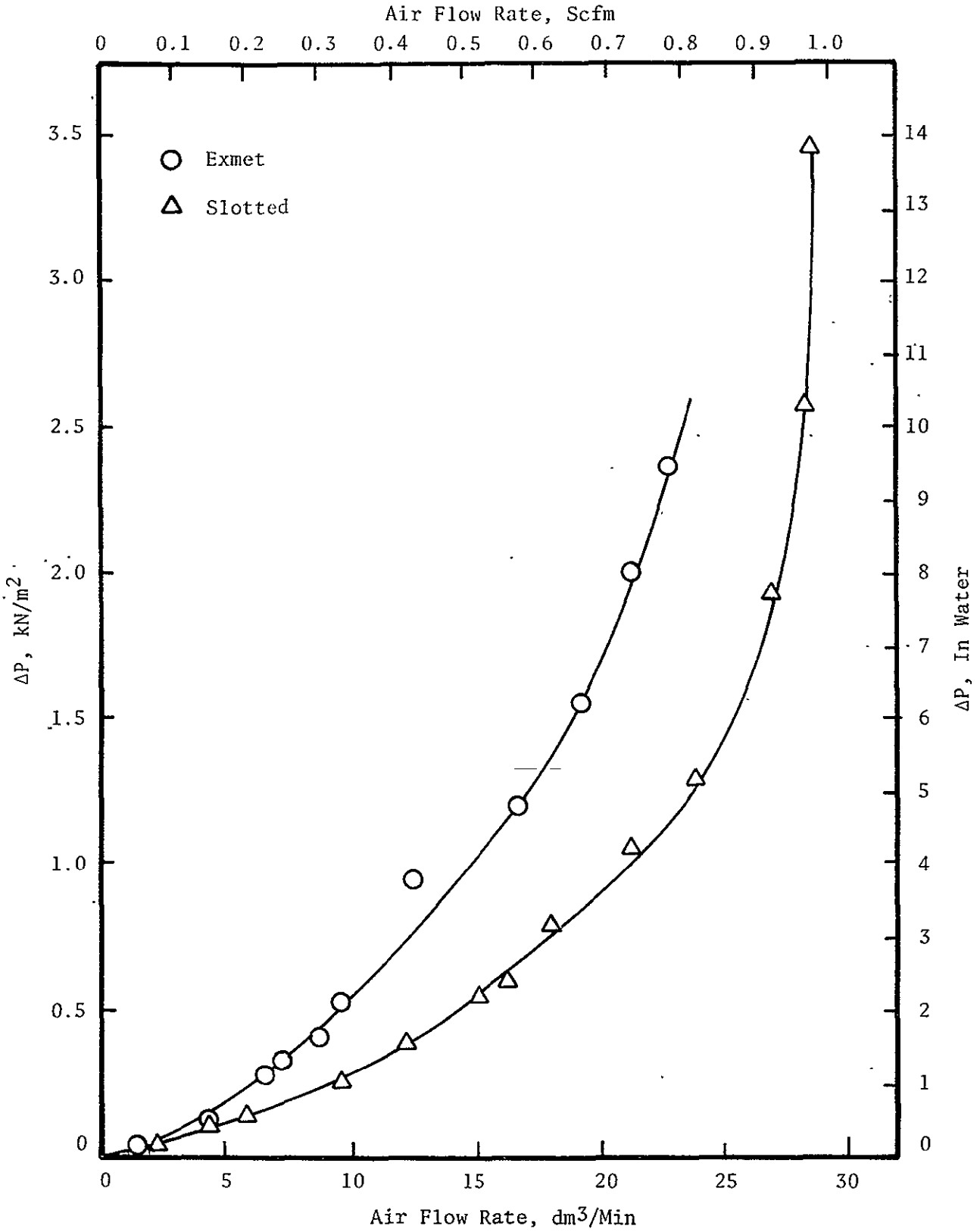

FIGURE 2 SINGLE-CELL PRESSURE DROP FOR EXMET AND SLOTTED AIR CAVITY SPACERS

Parametric Mapping of an EDC Cell

Typical analyses of concentrator cells are conducted assuming average electrolyte concentrations, temperatures and pCO_2 driving forces. In actuality, substantial thermal, pCO_2 and electrolyte concentration gradients exist within each cell, especially in the process air. These gradients are difficult to predict analytically and had not been previously experimentally quantified.

Cell Mapping

A single-cell concentrator was constructed to study the variation in process air stream parameters as a function of active cell area length and width. A plexiglass endplate was modified by drilling access holes in the area above the cathode compartment. Female-run tees were installed and thermocouples were inserted through the tees into the cathode compartment. The tee branches were connected to a dew point analyzer and process air LIRA. This combination allowed for the measurement of static pressure, temperature, dew point and pCO_2 at each sample port location. A schematic of these locations is shown in Figure 3. The thermocouple tips were inserted in the center of the air compartment without touching any cell components, such as the expanded metal spacers, to minimize heat loss through conduction. Prior to each specific test and after a baseline was established for a minimum of 72 hours, data was taken from each individual access port.

Experimental Results

The results of the tests are shown in Figures 4, 5, 6 and 7.

Pressure Differential Profile. Figure 4 shows the pressure differential profile across the cathode compartment of the cell based on the static pressure level measurements at the various sample port locations. The pressure drop is linear across the expanded metal (Exmet) spacers of the cell. Negligible variations in pressure levels were noted as a function of cell width. The data indicates that no process air flow maldistribution exists. The figure also shows that the pressure drop across the total cell divides approximately into equal thirds, with one-third each occurring in the entrance and exit grooves and one-third across the active cell area.

Temperature and Dew Point Profile. The dry bulb temperature of the process air rises quickly after entering the cell, as shown in the upper portion of Figure 5, and continues to increase until a maximum level is reached near the center of the cell. Beyond this maximum rise there is little change in temperature except for only a slight drop in the bottom and middle flow paths and a slight rise in the upper path. This may be attributed to the coolant flow pattern through the tubes attached to the external fins. The level portion of process air temperature profile in the exit half of the cell indicates that the cell has reached steady-state conditions with the process air in that section. The lower temperature rise through the center of the cell could well be caused by the current density pattern which tends to be greater near the edges than in the middle due to the cathode current collector construction, i.e., open center frame with spot-welded Exmet along the inner frame edges.

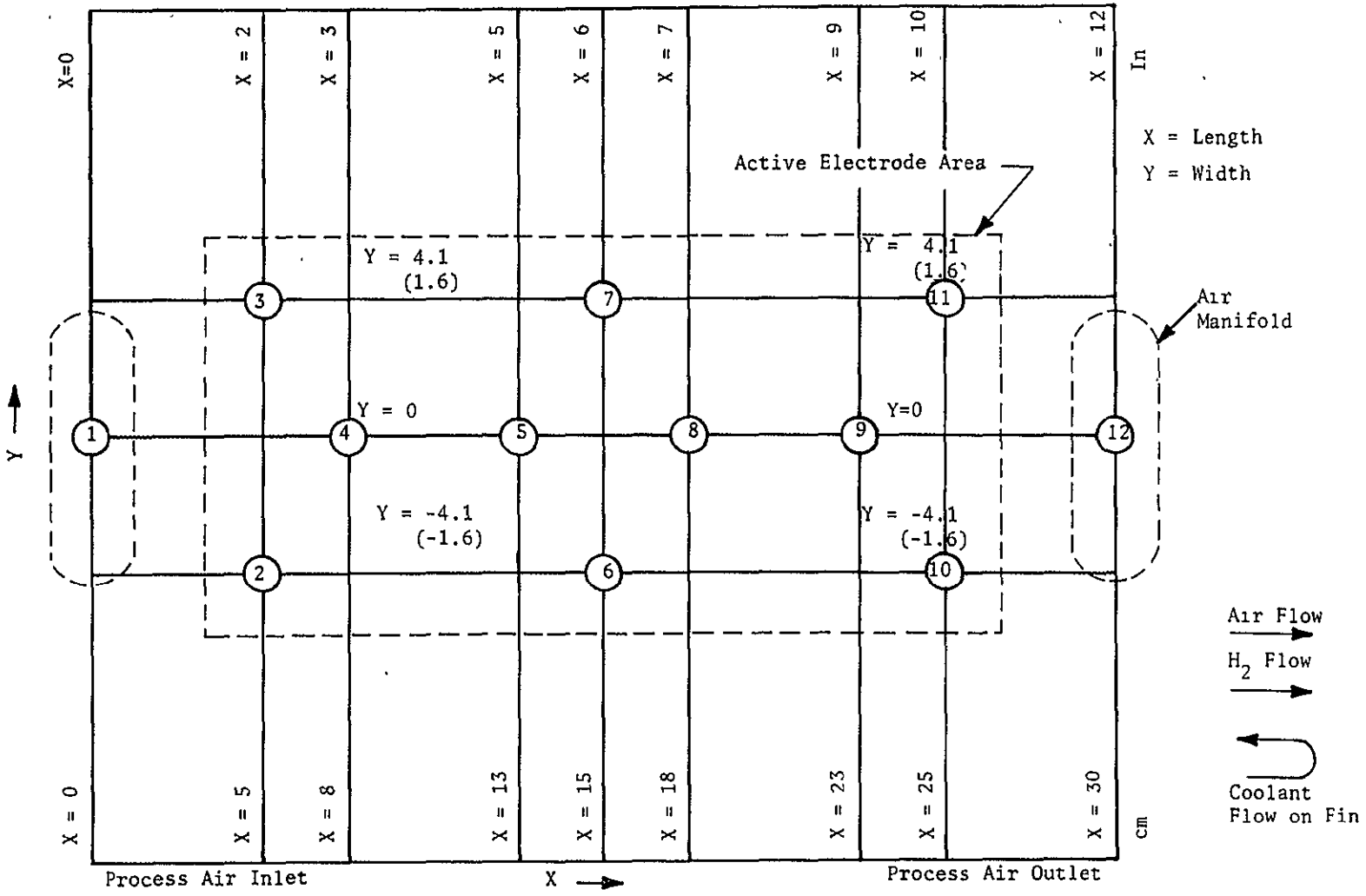

FIGURE 3 SAMPLE PORT LOCATIONS FOR EDC MAPPING TESTS

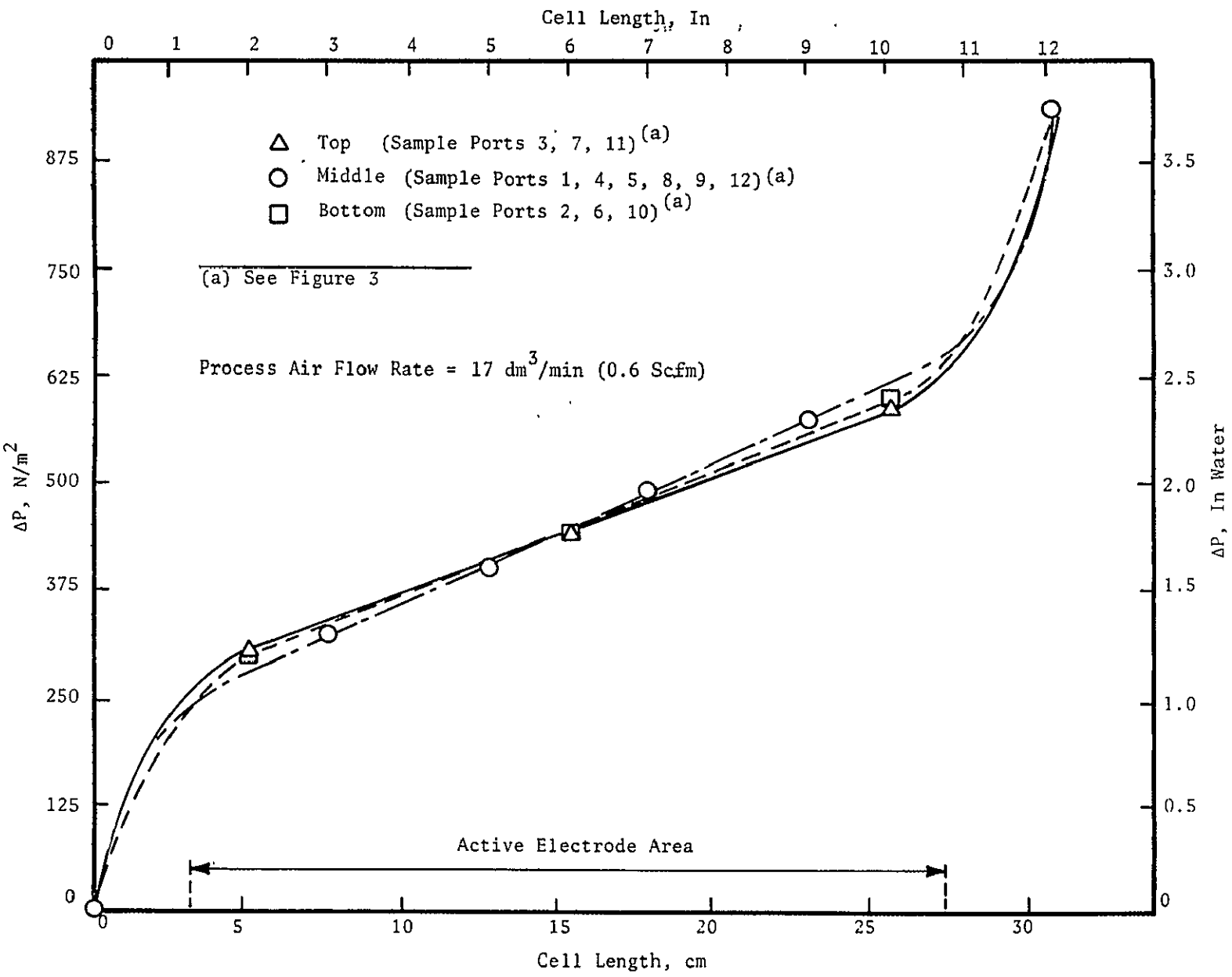

FIGURE 4 EDC PRESSURE DROP AS A FUNCTION OF CELL LENGTH

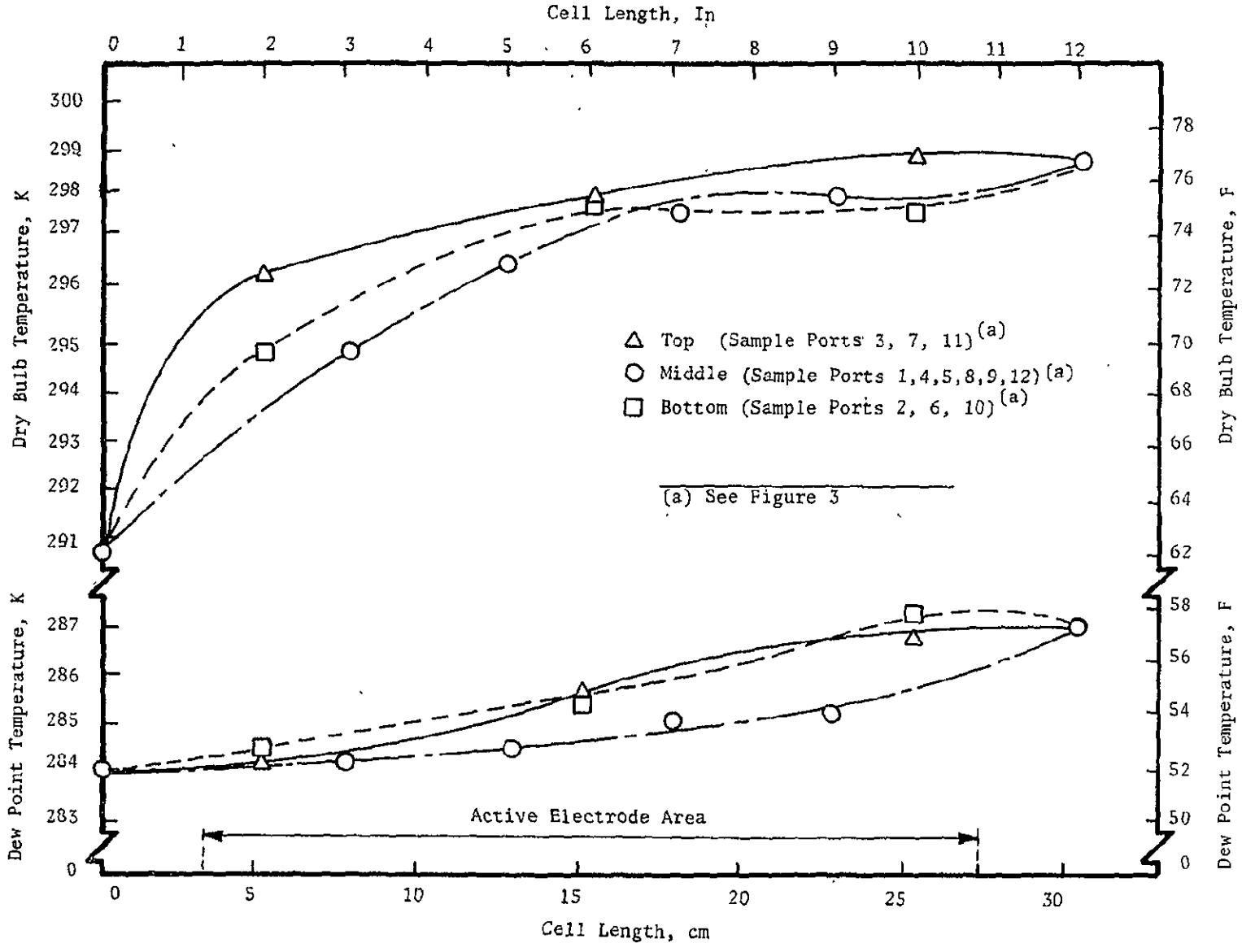

FIGURE 5 EDC DRY BULB AND DEW POINT TEMPERATURE AS A FUNCTION OF CELL LENGTH

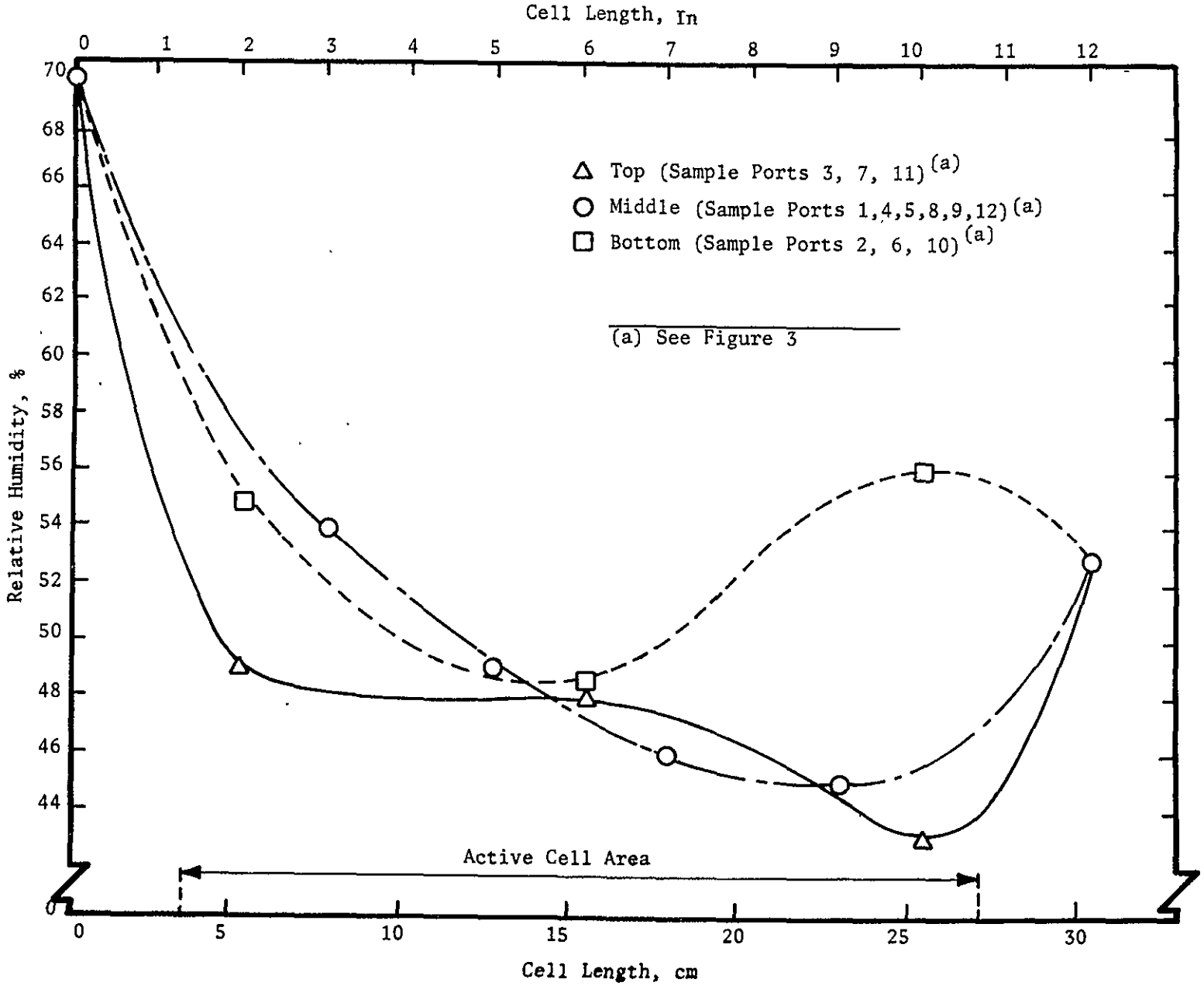

FIGURE 6 EDC RELATIVE HUMIDITY AS A FUNCTION OF CELL LENGTH

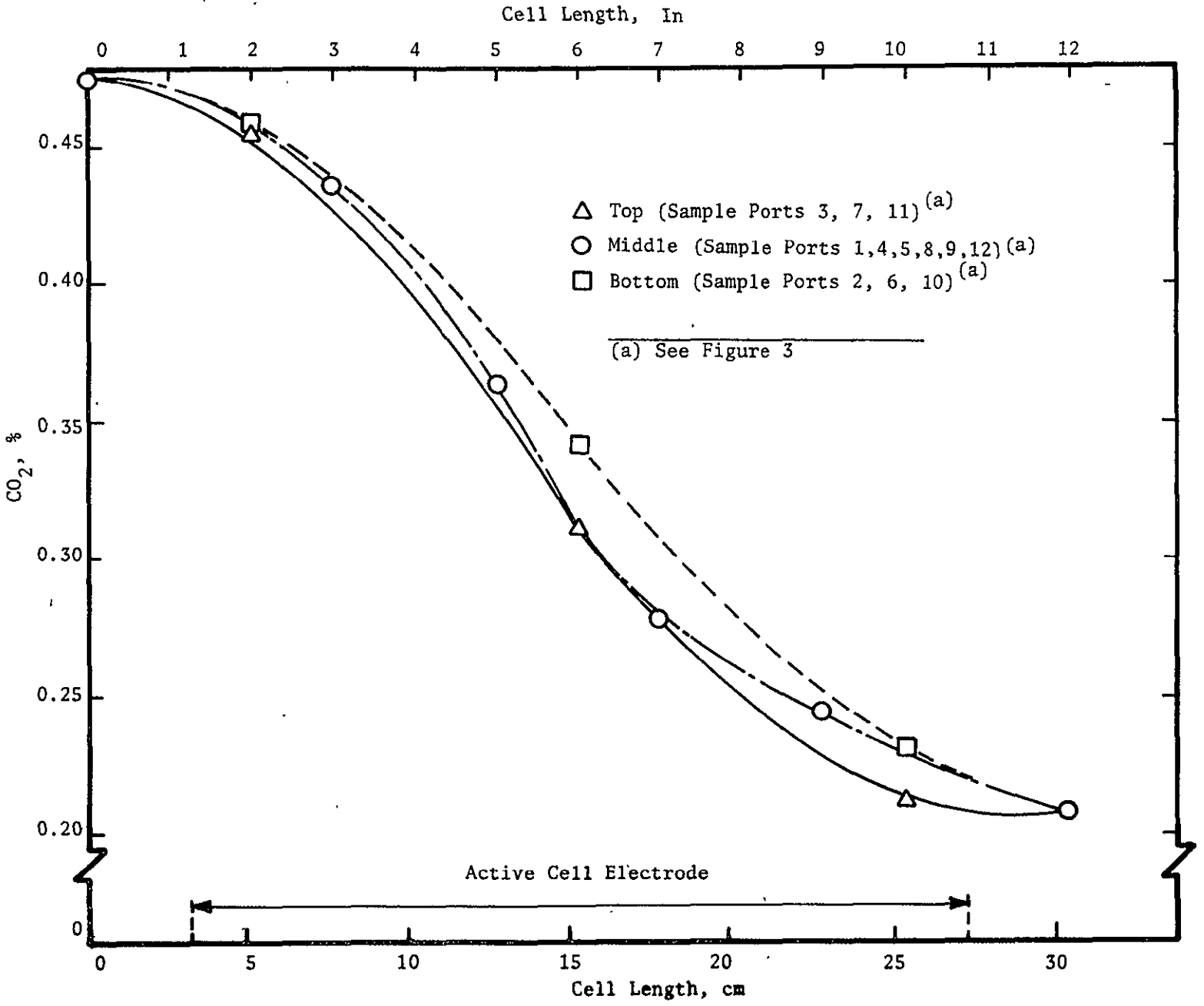

FIGURE 7 EDC pCO_2 AS A FUNCTION OF CELL LENGTH

The dew point rise is relatively linear across the cell as shown in the lower portion of Figure 5. The upper and bottom flow path increases in dew point are almost identical while the middle path, again due to possible minor current density maldistributions, indicates a slightly lower dew point rise.

Process Air Relative Humidity. Based on the process air dry bulb and dew point variations shown in Figure 5, the gradients can be determined. As shown in Figure 6, the RH of the process air drops very quickly upon entering the cell and then slowly rises. The sudden drop is caused by the initial steep rise in dry bulb temperature while the dew point increases very little per unit of cell length. The dry bulb temperature of the process air levels off quickly while the dew point continues to rise, resulting in a slight increase in the RH level. Process air dry bulb temperature variations caused by coolant loop flow patterns result in relatively large RH variations near the cell's exit. These large variations are due to changes in dry bulb and dew point temperatures in opposite directions.

Figure 6 shows that, over a major portion of the cell's active area, the process air RH is substantially less than the equilibrium value (70% RH) based on the initial electrolyte charge concentration (61.5% cesium carbonate (Cs_2CO_3)). Also, the process air RH is near the solubility level of Cs_2CO_3 which is approximately equivalent to a 48 to 50% RH at the cell's operating conditions. Since the cell operated successfully, the results show that the process air is not in equilibrium with the cell electrolyte and that a substantial water vapor partial pressure (pH_2O) differential exits between the electrolyte and the process air. This differential is that needed to transfer the water generated in the cell into the air stream.

Carbon Dioxide Removal Profile. Figure 7 shows the variation in percent CO_2 as a function of cell length. The CO_2 removal rate based on the percent CO_2 gradient across the cell electrode area follows, as expected, an exponential variation showing the dependence of CO_2 removal rate on pCO_2. The change in slope in percent CO_2 near the center indicates an accelerated decrease in CO_2 removed per unit cell area. This occurs near a CO_2 level of 0.33% (333 N/m^2 (2.5 mm Hg)) coinciding with the typical "knee" experienced in an efficiency versus pCO_2 curve for EDC cells. It is near this level that the limiting mechanism in CO_2 removal efficiency changes from reaction limiting to mass transport limiting.[3]

Cell Moisture Tolerance Study

Efficient operation of an EDC requires that the electrolyte-gas interfaces are maintained within proper limits, i.e., within the activated sites of the electrode. An aqueous electrolyte solution will reach equilibrium or steady-state with the water vapor pressure of the surrounding air by either accepting or rejecting water. If water generation is involved, as in the matrix/electrode composite of an electrochemical CO_2 concentrating cell, a water vapor driving force between the electrolyte and the surrounding air is needed to remove the water generated so that steady-state conditions can exist. Also, since water is generated at one electrode (anode) and a major portion of this water must be rejected at the other electrode (air cathode), a concentration gradient exists within the cell.

Electrolyte Volume Changes

For variations in operating conditions, such as for changes in process air RH, the pH_2O of the electrolyte must vary to regain steady-state conditions. The results of the variations in pH_2O are changes in the concentration of the electrolyte. These concentration changes, in turn, result in electrolyte volume fluctuations which, at low pH_2O levels, can cause cell dry-out to the point of electrolyte salt precipitation and gas crossover or, at high pH_2O levels, can cause electrolyte loss. For proper cell operation, i.e., maintaining system moisture balance, the parameters and cell configurations affecting the electrolyte volume must be understood and defined in order to establish limits of safe operation.

The effects of volume fluctuation can be controlled by selecting proper electrode-to-matrix thickness ratios. High ratios, i.e., thin cell matrix with thick electrodes, are desired for increased moisture tolerance. Adverse side effects of selecting large values for this ratio are diffusion problems caused by either CO_2 backdiffusion, reducing CO_2 removal efficiency; H_2 diffusion to the cathode, reducing cell electrical efficiency; or increased diffusion resistances to the CO_2 from the process air to the OH^- generation sites, again causing a decrease in the CO_2 removal rate and efficiency.[8]

Water Transport

For a given initial electrolyte charge concentration, the electrolyte volume retained in the electrode-matrix composite, and hence, electrolyte average concentration level, depends on the inlet process air dew point and dry bulb temperatures, the cell current and the cell temperature. Since electrolyte precipitation establishes a limit to cell operation, electrolyte concentration gradients (not only absolute concentration levels) become important. These gradients are directly related to the amount of water that is transported between the electrodes within the cell.

There are two phases of water transport: (1) the combination of molecular diffusion due to the concentration gradient and the bulk electrolyte flow due to capillary action within the matrix and (2) the water absorption by the process air due the difference in pH_2O between the air and the catholyte at the cathode-air interface.

The water transport through the matrix can be modeled using the Nernst-Planck equation for mass transport:

$$N_{H_2O} = D_{H_2O}\frac{dC_{H_2O}}{dx} + C_{H_2O}\bar{V} \qquad (5)$$

where

N_{H_2O} = flux of water

D_{H_2O} = diffusion coefficient of water through the electrolyte

C_{H_2O} = water concentration

dC_{H_2O}/dx = change in water concentration across the diffusion path

$\overline{V}$ = average velocity of electrolyte solution

The molecular diffusion is driven by the concentration change from the anode to the cathode. The amount of water which is transported from the anode across the cell is not only the water generated through the electrochemical reactions but also the water bound to the ions which transfer from the cathode across the cell. The bulk flow diffusion is due to capillary action of the matrix and electrodes.

The absorption of water by the air flow is given as:

$$N_{H_2O} = H_2O\ (pH_2O_{electrolyte} - pH_2O_{air})/RT \qquad (6)$$

where

N_{H_2O} = flux of water

pH_2O = diffusion index of water through air

pH_2O = partial water vapor pressure

R = gas constant

T = absolute temperature

The flux at steady-state should be equal to the water produced. The remaining water which is transported through the matrix to the cathode is needed to bind the newly formed ions.

Effects of Operating Parameters

Four major operating parameters directly affect a cell's moisture balance. They are cell current, cell temperature, process air pH_2O and process air flow rate. While the remaining parameters associated with operation of an EDC cell can also affect the cell's moisture balance, their effects are of a more indirect nature.

Electrical current has two major effects on the system moisture balance. First, the amount of water produced is a direct function of current level (Faraday's Law) and is independent of CO_2 transfer efficiency. Second, water is bound to each ion carrying current across the cell. Increasing the current increases the amount of water formed and the number of ions transferring water, resulting in a greater amount of water transport, hence greater concentration gradients.

The cell operating temperature affects the pH_2O of the electrolyte which is the driving force for water transport into the air. Therefore, the cell temperature has a direct effect on the moisture balance of the system.

The dew point of the process air is representative of the pH_2O of the air. Varying this condition has the effect of changing the driving force for water transfer into the air.

The diffusion coefficient of water into air is directly proportional to the air flow rate. Increasing the air flow will therefore increase the flux of water into the process air and result in a decrease in the needed differential in pH_2O at the interface.

Other conditions which affect the moisture balance are the process air temperature, intital charge concentration and the H_2 flow rate. The process air temperature has two indirect effects. The flux of water into air is inversely proportional to the absolute temperature. Therefore, any change in process air temperature will slightly change the flux. The other effect of process air temperature is on cell temperature and resulting temperature gradients in the direction of air flow which, in turn, affects the electrolyte pH_2O. The initial charge concentration establishes the operational ranges of the cell by limiting the amount of salt available for the moisture balance. Due to the relatively small flow rates the anode gas (H_2 and/or $H_2 + CO_2$) has little effect on the moisture balance of a cell.

Effect of Moisture Balance on EDC Performance

An increase in CO_2 transfer efficiency (TI) with decreasing RH has been experimentally observed and characterized as a function of the average RH within the process air compartment. (See results presented in the section entitled EDC Cell and Stability to Pressure Differentials.) As the average RH decreases, the electrolyte volume decreases. With a smaller volume the surface area for CO_2 diffusion into the electrolyte increases and/or the diffusion path for carbonate ion ($CO_3^=$) transfer decreases resulting in more efficient CO_2 transfer.

As the electrolyte concentration increases, however, the terminal voltage decreases due to a decrease in the conductivity of the electrolyte which results in a decrease in the cell's electrical efficiency. Also, a decrease in electrolyte volume causes the electrolyte to pull out of some of the active sites within the cell's electrodes, again reducing cell voltage. The latter, however, does not appear to decrease the CO_2 removal efficiency since the chemical reaction of OH^- and CO_2 to form $CO_3^=$ is not affected. The loss in cell electrical efficiency with decreasing RH has also been experimentally verified.

Predicting EDC Operational Limits

Two moisture balance-related operational limits exist: a lower limit, or dry out, with resulting gas crossover and an upper limit, or excessive moisture, with resulting electrolyte loss. The operational parameters of the EDC cell establish a demand electrolyte concentration at the air catholyte interface such that the water produced is removed by the process air stream. This demand concentration, along with the total amount of electrolyte salt within the cell fixed by the initial charge concentration, determines the specific volume of electrolyte that must exist within a cell at operational steady-state conditions. The lower limit is exceeded when this volume is less than the minimum operational volume of the cell and extreme performance degradation or even gas crossover occur. The upper limit is exceeded when the electrolyte volume is greater than the maximum operational volume capacity of a cell and electrolyte loss occurs.

For this analysis the minimum operational volume was defined as the quantity of electrolyte necessary in the electrode/matrix composite to maintain liquid (by capillary action) in the largest pores or pore paths present in the compressed asbestos matrix. The maximum operational volume was defined as the quantity of electrolyte that can be retained within the pores of the electrodes and cell matrix without forming electrolyte or moisture "beads" (liquid droplets) on the gas side of either electrode.

Based on analyses and experimentation performed under this activity, the maximum and minimum operational volumes of a CS-6 style cell were found to be 64% and 50%, respectively, of the total volume of the electrodes and cell matrix. Knowing these percentages and using electrolyte properties, such as specific volume versus concentration, the limits of process air inlet dew points for a given cell, electrolyte type and initial electrolyte charge concentration can be readily calculated.

Cell Optimization

In optimizing cell construction with respect to moisture balance, the selection of proper electrode-to-matrix thickness ratios can decrease the adverse effects of volume fluctuations within a system and result in a larger tolerance to operational process air RH ranges. In general, higher ratios (thick electrodes and thin cell matrix) are desirable for increased moisture tolerance. For example, a cell having an electrode-to-matrix thickness ratio of one (ratio of thickness of both electrodes to the thickness of the cell matrix) could withstand a volume reduction of nearly 50% from a fully-charged condition (both electrodes and matrix filled with electrolyte) before any liquid volume reduction within the matrix would occur. Relative porosities and pore sizes of the electrodes and matrix will, of course, affect the ratio values. As a general rule, the pore size of the matrix material must be lower than that of the electrodes to insure that the electrolyte will wet the matrix to maintain a positive gas barrier and provide for a continuous, electrically conductive medium.

Higher ratio values can be achieved by either decreasing the thickness of the cell matrix and/or increasing the electrode thickness. Two potential problems

do exist when decreasing the matrix thickness. The first is the occurrence of increased CO_2 backdiffusion, thus lowering CO_2 transfer rates, while the second is a decrease in the matrix differential pressure capability.

While increasing electrode thickness increases moisture tolerance, it can also decrease CO_2 removal rates and cell voltage due to the increase in CO_2 and O_2 diffusion path lengths. Previous experimental activities have shown, however, that increases in anode thickness have only minor effects on CO_2 removal efficiency while increased cathode thickness normally adversely affected CO_2 removal. These facts suggest that in optimizing an EDC cell with respect to performance and moisture tolerance by selection of the electrode-to-matrix thickness ratio, a thin cathode, thin matrix, and thick anode are desirable.

Once the thickness ratio and absolute thicknesses of the electrodes and matrix have been established, one additional aspect for cell moisture optimization must be considered. This aspect concerns the relative matrix and anode pore sizes. Since the anode has no demand concentration due to water transport and its thickness has negligible effects on cell performance, it can ideally serve as an internal electrolyte reservoir. The anode can, therefore, retain excess electrolyte during operation at high process air RH for use during operation at low process air RH. The electrolyte must be capable of being transferred in and out of the matrix and anode as dictated by the process air RH values. To insure this transfer and maintain positive gas separation and electrical continuity, the pore sizes of the anode must be larger than the pore sizes of the matrix.

Single-Cell Testing

Single-cell testing was conducted to support the analytical moisture balance studies. The tests were designed to obtain performance data as a function of varying electrolyte concentrations and volumes and to verify cell operational limits.

Electrolyte volume variations were obtained by two methods. With the first method, minor volume fluctuations were investigated by manually adjusting the process air inlet RH condition but maintaining a fixed salt content in the cell. With the second method, larger volume changes were studied by decreasing the equivalent electrolyte charge concentrations through the lowering of the total salt content of the cell. The decreases in equivalent charge concentrations were accomplished at zero current by conditioning the cell with process air at sufficiently high RH values to result in electrolyte loss, i.e., a decrease in total salt content within the cell. Volume variations at equivalent charge concentrations of 61.5 (baseline), 55, 50, and 35% Cs_2CO_3 were evaluated.

At each equivalent charge concentration the process air inlet dew point-to-module temperature differential (ΔT) was varied over one fixed range to cause the electrolyte volume variations. For a fixed ΔT, larger volume changes will result as electrolyte equivalent charge concentration decreases. Effects on cell performance could, therefore, be obtained as a function of both electrolyte concentration and volume.

The test results supported the analytical findings that a decrease in electrolyte volume causes a decrease in cell voltage, most likely caused by the decrease in electrolyte-electrode contact. This was illustrated for both the small volume fluctuation as well as for the large volume fluctuation.

The effects of volume fluctuations on CO_2 transfer efficiency for the varying equivalent charge concentrations and volumes showed the following. An initial decrease in electrolyte volume from the baseline 61.5% Cs_2CO_3 charge did, in general, cause an increase in TI to some maximum value. Further, volume decreases decreased TI with large changes in TI observed as the electrolyte volume decrease is accelerated. Equal electrolyte volumes achieved by varying the ΔT but starting with different initial equivalent charge concentrations (61.5% to 35% Cs_2CO_3) showed equal TI levels when starting with 61.5, 55, and 50% Cs_2CO_3 but showed decreased TI values for equal volumes when starting with 35% Cs_2CO_3.

The results of the volume variation tests were also used to determine and verify the operational moisture limits for a CS-6 style cell (see discussion above). The results showed a maximum and minimum allowable electrolyte volume of 64% and 50%, respectively, based on the total electrode and matrix volume of the cell.

Three-Cell Testing

The three-cell test was designed to evaluate the effectiveness and usefulness of the model when scaled to multiple cell modules. The testing was performed with CS-6 baseline electrode and matrix configurations and a charge concentration of 61.5% Cs_2CO_3. The three-cell module was liquid-cooled in an effort to maximize the consistency and repeatability of moisture conditions of the process air along the electrode surface area. Thermocouples were placed in the cathode air compartment to monitor the dry bulb temperature at different points along the cell's active area.

Following conditioning of the module at baseline operating conditions, a charge analysis was performed to determine, by weighing, the initial mass of electrolyte contained in each cell. The moisture conditions of the process air of the module were slowly changed until first electrolyte loss and then cross-over occurred. Following a crossover, the cells were remoisturized to the point of electrolyte loss. The amount of electrolyte lost was collected and measured to maintain a salt content history and the module, now with a new initial charge concentration, was operated to determine new sets of operational limits. The operating conditions at each set of operational limits were used to calculate the electrolyte volumes in each cell at each limit observed. These results were compared with the operational limits as predicted by the analytical model. The results verified the predictability of the model.

Liquid-Cooled EDC Studies

Cells of previous EDC modules were externally cooled using either air over external fins or liquid coolant through tubes attached to fins. Tests conducted with internally liquid-cooled concentrator cells had shown increased CO_2 removal efficiencies (particularly at low pCO_2 levels) when compared to baseline air-cooled cells. An extensive test program was conducted using a three-cell,

liquid-cooled EDC to characterize the electrochemical performance of liquid-cooled cells. Also, the possible mechanisms by which the increased performance of liquid-cooled cells is achieved was investigated.

Experimental Investigation

A three-cell, liquid-cooled concentrator was constructed with coolant flowing in parallel through the three cells utilizing "Z" configured flow paths. A serpentine coolant flow path was created through each cell and solid nickel cathode current collectors separated the cathode compartment from the coolant.

The coolant compartments were generated using the internal humidifier frames developed for the module of the one-man system (CX-1).[9] The serpentine flow path was created using silicone elastomer. The module was operated for 600 hours and all inlet, exhaust and performance parameters were monitored. During the test a current density and a pCO_2 span were performed.

The results of the tests are shown in Figures 8, 9, and 10. The performance of the three-cell module was superior to previous cell configurations operated. The module also demonstrated the capability of successfully operating with an inlet air RH range of 32% to 94% (see Figure 8) using Cs_2CO_3 as the electrolyte.

The effect of inlet air pCO_2 on TI showed a shift of the "knee" to the left near the 400 N/m^2 (3 mm Hg) pCO_2 level (Figure 9), resulting in increased TIs at lower pCO_2 levels. For example, a 25% improvement was observed in the TI at a pCO_2 of 333 N/m^2 (2.5 mm Hg) (2.5 compared to 2.0). The performance at all other pCO_2 levels was also above that of prior average levels as indicated on Figure 9 by a least squares fit curve of previous EDC performance data.[3]

Figure 10 shows the effect of current density on TI and cell voltage. The results obtained for the TI values, when compared to previous data, again show improved performance. For example, a 38% improvement in TI was observed at 43 mA/cm^2 (40 ASF) (1.8 compared to a typical value of 1.3). Cell voltages were equal to or slightly above typical air-cooled cell levels.

Possible Mechanisms of Improved Performance

The approach to the study was to investigate potential differences between liquid-cooled and externally air-cooled cells based on cell construction, process fluid interface conditions, and direct results of the heat removal mechanism (internal thermal gradients).

Cell Construction. The primary difference between the baseline air-cooled cell and the baseline liquid-cooled cell lies in the cathode compartment height and cathode current collector construction. A liquid-cooled cell uses a solid, 0.05 cm (0.020 in) thick nickel current collector with a 0.15 cm (0.060 in) thick expanded metal spacer spot-welded to the current collector to create the cathode compartment. An air-cooled cell, on the other hand, uses a frame-shaped, open cathode current collector with a 0.20 cm (0.080 in) thick expanded metal spacer attached within this frame to create the cathode compartment. For a given process air flow rate, the lower spacer height may result in an increase in

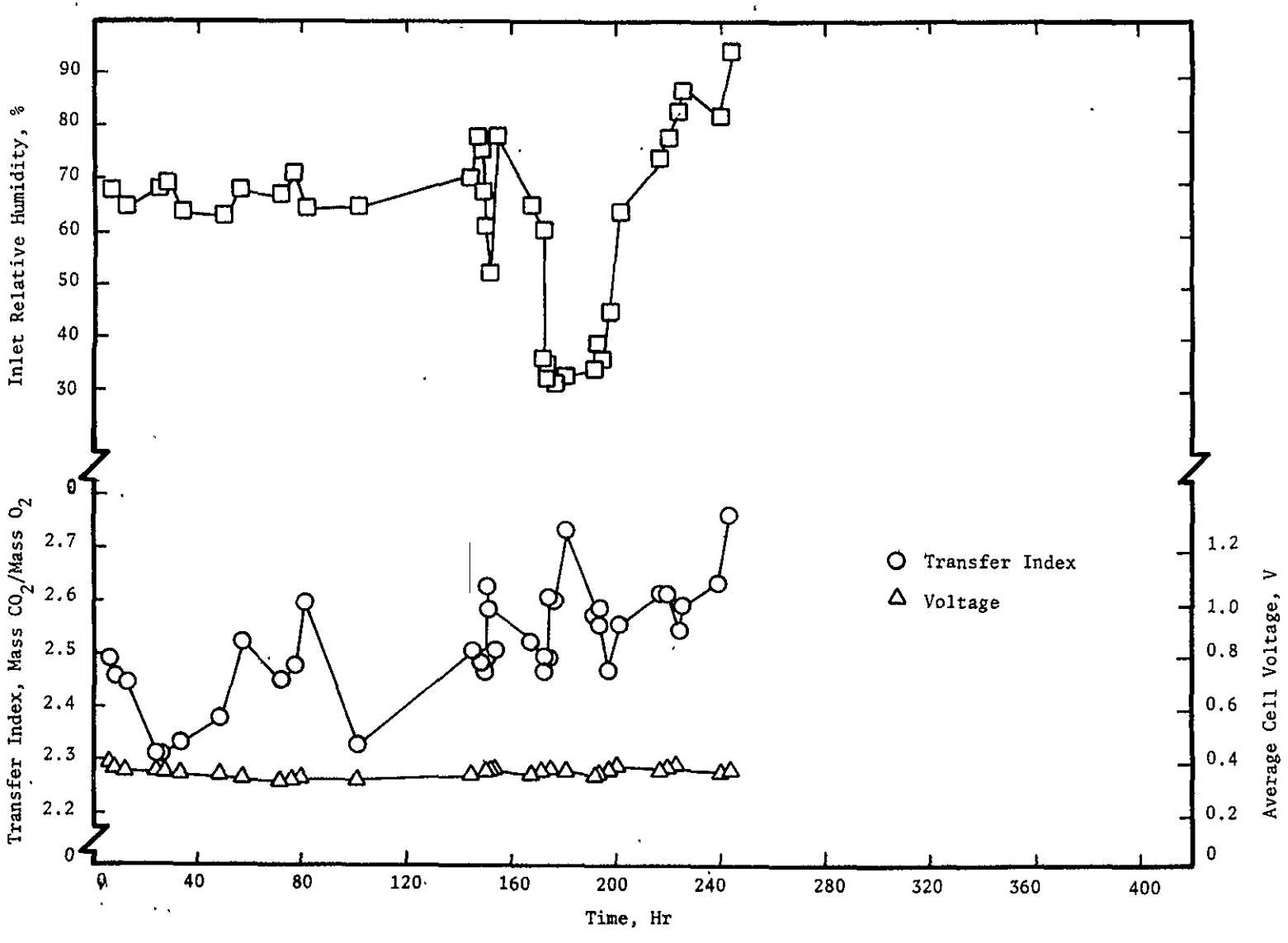

FIGURE 8 LIQUID-COOLED EDC PERFORMANCE AS A FUNCTION OF PROCESS AIR INLET RELATIVE HUMIDITY

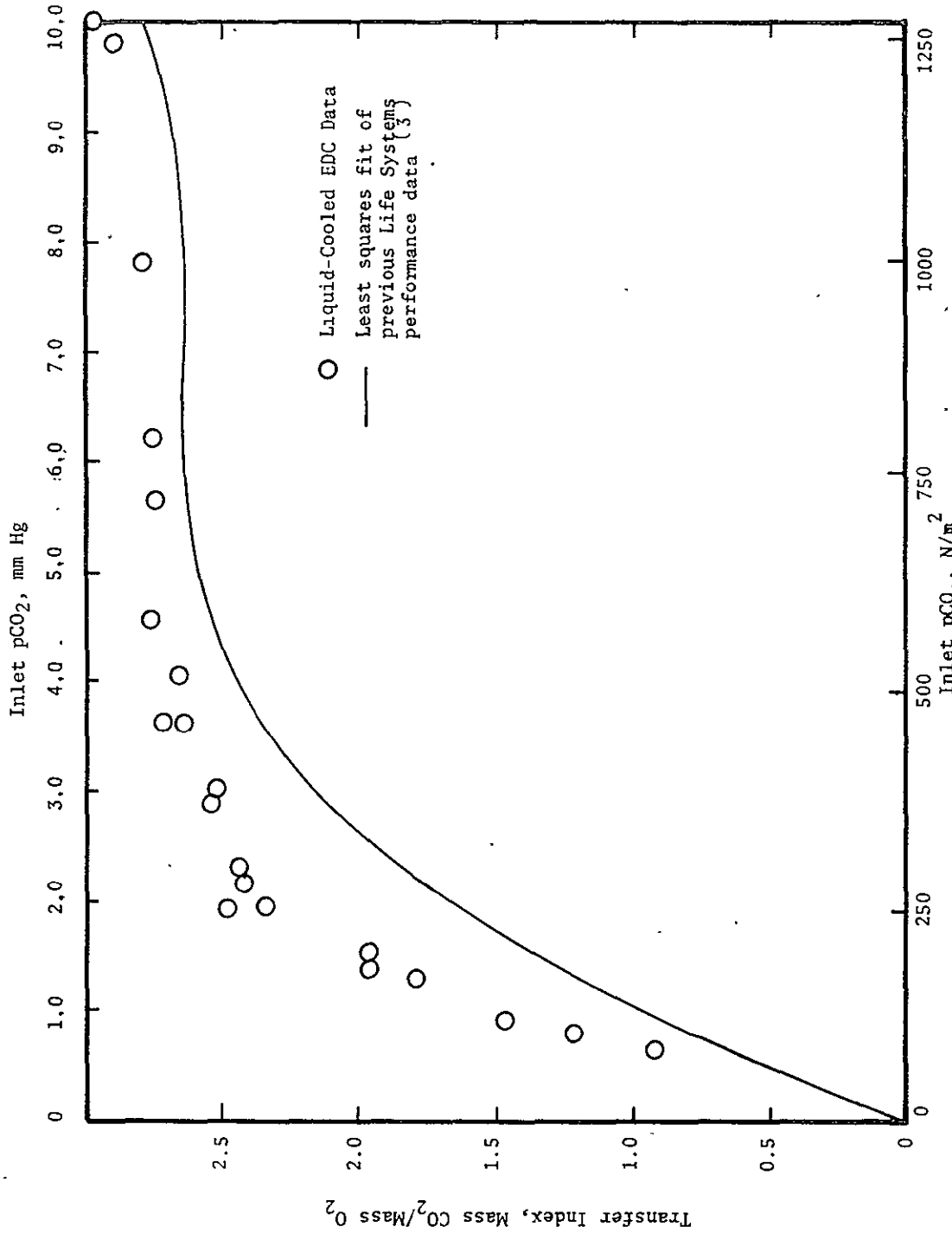

FIGURE 9 LIQUID-COOLED EDC PERFORMANCE AS A FUNCTION OF AIR INLET pCO_2

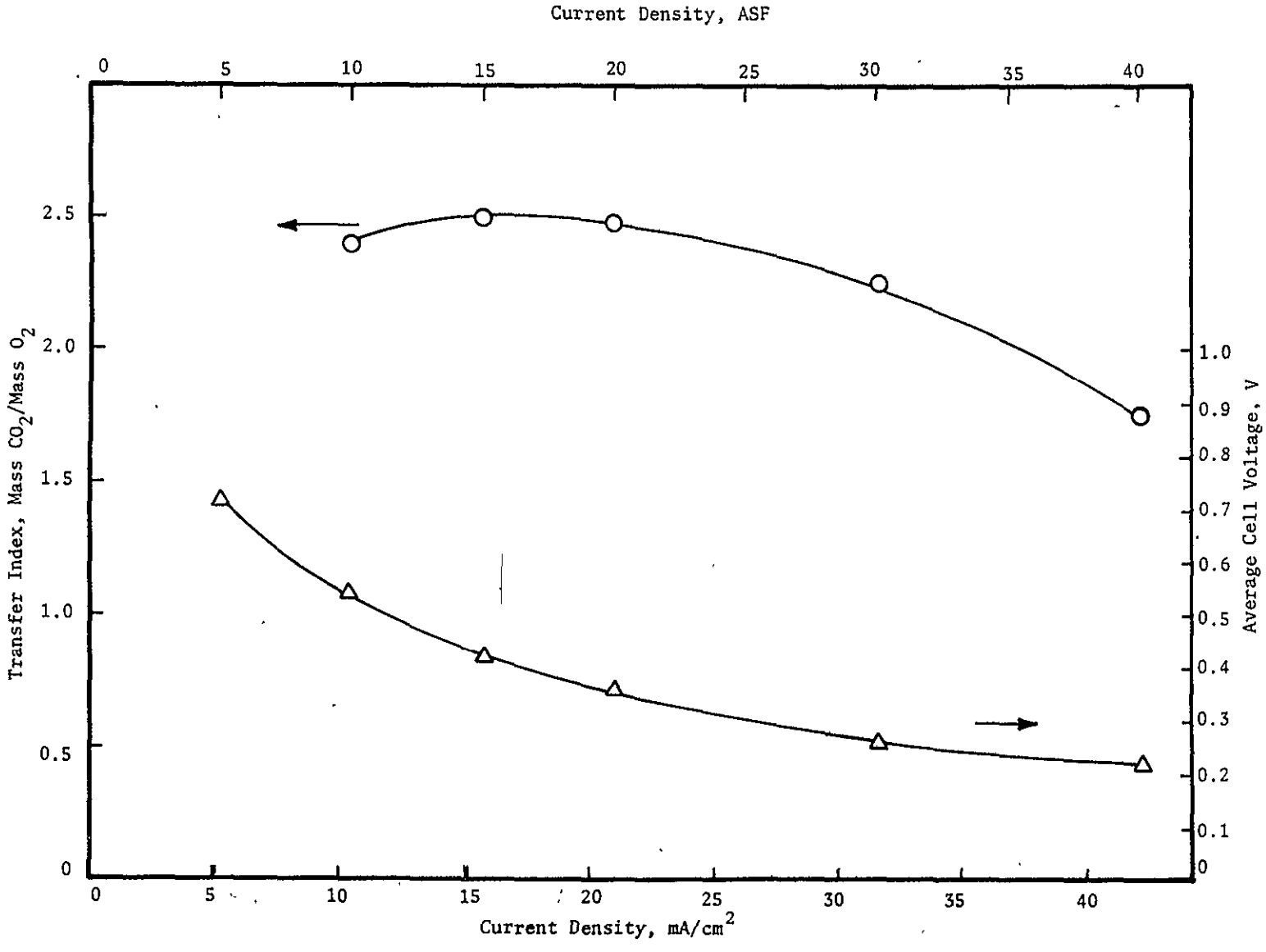

FIGURE 10 LIQUID-COOLED EDC PERFORMANCE AS A FUNCTION OF CURRENT DENSITY

process air turbulence within the cathode compartment, hence, increases in the CO_2 removal efficiencies. Also, the solid current collector used in liquid-cooled cells decreases the possibility of current density maldistributions. Higher current densities can occur near the edge of the open-type frame current collector since the current is primarily carried by the expanded metal spacer to the internal active cell areas as opposed to a solid nickel sheet.

To investigate the effects of the difference in cell structure, test results of air-cooled cells using solid cathode current collectors with 0.15 cm (0.060 in) thick cathode compartment spacers were analyzed. Also, a liquid-cooled cell was constructed using an air-cooled type, open-frame cathode current collector with a 0.20 cm (0.080 in) thick cathode compartment. For this construction, the liquid-cooled cavity was isolated from the process air stream using a 0.03 cm (0.010 in) thick polysulfone sheet.

Investigation of test results showed that the same increase in CO_2 removal efficiency resulted for liquid-cooled cells using either solid or open frame type current collectors. Also, no particular increase in CO_2 removal efficiency was observed for an air-cooled cell using a solid cathode current collector.

Process Fluid Interfaces. Large amounts of available test data for both liquid- and air-cooled cells were analyzed and CO_2 removal efficiencies at identical process fluid interface conditions were isolated and compared. Again, for similar interface conditions, higher CO_2 removal efficiencies were obtained with liquid-cooled cells as compared to externally air-cooled cells.

Internal Thermal Gradients. Elimination of the configuration differences and differences in interface parameters as a potential mechanism for increased CO_2 removal efficiencies left the effect of internal thermal gradients as the most likely candidate. The primary differences between the two heat removal techniques are the resulting temperature gradients imposed over the active area of a cell. Data taken from liquid-cooled single cells based on coolant and process air inlet and outlet conditions indicate that thermal and resulting air RH gradients are negligible over a liquid-cooled cell's active area. In air-cooled cells, on the other hand, the RH of the process air above the cathode can vary from 43 to 70% RH (see Figure 6). Equilibrium Cs_2CO_3 concentrations for such a range in RH are 72 to 60% in weight, respectively. This range in concentration corresponds to a ratio in specific electrolyte volumes of 1:1.6, indicating that a 60% increase in electrolyte volume is experienced in the high RH regions as compared to the low RH regions of the cell.

Moisture balance studies have shown a dependency of CO_2 transfer efficiency on the electrolyte volume retained within the electrode-matrix-electrode composite. In general, high volume retention of electrolyte in a specific area will result in lower TIs while areas of low electrolyte volume generally have higher TIs (see Cell Moisture Tolerance Study, above).

The operating conditions for a liquid-cooled cell with its uniform temperature and RHs across the cathode surface can be tailored to achieve optimum, uniform electrolyte concentration and volume. The result is a uniform current density with optimum CO_2 transfer for the given conditions. In an air-cooled cell, the

average electrolyte concentration can be optimized but the deviations, both in the dry or wet direction from the optimum concentration and volume, will result in decreases in overall CO_2 transfer efficiency.

Spectrographic Analysis of EDC Exhaust Gases

Mass spectrographic analyses were made of EDC gases as another step toward total characterization of the EDC concept. The CS-6 for the SSP was used for the testing. The CS-6 exhaust gases were analyzed for impurities and possible electrolyte aerosols. The anode exhaust was also analyzed to identify if air contaminants possibly present in the process air could be transferred to the anode side and harm the catalysts of a CO_2 Reduction Subsystem downstream of the EDC. A sample of the anode exhaust was also taken near the end of the two-minute shutdown nitrogen (N_2) purge to assure that all combustible gases were being removed from the subsystem. To establish a point of reference, both the CS-6 process air and H_2 supplies were analyzed.

Process Air Analysis

All sample cylinders were cleaned with N_2 and high purity argon (Ar). Samples were taken when the subsystem was operating at "baseline," "wet" and "dry" conditions with respect to electrolyte-process air humidity tolerance. The results of the analyses are shown in Table 1. The numbers shown in the table are corrected for any Ar in excess of that normally found in ambient air. Such excess Ar was considered residual from cylinder flushing prior to sample collections. The N_2 and O_2 levels of all three samples are consistent and agree with theoretical air precentages of 78% and 21%, respectively. The pCO_2 level in all three exhaust samples are in agreement with the pCO_2 measurements taken with the infrared analyzer (LIRA) during the testing. As can be seen from the results presented in Table 1, no trace contaminants, impurities or electrolyte aerosols were detected over the typical range of operation in process air humidities. The analysis of the sample of the process air supply to the CS-6 (operating in an open loop manner) showed no detectable signs of contamination.

Anode Gas Analysis

The results of the anode gas analysis are shown in Table 2. The results show that there is no transfer or addition of impurities by the cell that could harm any CO_2 reduction unit catalyst. Again, an analysis of the H_2 supply gas was included for reference. A comparison between the results of the analyses and data taken during testing shows excellent agreement as shown below:

H_2 Balance

H_2 + CO_2 flow (experimental with wet test meter)	9.55 dm^3/min
H_2 in exhaust stream (analysis)	72%
H_2 flow out (calculated)	6.88 dm^3/min
H_2 flow in (experimental with wet test meter)	9.8 dm^3/min

TABLE 1 PROCESS AIR ANALYSES

Element	Cathode Exhaust			Cathode Supply, Vol %
	Baseline, Vol %	Wet, Vol %	Dry, Vol %	
Nitrogen	77+	77+	77+	77+
Oxygen	20.3	20.8	20.8	20.9
Argon	0.94	0.94	0.94	0.93
Carbon Dioxide	0.24	0.25	0.27	0.075 (a)
Hydrogen	0.018	0.014	0.008	<0.001
Helium	ND (b)	ND	ND	ND
Carbon Monoxide	ND	ND	ND	ND
Methane	ND	ND	ND	ND
Sulfur Dioxide	ND	ND	ND	ND
Nitric Oxide	ND	ND	ND	ND

(a) Upstream of CO_2 addition point
(b) ND = None Detected, less than

Helium	0.001%
Carbon Monoxide	0.02%
Sulfur Dioxide	0.003%
Nitric Oxide	0.0015%
Methane	0.002%

TABLE 2 ANODE GAS ANALYSES

	EDC Anode (H_2 + CO_2) Exhaust		
Element	Baseline, Vol %	Wet, Vol %	Anode Supply, Vol %
Hydrogen	72+	76+	Balance
Nitrogen	0.74	1.4	0.038
Carbon Dioxide	26.6	22.2	0.0027
Oxygen	0.0013	0.07	ND[a]
Argon	0.027	0.34	0.0066
Helium	ND	ND	ND
Carbon Monoxide	ND	ND	ND
Methane	ND	ND	ND
Sulfur Dioxide	ND	ND	ND
Nitric Oxide	ND	ND	ND

(a) ND = None Detected, less than

Helium	0.001%
Carbon Monoxide	0.02%
Methane	0.002%
Sulfur Dioxide	0.0015%
Nitric Oxide	0.003%

H_2 consumed (no. of cells) x (A) x (7.54 $\frac{cc/min}{cell-A}$)	3.4 dm^3/min
H_2 flow out	6.4 dm^3/min
Error	7.5%

CO_2 Balance

CO_2 transferred (experimental with LIRA)	2.43 dm^3/min
$H_2 + CO_2$ flow (experimental with wet test meter)	9.55 dm^3/min
CO_2 in exhaust stream (analysis)	26.6%
CO_2 flow out (calculated)	2.55 dm^3/min
Error	3%

Similar treatment of the "wet" sample analysis yielded comparable results.

Nitrogen Purge

The results of the N_2 purge analysis are shown in Table 3. The analysis shows that all combustible gases are removed from the subsystem during the purge sequence.

EDC Cell Stability to Pressure Differentials

Prior to the conversion of the CX-6 to SSP specifications, the EDC operated with a pressure differential of less than 6.9 kN/m^2 (1 psid) between the H_2 and air compartments. Space Station Prototype requirements called for a pressure differential greater than 31 kN/m^2 (4.5 psid) to meet water accumulator operating requirements downstream of the Sabatier Reactor in the CO_2 Reduction Subsystem.

Immediately after establishment of the elevated anode gas backpressure requirement a program was initiated to systematically characterize EDC performance at SSP baseline conditions by gradually increasing backpressure levels to 34.5 kN/m^2 (5 psid). These tests were performed sequentially with single cells, three-cell submodules, a one-man capacity subsystem, the CX-6 and finally the CS-6.[5] Operating times with the various EDC configurations ranged from several hundred to an excess of one thousand hours of operation. While these tests established the EDC's capability to withstand the 34.5 kN/m^2 (5 psid) differential at baseline conditions, they did not include evaluation of the module's tolerance to pressure differentials for variations in other operating parameters.

The key parameters affecting a cell's stability to pressure differentials at a given current level are the process air dew point, dry bulb temperature and module temperature. These parameters control the electrolyte volume retained in the cell's matrix and electrodes. For an increased H_2-to-air pressure differential, adverse effects such as electrolyte being forced into the cathode compartment or gas crossovers at locations of maximum matrix pore sizes, will occur at different values for key parameters than at a zero pressure differential.

TABLE 3 NITROGEN PURGE EXHAUST ANALYSIS

Element	Volume, %
Nitrogen	Balance
Oxygen	ND[(a)]
Argon	0.004
Carbon Dioxide	ND
Hydrogen	ND
Helium	ND
Carbon Monoxide	ND
Methane	ND
Sulfur Dioxide	ND
Nitric Oxide	ND

(a) ND = None Detected, less than

Oxygen	0.001%
Carbon Dioxide	0.001%
Hydrogen	0.004%
Helium	0.001%
Carbon Monoxide	0.02%
Methane	0.001%
Sulfur Dioxide	0.002%
Nitric Oxide	0.001%

A measure of moisture tolerance that has been used in evaluating EDC performance is the temperature differential between the module temperature (equivalent, by definition, to process air outlet temperature) and the dew point of the process air at the inlet (ΔT).[9] The SSP baseline value for this differential had been initially projected as 11K (20F), but was to be verified by results of this investigation. The range of temperature differentials selected for testing was from 10K to 14K (18F to 25F).

Test Procedure

The one-man capacity CX-1, with a 15-cell module, was selected for the test. The system was operated at several sets of constant operating conditions for extended periods of time while maintaining a constant elevated H_2 backpressure of 31.0 to 34.5 kN/m^2 (4.5 to 5.0 psid) and a ΔT of 5.5 ±0.4K (10 ±0.7F) to establish baseline module performance. After establishing baseline performance, ΔT tolerance of the module was characterized by maintaining the module's temperature constant at 292 ±0.3K (66.5 ±0.5F) while slowly raising the inlet air dew point, thus decreasing the ΔT until moisture was visible in the process air exhaust manifold. This procedure established the lowest permissible ΔT value. The upper ΔT value was determined by lowering the inlet air dew point until a significant drop in cell voltage was observed, thus signifying incipient H_2 crossover. Since moisture level changes are slow in reaching equilibrium, the ΔT excursions were made slowly and extended over several hundred hours. A maximum average rate of change of 0.06K (0.1F) per hour was adopted.

Experimental Results

The results of the test are shown in Figures 11 and 12. Figure 11 shows average cell voltage, TI and module-to-inlet-air-dew-point ΔT for the total 1,110 hours of operation at elevated H_2 backpressure. Figure 12 shows the same parameters expanded over the last 430 hours of operation during which the ΔT spans were performed.

After 680 hours of operation at elevated H_2 backpressure, and after two excursions to different cabin pCO_2 (400 N/m^2 and 360 N/m^2 (3.0 mm Hg and 2.7 mm Hg)), the dew point of the inlet air was slowly raised until moisture was observed. The dew point was then lowered, raised again and then lowered until a significant cell voltage decrease resulted. The latter occurred at 1,110 hours of operation.

The first signs of moisture were observed at a ΔT value of 8.8K (14F) while incipient H_2 crossover (H_2 backpressure drop) was observed at a ΔT of 13K (24F) (also start of sudden cell voltage drop). The figures show that the TI increases and decreases closely followed ΔT increases or decreases. This was expected and is attributed to electrolyte volume changes and resulting changes in liquid gas interface locations as discussed previously.

The range in module air inlet RH was 88% to 92% while the range in air outlet RH was from 54% to 72%. These ranges correspond to 47% to 38% and 68% to 59% by weight of Cs_2CO_3 concentration (assuming air-electrolyte equilibrium). The resulting localized maximum volume fluctuation possible, based on the 38% and 68% concentrations, is 1.75:0.68 or 2.5:1. This value is slightly lower than the typically expected maximum volume ratio of 3:1 established for similar cells

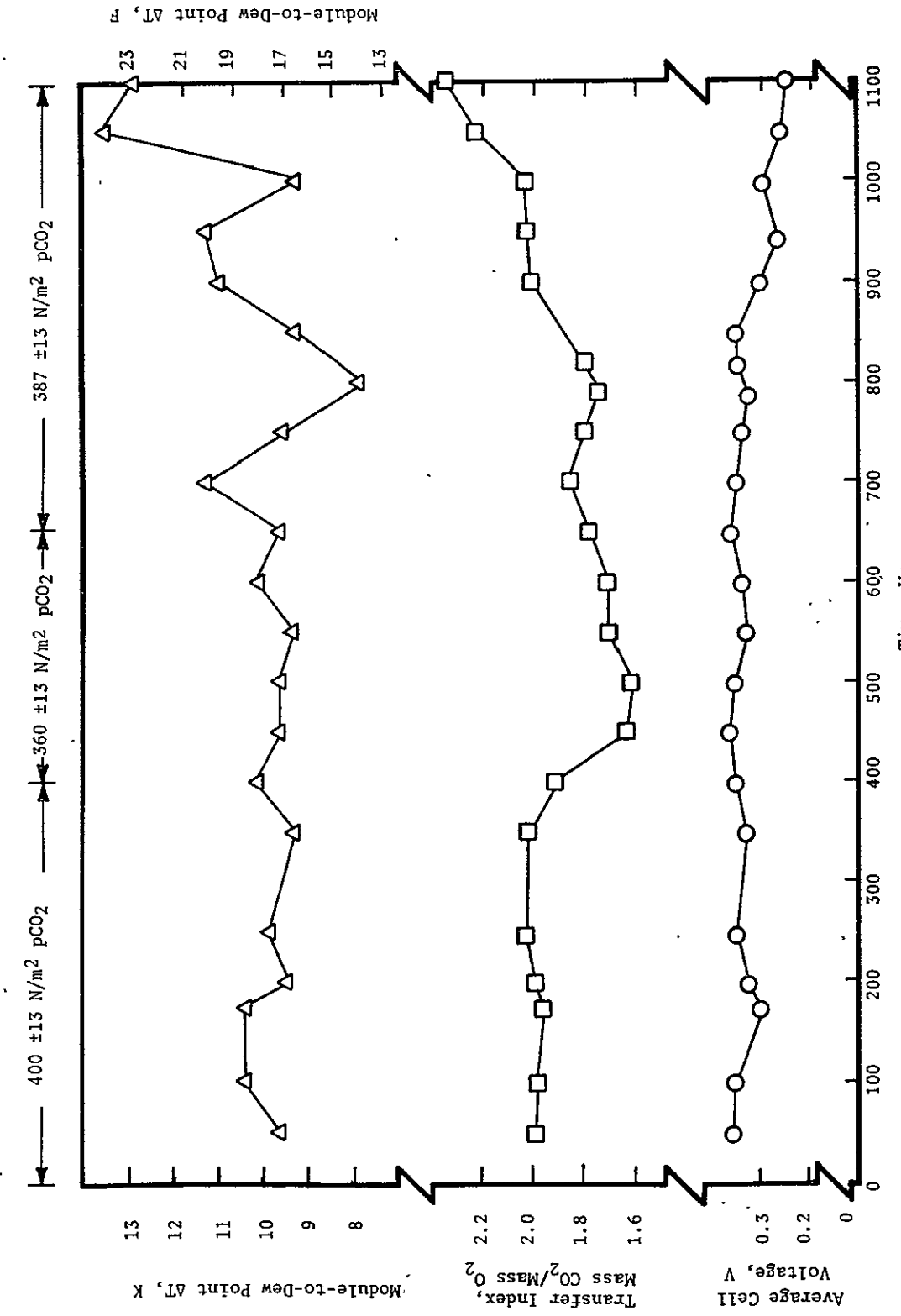

FIGURE 11 ELEVATED HYDROGEN BACKPRESSURE CHARACTERIZATION TEST

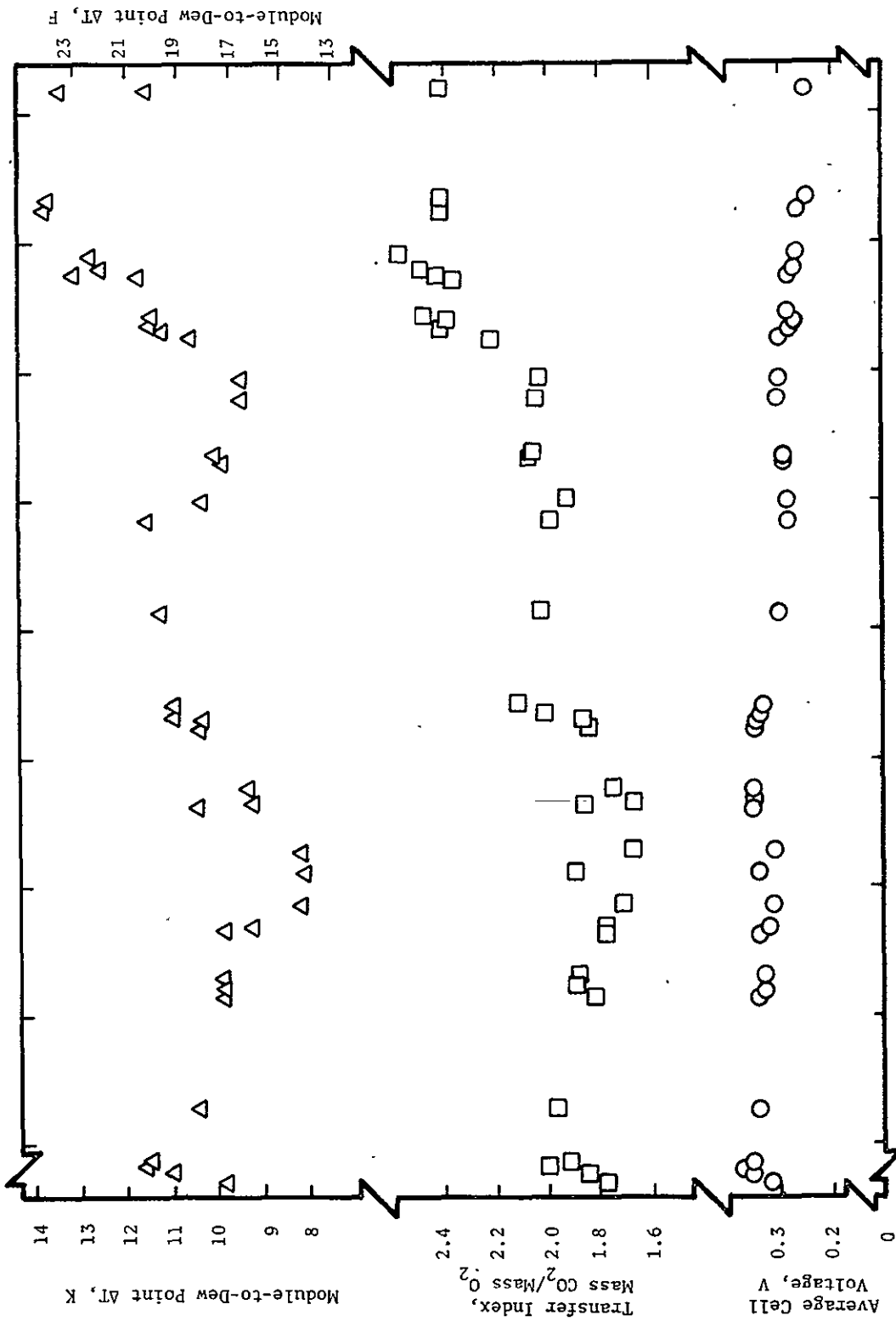

FIGURE 12 PERFORMANCE CHARACTERIZATION AT ELEVATED HYDROGEN BACKPRESSURE FOR CHANGES IN MODULE-TO-DEW POINT ΔT

without H_2 backpressure. Based on the results, i.e., a maximum ΔT range of 8.8 to 13K (14 to 24F), a baseline ΔT of 10.5K (19F) was adopted for SSP operation.

ADVANCED EDC MODULE DEVELOPMENT

Based on the results of the Technology Advancement Studies, projected needs for spacecraft air revitalization and past EDC developments, an Advanced EDC Module (AEDCM) was designed, fabricated, assembled and tested. The new generation design was based on the philosophy that:

1. The number of cells per module and the active electrode area per cell should be increased above that of previous modules to allow for multi-man scale-up without excessive increases in the number of modules

2. The cell design should allow either internal air or liquid cooling for decreased thermal gradients and increased application flexibility

3. The design should allow for variable electrode-matrix-electrode thickness ratios to increase humidity tolerance

4. The module should be designed for low weight, volume and process air pressure drop without sacrificing electrical or CO_2 removal efficiencies

Module Design Considerations

Prior to the detailed design of the AEDCM, the capacity of the module was selected, the heat and mass balances were calculated and major areas of potential weight and volume reductions (based on previous cell and module hardware) were identified.

Module Size

The module was sized to remove the CO_2 generated by a crew of four using a nominal metabolic CO_2 generation rate of 1 kg/man-day (2.2 lb/man-day). The module was to remove the required CO_2 from a cabin atmosphere having a pCO_2 of 400 N/m^2 (3.0 mm Hg) or less.

A four-man capacity size was selected to (1) demonstrate the advanced design concept of the multi-man level, but still limit hardware costs and (2) relate module size to possible flight applications, such as the Shuttle Orbiter.

Heat and Mass Balance

The AEDCM must interface with cabin air, the spacecraft liquid coolant source (liquid-cooled module only), the O_2 Generating Subsystem or on-board H_2 source (the H_2 anode gas source) and the CO_2 Reduction Subsystem or overboard vent.

The vehicle cabin atmosphere data for the module design was selected based on a nominal range in cabin temperature, humidity and pCO_2 while the flow rates were based on a nominal metabolic CO_2 generation rate of 1.0 kg/man-day (2.2 lb/man-day) (see Table 4). The design cell voltage was 0.4V/cell while the design CO_2

TABLE 4 AEDCM DESIGN SPECIFICATIONS

Crew Data	
Number of Crew	4
CO_2 Generation, kg/day (Lb/Day)	
Per Man	1.0 (2.20)
Total	4.0 (8.80)
Cabin Atmosphere Data	
Operational Gravity	0-1G
Total Pressure, kN/m^2 (Psia)	101.3 ±1.4 (14.7 ±0.2)
O_2 Partial Pressure, kN/m^2 (Psia)	22.0 (3.2)
Diluent	N_2
Temperature, K (F)	291 to 297 (65 to 75)
Humidity	
Dew Point Range, K (F)	281 to 289 (46 to 57)
RH Range, %	35 to 90
CO_2 Partial Pressure, N/m^2 (mm Hg)	373 to 400 (2.8 to 3.0)

removal efficiency was 91% (TI = 2.5) resulting in a consumption of 0.39 kg/man-day (0.87 lb/man-day) of O_2.

Figure 13 shows the heat and mass balance for the four-man capacity AEDCM at baseline operating conditions and for the above design parameters.

Weight and Volume Optimization

The most dominant weight contributors in previous EDC module designs were the anode current collectors with external cooling fin extensions and the module endplates, comprising 61.5% of the total cell weight and 23.4% of the total module (one-man capacity) weight, respectively.[4] Also, internal process air manifolding contributed significantly to module weight.

A design study was completed to evaluate techniques to reduce the weight of these components and cell and module weights in general, based on a total-weight-to-active-electrode-area ratio.

Anode Current Collectors. Selection of internal cooling (either liquid or air) eliminated the need for thick metallic heat conduction paths from the cell interior to the externally air-cooled fins. This function was previously provided by the anode current collectors. By sizing the anode current collectors to satisfy only the electrical conduction requirement, a sufficiently thin metallic layer resulted to allow electroplating the collector directly onto the anode cavity surface of the polysulfone cell frame. Following a feasibility study of electroplating polysulfone, including sample evaluations, the technique was selected for the AEDCM design.

By combining the anode current collector and the cell frame into a single electroplated polysulfone component, the projected cell weight and volume reduction was 66% and 34% per unit active cell area respectively. Combining these two cell parts also eliminated the anode compartment (H_2) seals, increasing the cell's reliability and safety aspects.

Greater dimensional stability was also possible by allowing the current collecting surface, electrode support surface and matrix sealing surface within a single molded part on the same side of the mold separation plane, thus eliminating effects of mold half misalignment during the injection molding process.

Endplate Size Versus Cell Area. Elimination of the anode current collectors as a major cell weight contributor leaves the endplates as the single most predominant weight factor in the AEDCM. The endplate construction is important to insure uniform current collector contact and electrode-matrix compression.

The total electrode area required within a module is determined by the CO_2 removal requirements and the operating conditions and interfaces. The number of individual areas or cells into which the total area requirement is divided is, to a large degree, based on a trade between cell weight versus endplate weight. At a high number of cells per module, the cell weight dominates (larger frame area per electrode area) while, at a low number of cells, the endplate weight becomes more significant, since endplate weight and thickness (volume) is a direct function of the electrode area per cell.

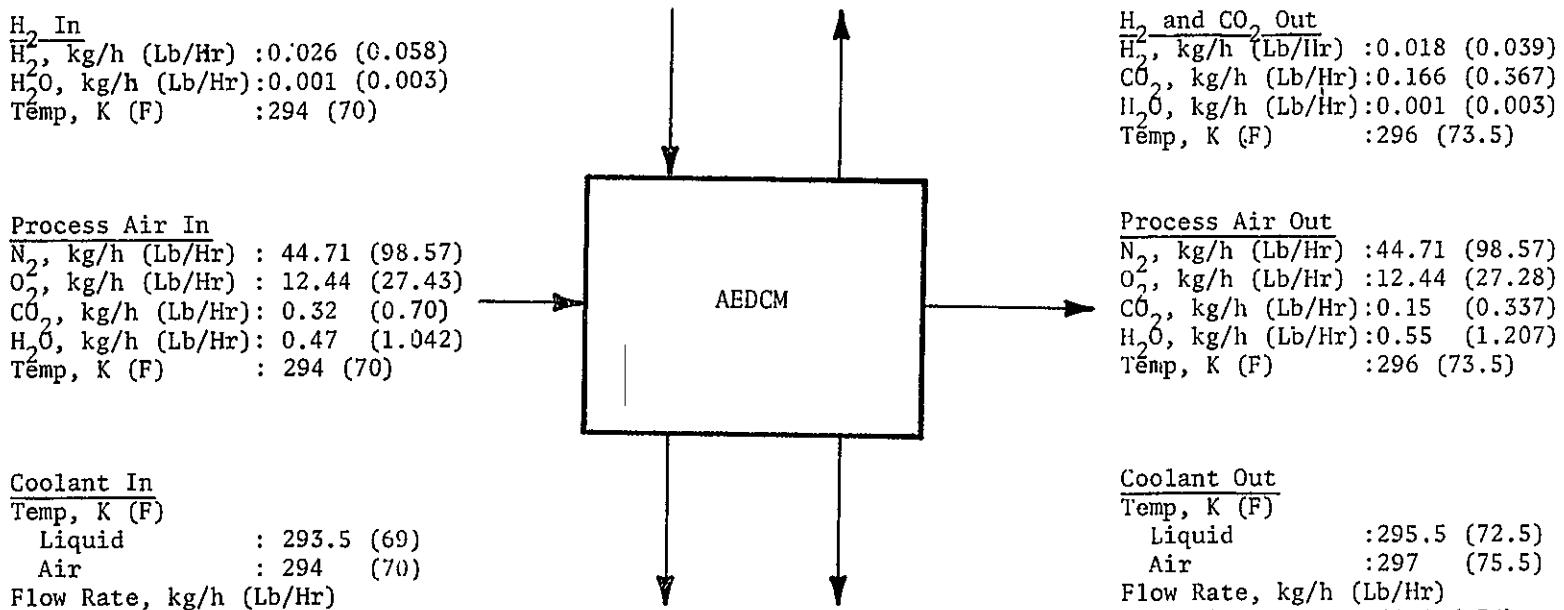

FIGURE 13 AEDCM HEAT AND MASS BALANCE

Practical limitations such as the maximum number of cells that can be successfully stacked between two endplates for a large number of small cells, as well as the value of the electrical current that must be conducted between and to the cells for a low number of large cells, may become governing in cell area selection.

Prior to the final design of the AEDCM, a decision was made to construct the advanced cells from a multiple of the baseline electrode size 0.023 m^2 (0.244 ft^2)) used previously by the Contractor in the one-man and the two six-man CO_2 Removal Subsystems, as well as in a majority of the supporting technology experiments.[3,4,5] This decision was based on a desire to retain proven and established electrode technology and performance for the AEDCM. Figure 14 shows the possible arrangements and overall cell dimensions using standard electrodes and a projected frame width of 1.27 cm (0.50 in).

Based on the analysis performed, two standard electrodes per advanced cell frame proved the best choice for a four- to six-man capacity module.

Module Fluid Manifolding. External manifolding of the process air and/or cooling air eliminates the cell frame and endplate weights and volumes necessary to enclose and seal an internal manifold. Also, internal manifolding makes the AEDCM "process air line replaceable." Figure 15 illustrates the proposed module air manifolding for both air- and liquid-cooled designs.

In contrast to the air manifolding, the liquid coolant (water) and H_2 were retained as internally manifolded to ensure positive sealing with a minimum in module weight and volume penalty. The relatively small liquid coolant and H_2 volumetric flow rates require only small internal manifold cavities and the associated cell framing for the manifold enclosure has only minimal impact on module weight and volume.

Internal Cooling. Internal air- and liquid-cooling had been selected for the AEDCM cell design based on the following advantages:

1. Elimination of large internal temperature gradients

2. Elimination of separate anode current collector/fins

3. Allowance for an internal cell temperature control above and below the process air temperature (liquid-cooled only), thus increasing the humidity operating range and allowing for precise moisture balance control

4. Provisions for better heat removal capacity for cell operation at higher current densities

Internal cooling, however, causes a slight penalty in the number of cells which can be stacked per inch of module. Previous EDC module cells could be stacked at 3.22 cells per inch compared to 2.66 per inch for the AEDCM. However, the larger electrode area per cell and reduced module volume due to the elimination of the cooling current collector fins and internal air manifolding more than offset the apparent volume penalty. A net cell volume reduction per active electrode area of 35% was projected.

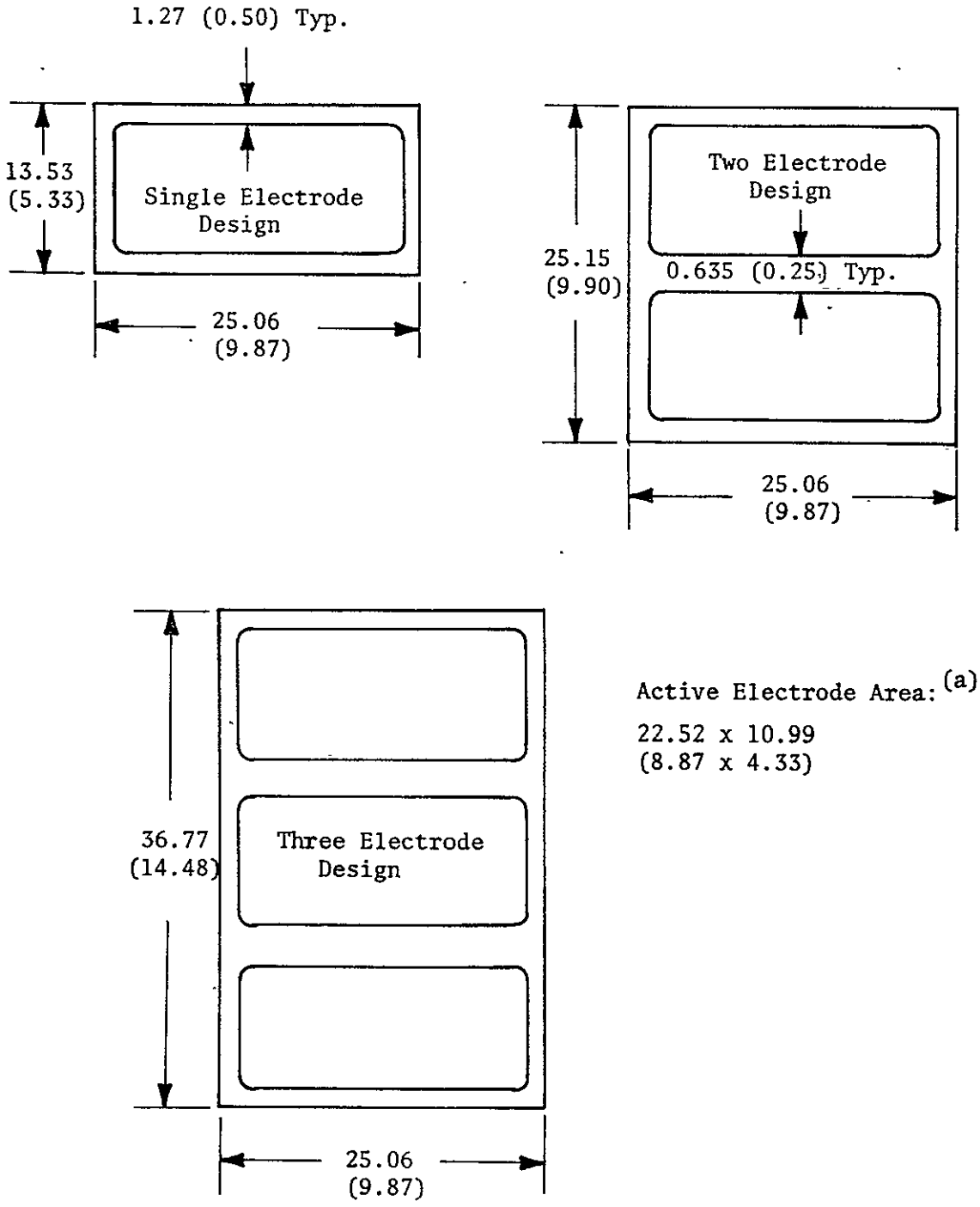

(a) All dimensions in cm (In)

FIGURE 14 PARALLEL STACKUP OF EDCM ELECTRODE AREAS

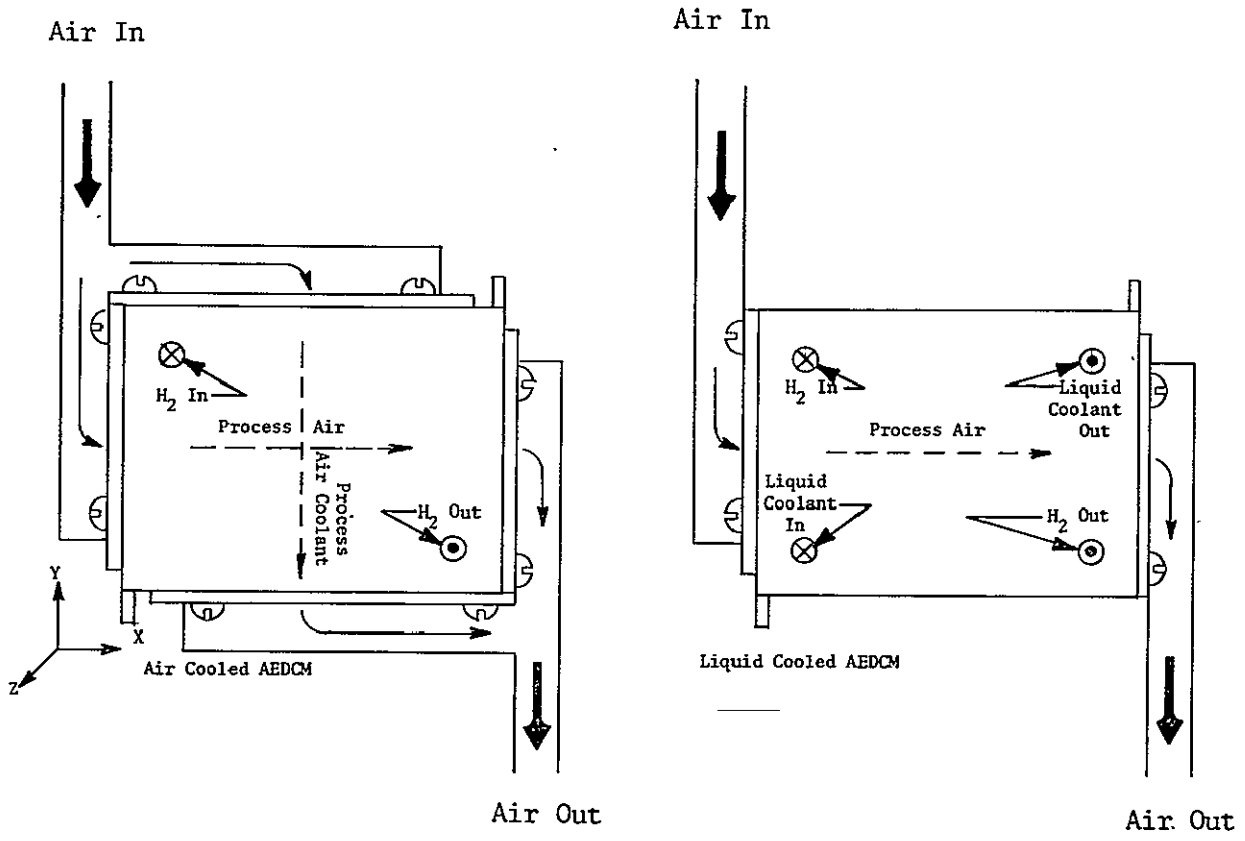

FIGURE 15 EXTERNAL AIR MANIFOLDING FOR THE AEDCM

Basic Cell Configuration

The basic cell configuration used for the AEDCM design was similar to that used in previous EDC cells. Figure 16 is a functional cell schematic showing this configuration and the fluid and electrical interfaces.

Basic Module Configuration

The previous module baseline configuration was retained. Cells are stacked between two sets of parallel insulation and structural endplates. Process air and coolant (liquid or air) flow through all cells in parallel. Hydrogen flows in series through all cells of a module. All cells are electrically connected in series and are "in situ" maintainable.(4)

Cell Part Fabrication

Each cell of the AEDCM consists of four assemblies. They are the cathode current collector assembly, the cathode frame assembly, the cell matrix assembly, and the cell housing assembly. Figure 17 shows the first three assemblies as well as the individual parts that make up the cell housing assembly.

The cathode current collector assembly is fabricated from 0.051 cm (0.020 in) thick nickel sheet to which cooling fins and two expanded metal (Exmet) cathode compartment spacers are attached. The cooling fins are formed by a ribbed, or corrugated, nickel sheet brazed to the flat collector plate. This creates a series of individual slots and fins through which the cooling air or liquid coolant flows to remove the waste heat generated by the electrochemical reaction. The two Exmet spacers are spot-welded to the opposite (from the cooling fins) side of the current collector sheet to form the two individual parallel cathode compartments of each single cell. The current collector assembly, therefore, combines the functions of creating the cathode compartment, providing for waste heat removal and distributing the current across the cathode areas.

The cathode frame assembly consists of an injection-molded polysulfone compression frame with two rectangular openings for the two 0.023 m^2 (0.244 ft^2) electrodes (cathodes). The electrodes are heat-bonded to the frame to form the assembly.

The cell matrix assembly is fabricated from chrysotile white asbestos. The matrix is one single piece extending over both active area sections of each individual cell.

The cell housing assembly consists of an injection-molded polysulfone cell frame with integral anode current collectors plated onto the polysulfone in the region of the active cell areas. To form the total housing assembly, two 0.102 cm (0.040 in) thick expanded nickel spacers are first placed onto the plated metallic surfaces of the cell frame. Two anode electrodes are subsequently heat-sealed to the frame to retain, or capture, the expanded metal spacers and to form the anode compartment. The plated-on anode current collectors consist of an initial layer of electroless nickel plate, followed by a layer of electroplated silver. A flash of gold plating is then applied to the silver surface. Electrical access to the plated current collectors is achieved through nickel tabs molded into the cell frame during the time of the injection molding process.

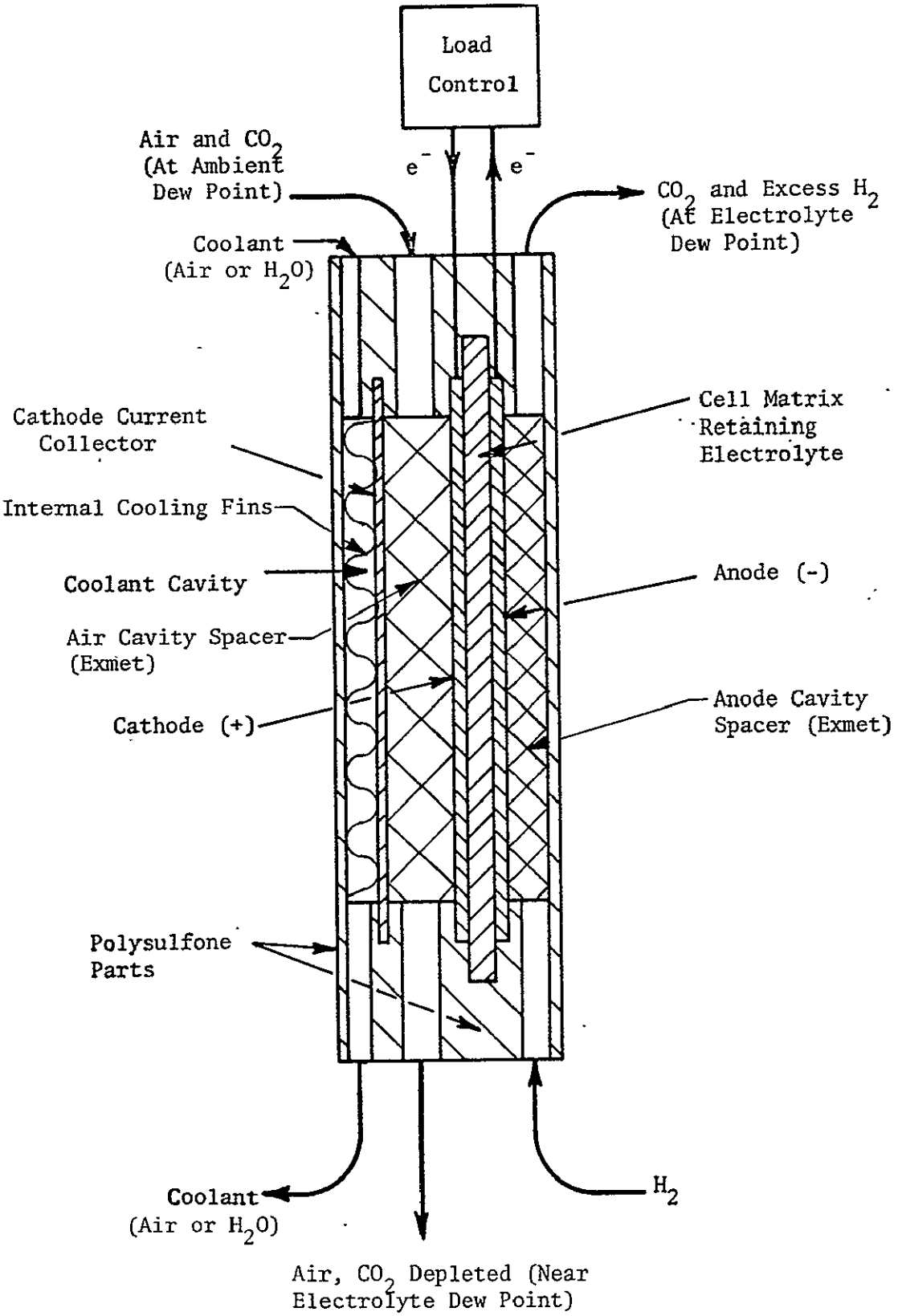

FIGURE 16 SINGLE-CELL SCHEMATIC

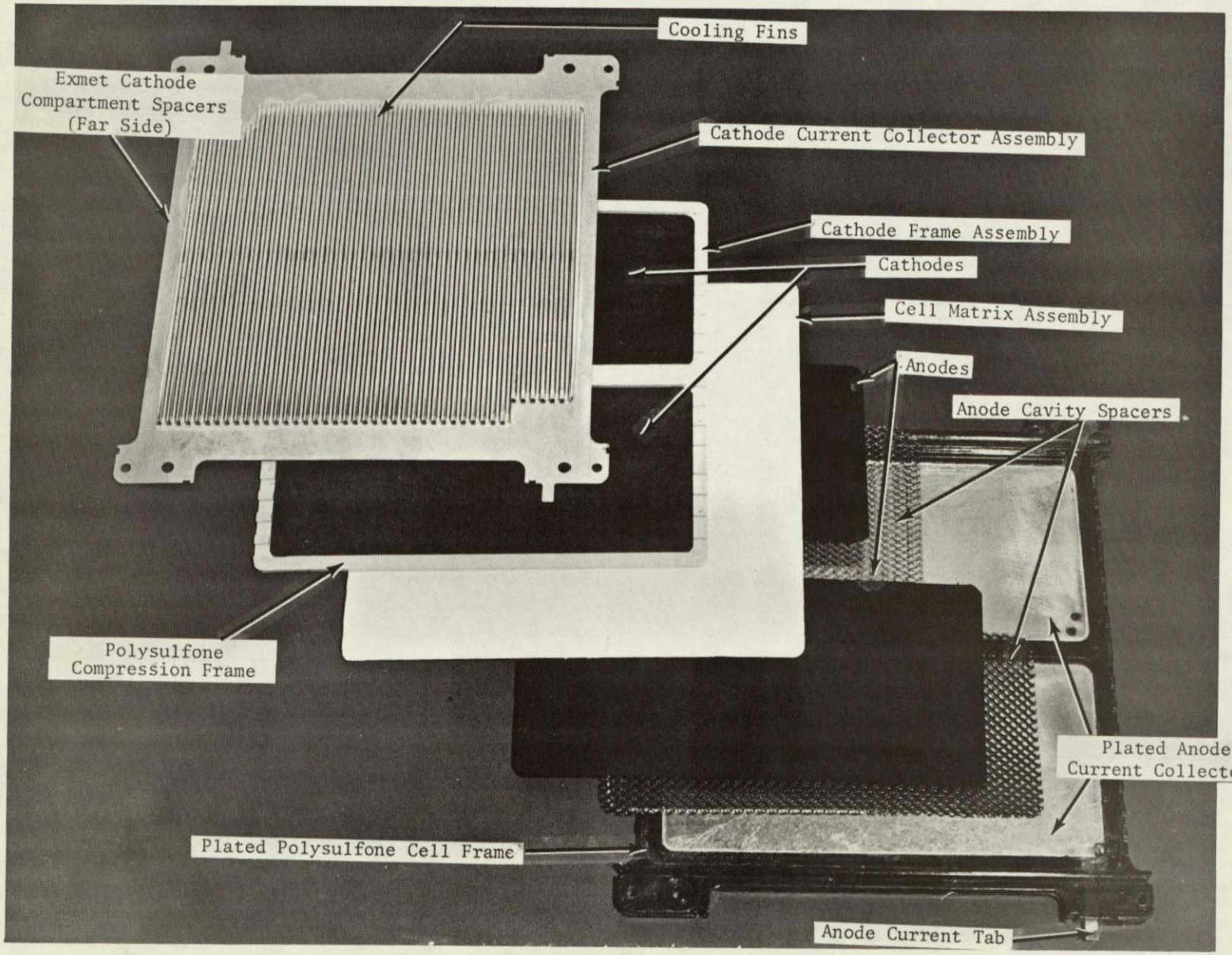

FIGURE 17 AEDCM CELL PARTS AND ASSEMBLIES

Manifolding, internal to each cell frame, provides for series H_2 flow for the two active cell areas of each individual cell. Each cell housing assembly provides a cooling cavity for the cooling fins of an adjacent cell in a module. This cooling cavity may either be configured for air cooling or liquid cooling, depending on mold inserts used during the injection molding process of the polysulfone cell frame. Figures 18 and 19 show the front and back views of plated, injection-molded cell frames for internal air cooling and liquid cooling, respectively.

To assemble a single cell or a multi-cell module requires, in addition to the cell parts discussed above, two insulation plates and two structural endplates. Figure 20 shows single cell parts and assemblies, together with two insulation plates and two structural endplates. Each single or multiple cell stack is retained by 14 tension bolts. Intercell sealing for the H_2 passages and liquid coolant passages is accomplished by O-rings. Sealing of the process air or of the internal cooling air compartments from ambient is achieved by using straight pieces of circular cross section, O-ring material.

Volume and Weight Reductions Demonstrated

A cell and module weight and volume comparison was made between the CS-6 style hardware and the AEDCM hardware.

Cell Level Comparison

Combining the cell housing and anode current collector into one single part accounts for the majority of the cell weight reduction, while the increase in active electrode surface area from 0.023 to 0.045 m^2 (0.244 to 0.488 ft^2) accounts for the majority of the cell volume reduction. Table 5 compares the CS-6 type EDCM to the AEDCM cell weights and volumes. As shown in the table, the total cell weight was decreased from 1064 to 560 g (2.34 to 1.12 lb) per standard (equal) electrode area, a decrease of 52%. Similarly, the AEDCM cell yields a volume reduction from 545 to 401 cm^3 (33 to 24.5 in^3), or 26%.

Module Level Comparison

The AEDCM was designed to operate at a current density of 30.13 mA/cm^2 (28 ASF). A 20-cell module is therefore sufficient to remove the CO_2 generated by four men. A four-man capacity EDC, using CS-6 style modules, would require four 16-cell modules. Table 6 is a comparison of the CS-6 style and AEDCM module weights and volumes for a four-man capacity system. The major weight savings for the AEDCM at the four-man system level are due to the weight savings at the individual cell level, the increased capacity of the AEDCM to operate at the 30.1 mA/cm^2 (28 ASF) instead of the 21.5 mA/cm^2 (20 ASF) level (37.5% area reduction), and the decrease in the number of endplates required. The latter is a direct result of the increase in active area per cell and the increase in number of cells per module. As shown in the table, the four-man module weight is decreased from 116 to 42 kg (256 to 92 lb), or a 64% decrease, while the four-man module volume shows a decrease from 0.0472 to 0.0201 m^3 (1.67 to 0.71 ft^3), or 57%.

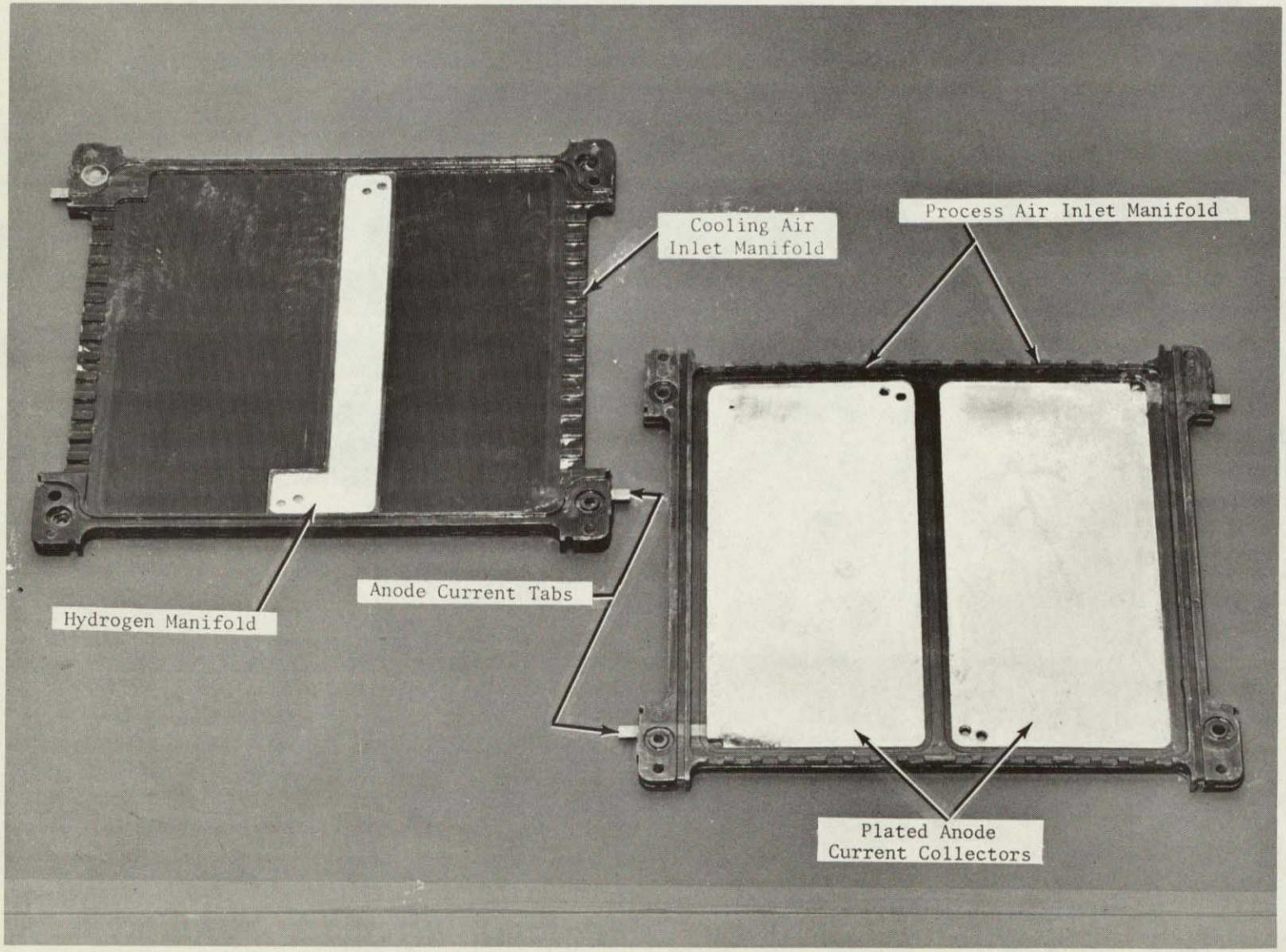

FIGURE 18 INJECTION MOLDED CELL FRAME FOR INTERNAL AIR COOLING

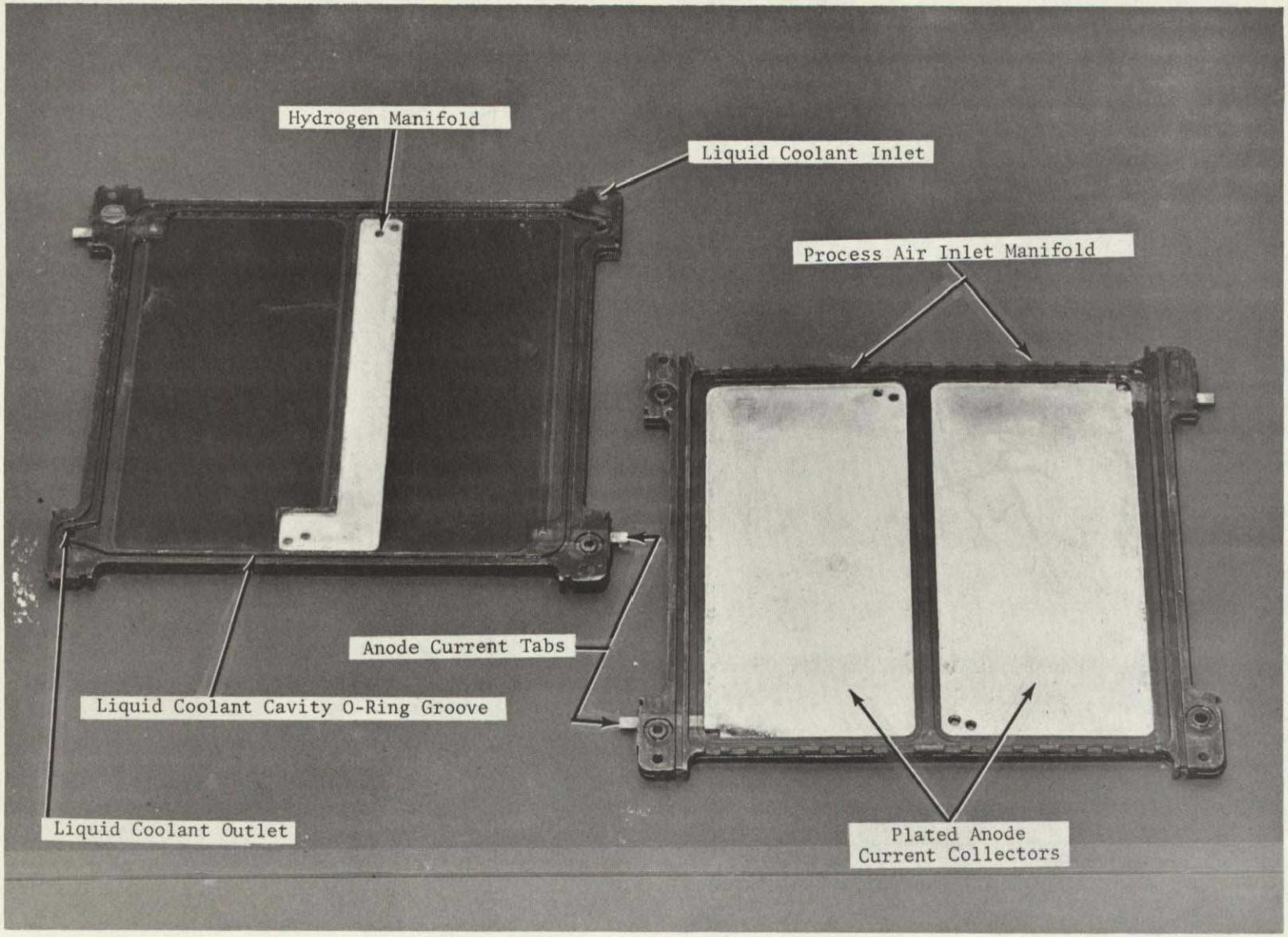

FIGURE 19 INJECTION MOLDED CELL FRAME FOR LIQUID COOLING

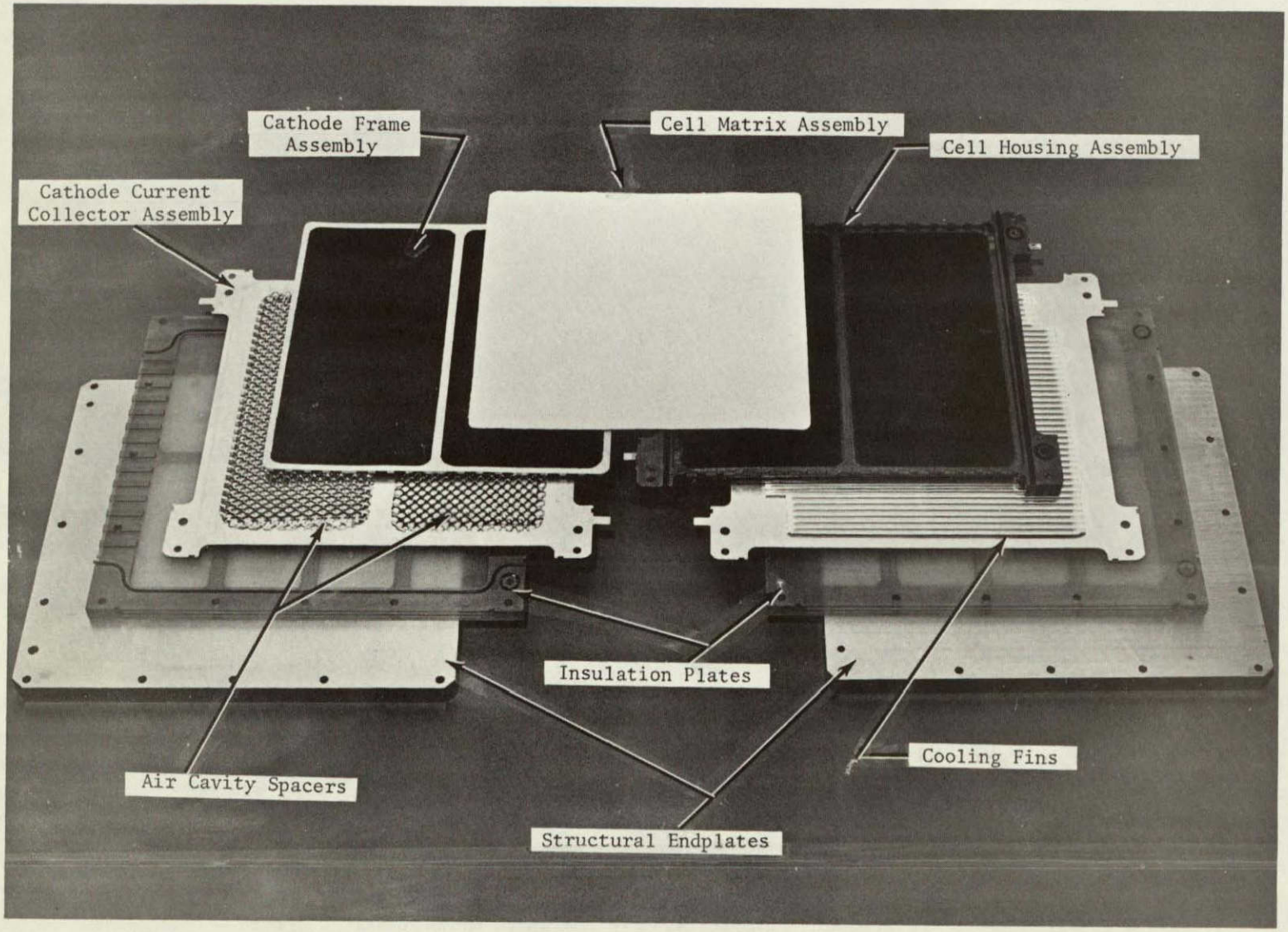

FIGURE 20 AEDCM SINGLE CELL WITH ENDPLATES

TABLE 5 COMPARISON OF EDCM AND AEDCM CELL DESIGNS

	EDCM (CS-6)	AEDCM
Active Electrode Area, cm^2 (In^2)	226.5 (35.1)	452.9 (70.2)
Cell Frame Weight, g (Lb)	84.0 (0.18)	301.0 (0.66)
Current Collector Weight, g (Lb)		
Anode	654.0 (1.44)	56.0 (0.12)
Cathode	146.0 (0.32)	311.0 (0.69)
Misc. Cell Parts, g (Lb)	180.0 (0.40)	352.0 (0.78)
Complete Cell		
Weight, g (Lb)	1064.0 (2.34)	1020.0 (2.25)
Overall Dimensions, cm (In)	0.79 x 34.93 x 19.76 (0.31 x 13.75 x 7.78)	1.09 x 28.35 x 25.96 (0.43 x 11.16 x 10.22)
Volume, cm^3 (In^3)	545.27 (33.16)	802.20 (48.95)
Weight per Active Electrode Area, g/cm^2 (Lb/In^2)	4.70 (0.07)	2.25 (0.03)
Volume per Active Electrode Area, cm^3/cm^2 (In^3/In^2)	2.41 (0.95)	1.77 (0.70)
Percent Reduction (Based on Active Electrode Area)		
Weight	-	52%
Volume	-	26%

TABLE 6 COMPARISON OF EDCM AND AEDCM FOUR-MAN MODULES

	EDCM	AEDCM
Number of Modules Required	4	1
Number of Cells per Module	16	20
Cell Weight per Module, kg (Lb)	17.00 (37.44)	20.43 (45.00)
Total Weight per Module, kg (Lb)	29.6 (64.00)	41.88 (92.24)
Total Four-Man Weight, kg (Lb)	116.22 (256.00)	41.88 (92.24)
Weight Reduction, %	-	64
Overall Dimensions per Module, cm (In)	15.77 x 21.44 x 34.93 (6.21 x 8.43 x 13.75)	27.31 x 25.96 x 28.35 (10.75 x 10.22 x 11.16)
Volume per Module, m^3 (Ft^3)	0.0118 (0.42)	0.0201 (0.71)
Total Four-Man Volume, m^3 (Ft^3)	0.0472 (1.67)	0.0201 (0.71)
Volume Reduction, %	-	57

Figure 21 is a photograph of an assembled air-cooled AEDCM. The module shown in Figure 21 is sized for a four-man CO_2 removal capacity, but has 21 cells compared to the 20-cell design value. The additional cell was added for performance derating during initial module testing.

Advanced Cell and Module Testing

The advanced cell and module test program consisted of (1) establishing a cell and module electrolyte charging procedure, (2) single cell functional testing, and (3) AEDCM parametric testing. A total of 871 hours of operation were accumulated with the four-man capacity module. As part of the test program, a comparison between CS-6 style cell performance and AEDCM cell performance was performed.

Electrolyte Charging Procedures

The advanced module design required a change in the procedures employed previously to charge the matrices of the EDC cells with electrolyte. The CS-6 style modules were assembled dry, subsequently evacuated and filled with electrolyte for matrix and electrode soaking. Since the advanced module does not have a closed process air manifold, this method is not applicable. However, the importance of vacuum charging of the electrodes and matrices, compressed to their operating thickness, is of utmost importance for proper electrolyte volume retention in each individual cell.

An electrolyte charging technique was developed for the advanced module using a specially constructed charging fixture fabricated from plexiglass. A cell assembly, consisting of its cell housing, cell matrix and cathode frame assemblies, is placed in the fixture. The charging fixture is sealed and evacuated, causing proper compression to be applied to the cell. The whole interior cavity of the charging fixture is then vacuum-filled with electrolyte. The electrolyte is drained from the fixture, excess electrolyte is removed from the cell parts and the cell is sealed in plastic, ready for subsequent assembly into a module.

The fixture is equipped with fluid taps to allow for in situ ΔP checking of each individual cell while located within the charging fixture.

Single-Cell Functional Testing

An advanced single cell was charged with electrolyte and assembled for testing. As part of the charging procedure, the single cell was successfully pressure checked to >34.5 kN/m^2 (>5.0 psig) above ambient for leaks between the anode and cathode compartment. The cell was installed into a single-cell test stand and operated at CS-6 baseline conditions.

For the baseline process air flow rate of 34 dm^3/min (1.2 scfm), the pressure drop through the cathode compartment was less than 125 N/m^2 (0.5 in of water). At equivalent air flows the CS-6 style modules exhibited a pressure drop of 872 N/m^2 (3.5 in of water). This resulted in a 86% reduction in cathode compartment air pressure drop.

Once process gases were supplied to the cell, an open circuit voltage of 1.15V was observed. At 21.5 mA/cm^2 (20 ASF), the transfer efficiency of the cell was 80% or a TI of 2.2. The cell voltage at 21.5 mA/cm^2 (20 ASF) was 0.38V.

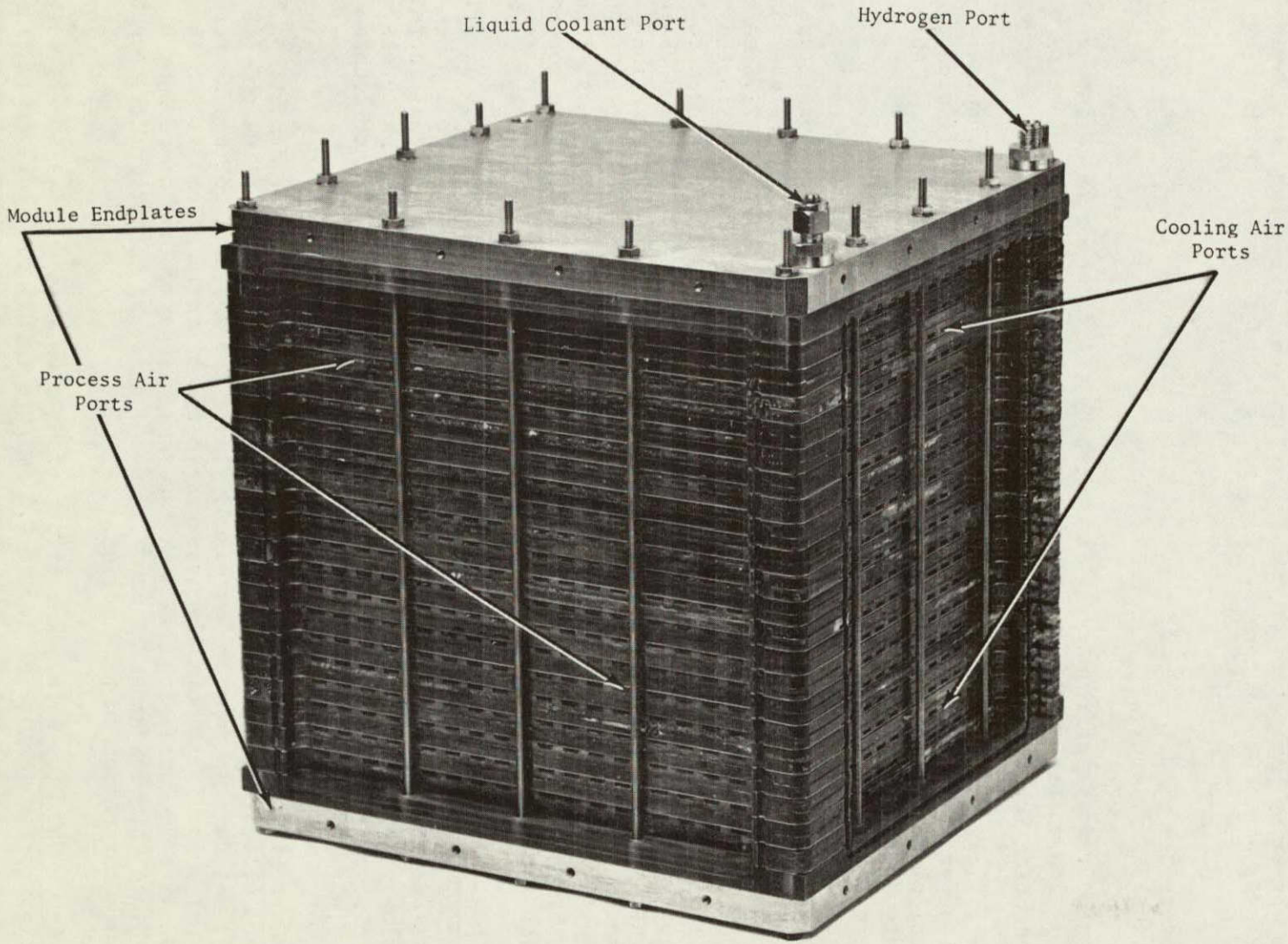

FIGURE 21 FOUR-MAN AEDCM

AEDCM Parametric Testing

Parametric testing was performed to characterize the effects of variations in the system operating parameters on module performance. The parameters varied include process air pCO_2, process air flow rate, current density and H_2 flow rate.

Two parameters are used to describe EDC module performance, CO_2 removal efficiency and electrical efficiency.

Carbon dioxide removal efficiency is reflected by the TI which is defined as the mass of CO_2 removed per mass of O_2 transferred. Based on the stoichiometry of the $CO_3^=$ reaction involved, the theoretical TI is 2.75.

Electrical efficiency is reflected by cell voltage. Since an EDC produces electrical power, a high cell voltage indicates a high electrical efficiency. The theoretical voltage for the electrochemical process is 1.23 volts. Table 7 is a summary of the parametric performance curves.

Effect of pCO_2. Figure 22 shows the effect of pCO_2 for a range of 0 to 1346 N/m^2 (0 to 10.1 mm Hg) on TI and average cell voltage. The effects on TI are shown for current density levels of 10.8, 21.5 and 40.9 mA/cm^2 (10, 20 and 38 ASF) while the effects on voltage are shown for a current density of 21.5 mA/cm^2 (20 ASF) only. Transfer index increased quickly with increasing pCO_2 in the diffusion limited pCO_2 range (0 to 400 N/m^2 (0 to 3 mm Hg)) and continued to increase less sharply in the remaining reaction limited range. With increasing current density, the difference between mass transfer limiting and reaction limiting mechanisms decreased as reflected by the shallower sloped curves. The figure shows a slight decrease in cell voltage with increasing pCO_2, most likely caused by the change in electrolyte composition (increasing bicarbonate concentration with increasing pCO_2).

Effect of Process Air Flow Rate. Figure 23 shows the effect of process air flow rate on TI for 22 to 47 dm^3/min/cell (0.8 to 1.66 scfm/cell) and over a pCO_2 range of 151 to 1346 N/m^2 (1.13 to 10.1 mm Hg). The TI shows a gradual increase with air flow rate, more pronounced at lower pCO_2 levels than at high levels. Also, the pCO_2 effect on overall TI level is again indicated. No noticeable effect of air flow rate on cell voltage was observed.

Effect of Current Density. Figure 24 shows the effect of current density on TI and average cell voltage for a current density range from 16 to 41 mA/cm^2 (15 to 38 ASF). As current density increased, TI and average cell voltage decreased. A maximum value for TI is normally observed in the 11 to 16 mA/cm^2 (10 to 15 ASF) region with TI decreasing for both lower and higher values of current density. Since this low range is normally not considered for practical operation, the AEDCM was not tested in this region.

Effect of Anode Gas Flow Rate. The effect of H_2 flow rate on TI and cell voltage was investigated for a range of 1.0 to 4.0 dm^3/min (0.035 to 0.141 scfm). This amount of H_2 is 1.3 to 3.0 times that required by the electrochemical reaction at 21.5 mA/cm^2 (20 ASF). Only a slight increase in TI and cell voltage was observed with increasing H_2 flow rate.

TABLE 7 SUMMARY OF AEDCM PARAMETRIC PERFORMANCE CURVES

Performance Curve	Parameter Varied	Range	Temperature, K (F)	Inlet Dew Pt., K (F)	Pressure	pCO_2, N/m^2 (mm Hg)	Air Flow, dm^3/Min/Cell (Scfm/Cell)	Current Density mA/cm^2 (ASF)
Figure 22	Process Air pCO_2, N/m^2 (mm Hg)	0 to 1346 (0 to 10.1)	294.5 ±0.5 (71 ±1)	286 ±0.5 (55 ±1)	Ambient[a]	Variable	34 (1.2)	10.8 to 40.9 (10 to 38)
Figure 23	Process Air Flow Rate, dm^3/Min/ Cell (Scfm/Cell)	22 to 47 (0.8 to 1.66)	294.5 ±0.5 (71 ±1)	286 ±0.5 (55 ±1)	Ambient	Variable	Variable	21.5 (20)
Figure 24	Current Density, mA/cm^2 (ASF)	15 to 38 (16 to 41)	294.5 ±0.5 (71 ±1)	286 ±0.5 (55 ±1)	Ambient	391 ±8 (2.93 ±0.06)	21 (0.75)	Variable
Figure 25	H_2 Flow Rate, dm^3/Min (Scfm)	1.0 to 4.0 (0.035 to 0.141)	294.5 ±0.5 (71 ±1)	286 ±0.5 (55 ±1)	Ambient	391 ±8 (2.93 ±0.06)	34 (1 2)	21.5 (20)

(a) Ambient pressure = 97.3 to 100 kN/m^2 (730 to 750 mm Hg)

ORIGINAL PAGE IS
OF POOR QUALITY

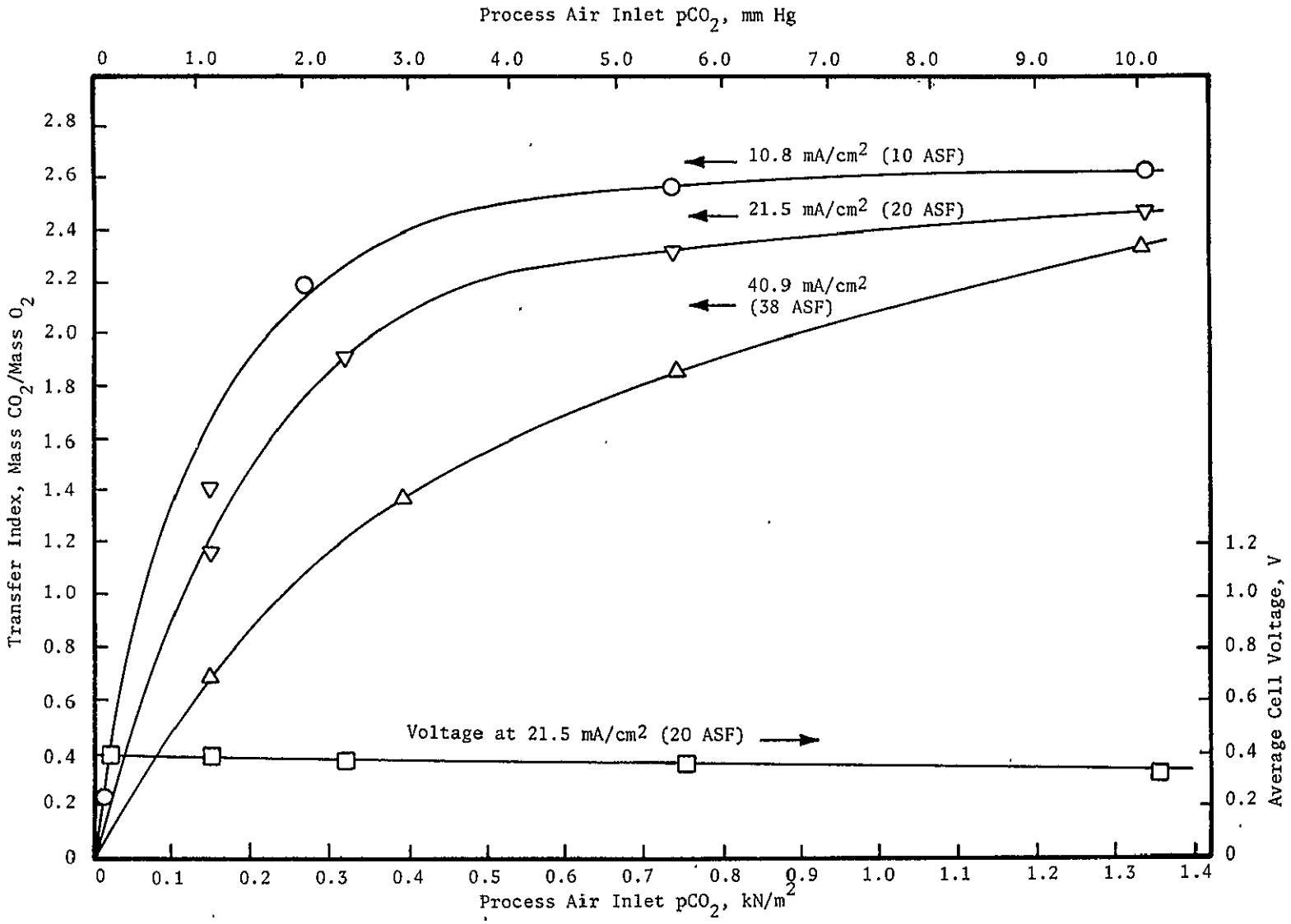

FIGURE 22 AEDCM PERFORMANCE AS A FUNCTION OF PROCESS AIR INLET pCO_2

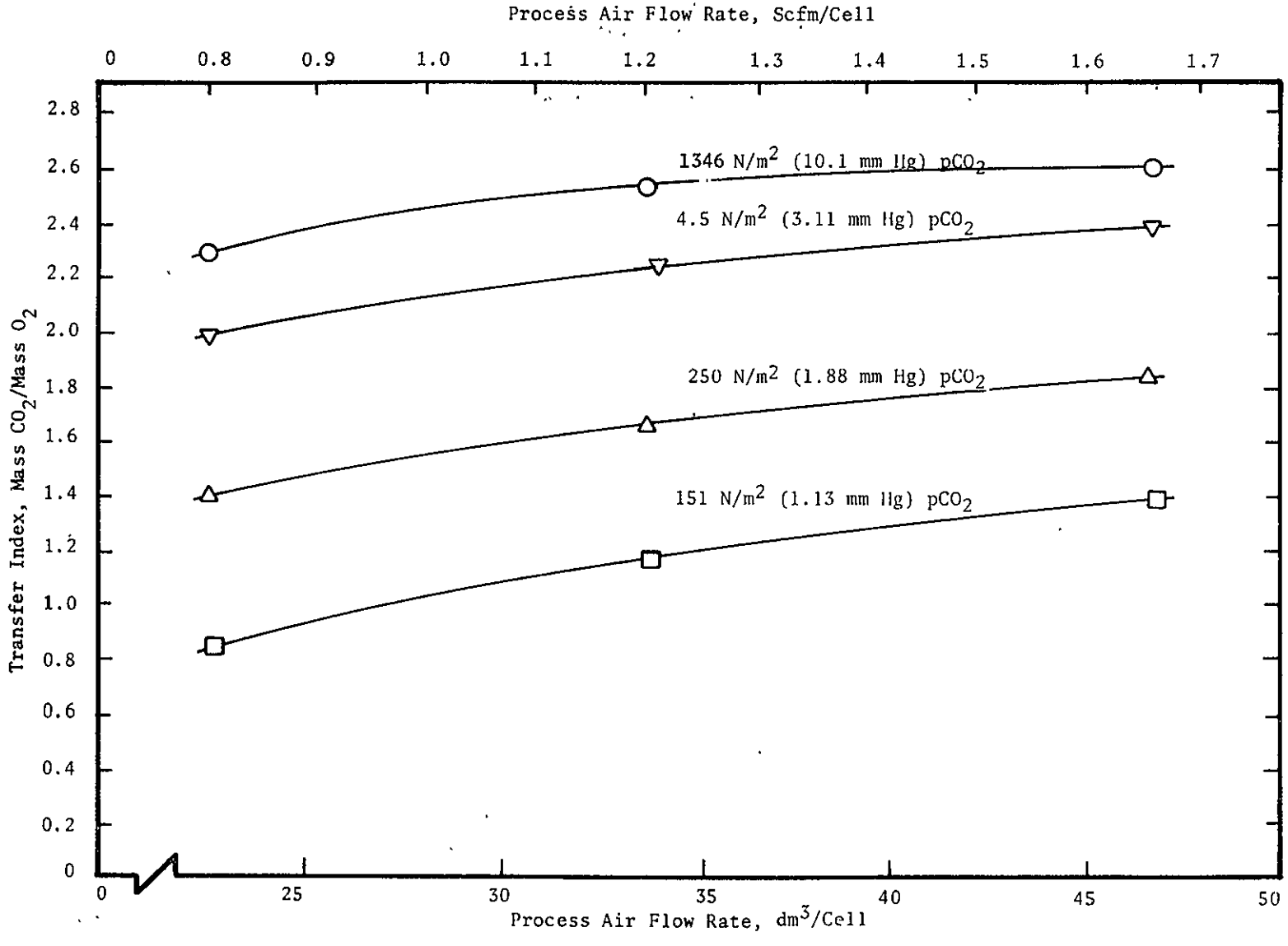

FIGURE 23 AEDCM PERFORMANCE AS A FUNCTION OF PROCESS AIR FLOW

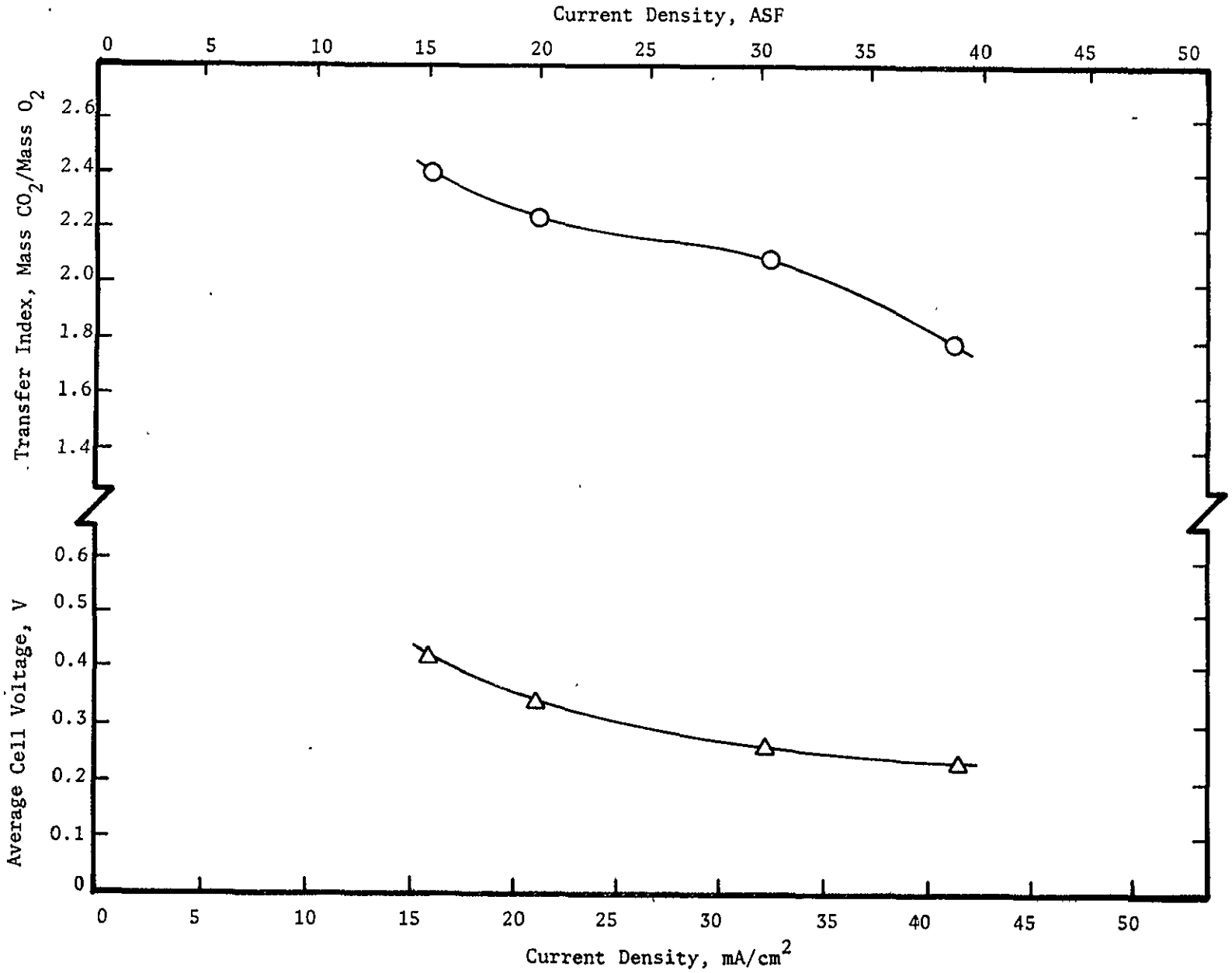

FIGURE 24 AEDCM PERFORMANCE AS A FUNCTION OF CURRENT DENSITY

The effect of anode gas flow rate on pressure drop for the new AEDCM was also investigated. Figure 25 shows the effect of the flow of H_2, only, and a 2:1 H_2 to CO_2 mixture on the anode compartment pressure drop (ΔP). The ΔP increased with the increase in the anode gas flow rate. The H_2/CO_2 mixture exhibited a ΔP approximately 1.15 times that of the pure H_2.

AEDCM/CS-6 Module Performance Comparison

Carbon Dioxide Removal Efficiency. Figure 26 shows the comparison curves for TI as a function of process air pCO_2 for CS-6 modules and the AEDCM. The performances of the two modules are similar, with the AEDCM exhibiting slightly better performance at low pCO_2 levels (0 to 400 N/m^2 (0 to 3 mm Hg)) and the CS-6 style modules exhibiting the slightly better performance at the higher pCO_2 levels.

Cell Voltage. Cell voltage levels, as a function of the major operating parameters, obtained with the AEDCM were within experimental error when compared to the voltages obtained with CS-6 style modules. Figure 27 shows this closeness as a function of current density, the operating parameter which has major impact of EDC cell voltage.

Process Air Pressure Drop. One of the primary AEDCM design objectives was to decrease process air pressure drop without sacrificing CO_2 removal efficiency since blower power requirements are a direct function of pressure drop. The comparable TI levels have been demonstrated in the data presented in Figure 26.

Figure 28 is a comparison of the process air pressure drops as a function of process air flow rate per unit area for the AEDCM and CS-6 style modules. As can be seen, a decrease of an order of magnitude was achieved with the new design. Figure 29 shows the AEDCM process air pressure drop as a function of air flow rate. The AEDCM baseline design air flow rate is also indicated.

Anode Gas Pressure Drop. The reduction in anode gas compartment height and the number of anode gas compartments connected in series (40 versus 16) in the AEDCM as compared to the CS-6 style modules resulted in a tenfold increase in anode gas compartment pressure drop. As was shown in Figure 25, however, this pressure drop is still less than 13 kN/m^2 (2 psid) in absolute value and the increase has negligible effects.

CS-6 COMPONENT NOISE AND WEIGHT REDUCTION STUDIES

In an attempt to reduce the noise and weight levels of the CO_2 Collection Subsystem for SSP application (CS-6), possible reductions in the commonality process air blower noise and in the subsystem module weights were examined.

CS-6 Blower Noise Study

The CS-6 used two of the SSP commonality blowers to circulate the process air through the electrochemical modules. These blowers proved excessively noisy and a study was initiated to investigate the possibility of reducing the blower noise by replacing the SSP blowers with quieter yet equal capacity blowers. The blowers used in the CX-6 were extremely quiet but had not been qualified in accordance with NASA flammability and outgassing specifications.

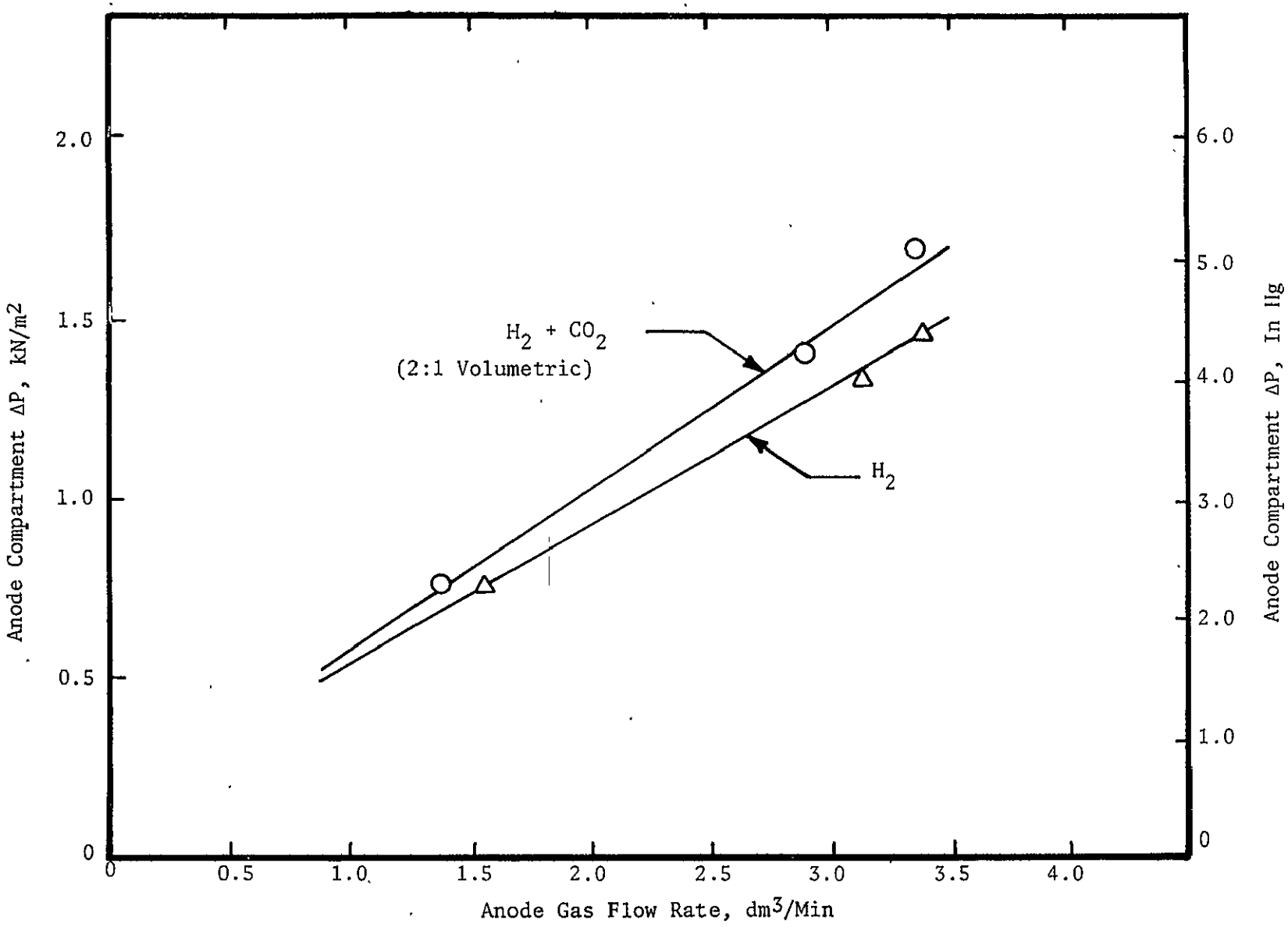

FIGURE 25 AEDCM ANODE COMPARTMENT ΔP AS A FUNCTION OF ANODE GAS FLOW RATE

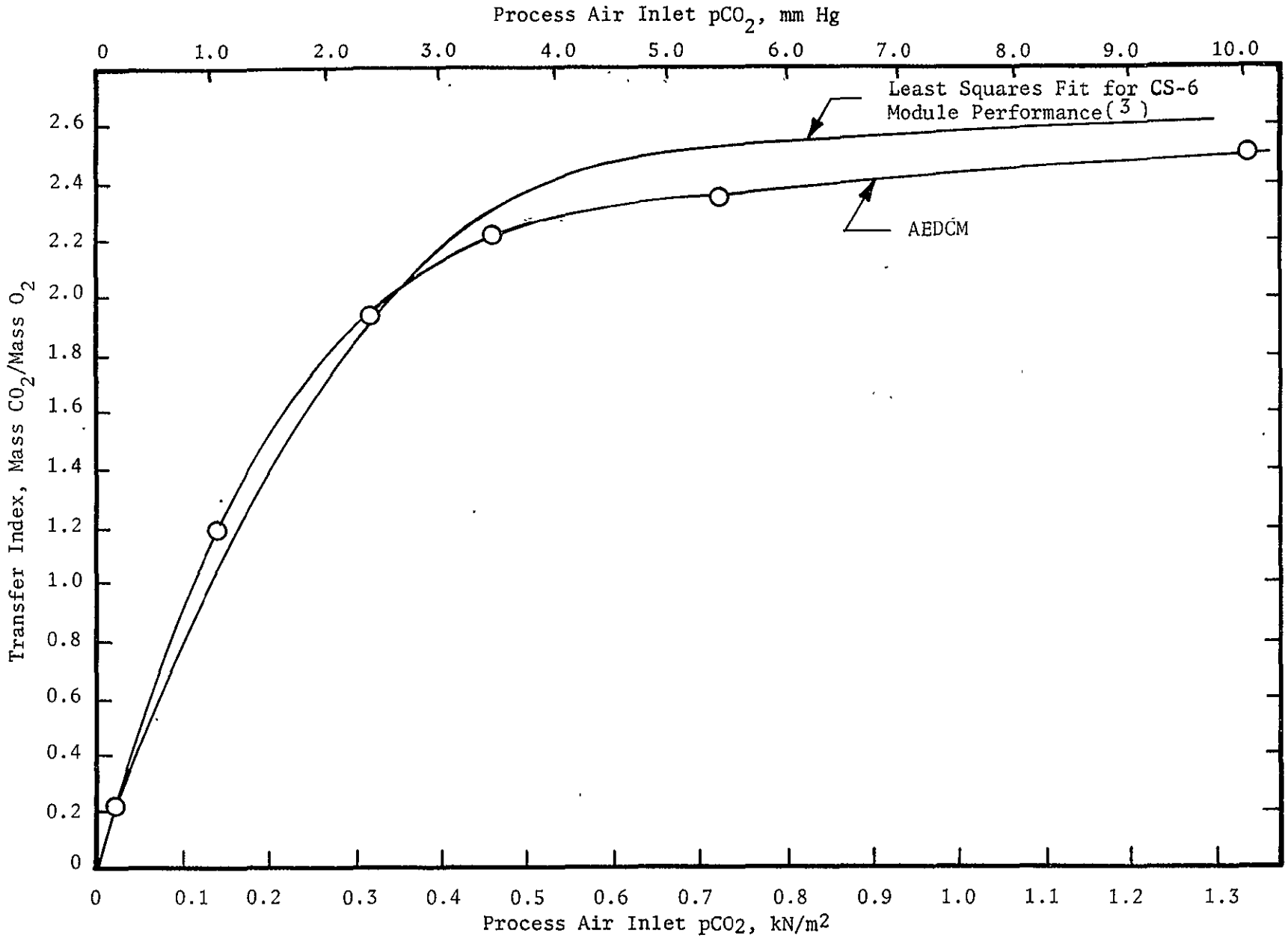

FIGURE 26 AEDCM AND MATH MODEL TI COMPARISON

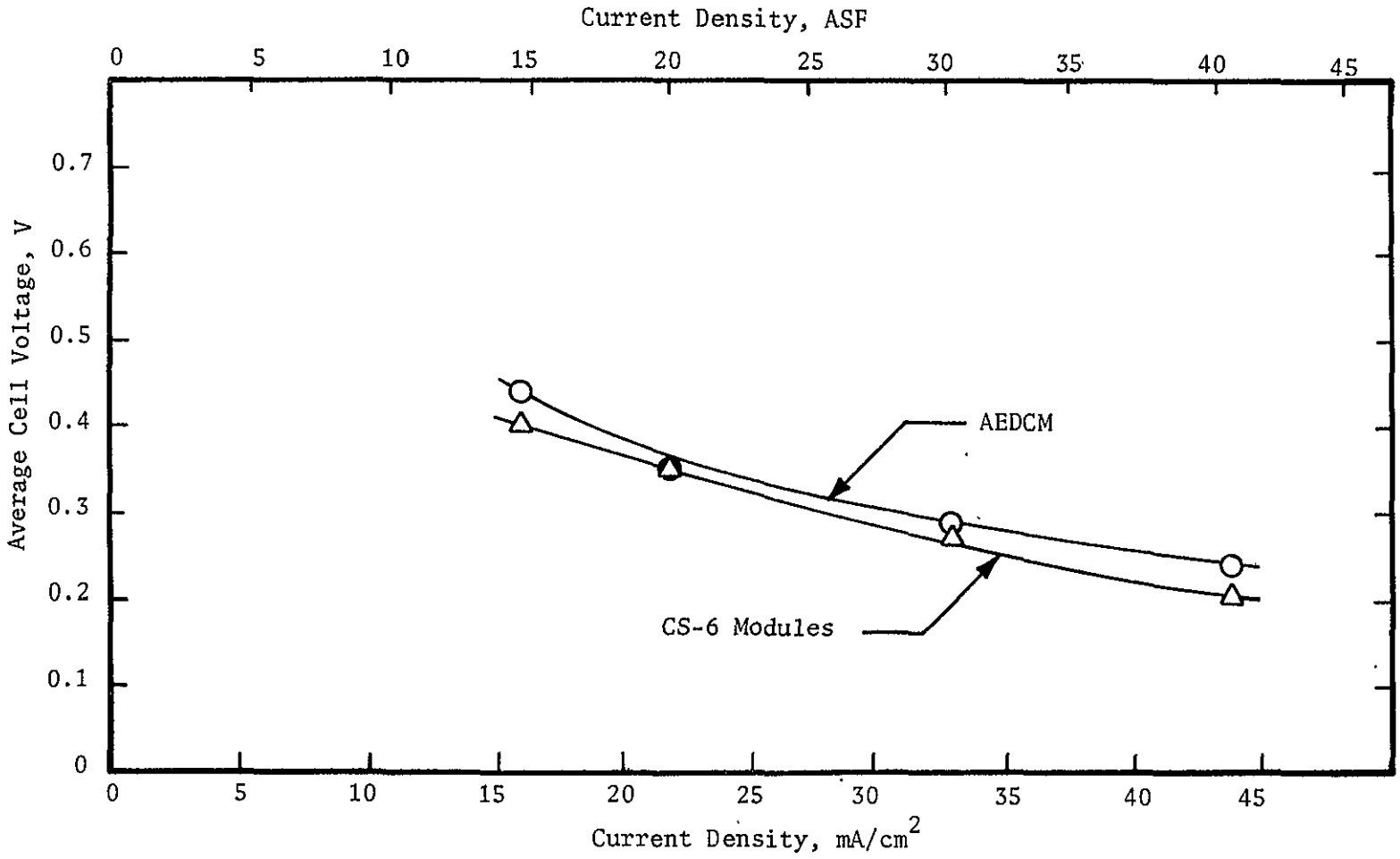

FIGURE 27 AEDCM AND CS-6 VOLTAGE COMPARISON

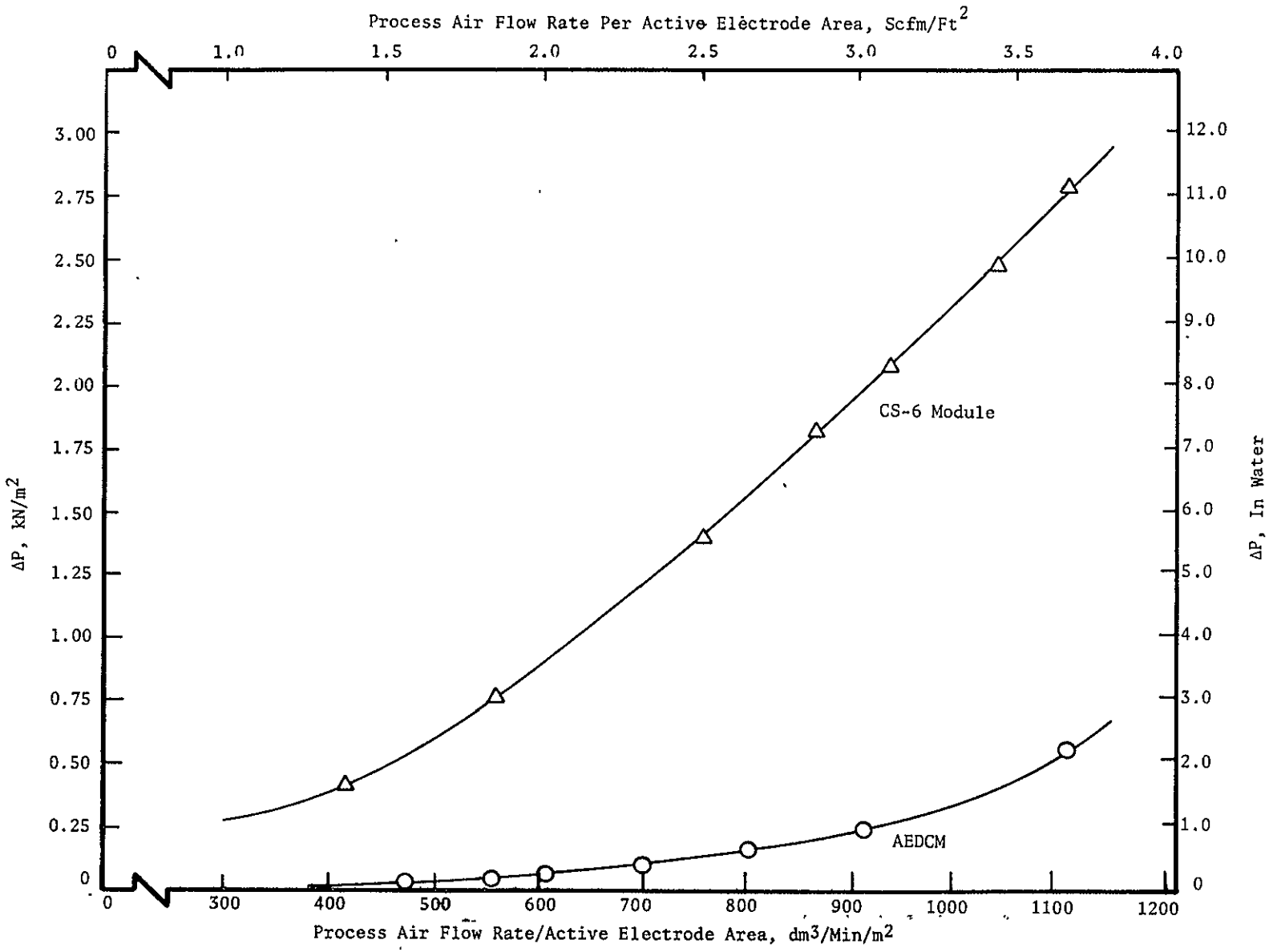

FIGURE 28 AEDCM AND CS-6 PROCESS AIR PRESSURE DROP COMPARISON

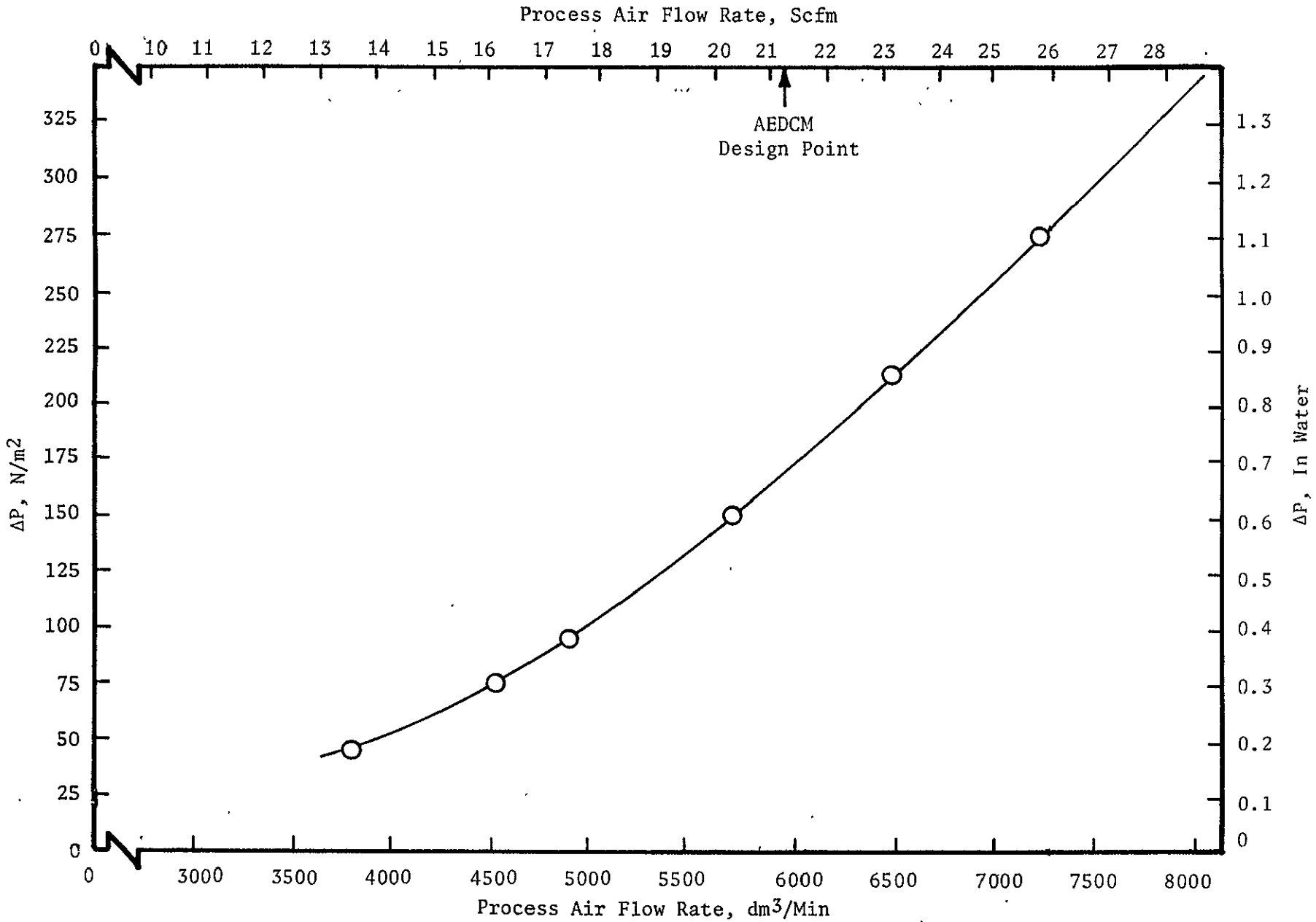

FIGURE 29 AEDCM PROCESS AIR PRESSURE DROP

CS-6 Blower Specifications

The CS-6 SSP commonality process air blowers are of the centrifugal fan type and deliver 991 dm^3/min (35 scfm) at 3.24 kN/m^2 (13 in water) static pressure. Each unit weighs 1.87 kg (4.12 lb) and occupies a volume of 4.27 dm^3 (260 in^3). The power requirements are 210W at 200 VAC, 400 Hz, three-phase and the operating fan speed is 11,000 rpm.

When bench tested, the noise levels were 93 dB at 2.75 m (9 ft) and 102 dB at 0.9 m (3 ft), with 50% of the inlet restricted, as required by the manufacturer's specification.

Literature Search

A literature search was performed to identify the availability and suitability of standard, off-the-shelf blowers or possibly identifying a single, special blower assembly which could provide simultaneous high flow, low pressure cooling air and low flow and high pressure process air. The criteria used to identify possible blowers were:

1. Air flow and static pressure capability
2. Noise
3. Volume
4. Weight
5. Power
6. Flight acceptability

For the purpose of blower identification, no relative importance was given to the six factors. Reliability and price were not included in the selection criteria inasmuch as reliability information is not readily available and is usually experimentally determined while price is a function of quantity and availability (off-the-shelf commonality items are less expensive than one of a kind).

Two candidate replacement blowers were identified: the CX-6 process air blower and the suit compressor used on Apollo spaceflight missions. The CX-6 blower was included in the study because it had demonstrated acceptable flow performance at a low noise level. The suit compressor was included because it, more than any other blower researched, fit all the requirements established for evaluation. Figure 30 shows the three units examined in the study.

Performance Comparison

The air performance of the three blowers range from 991 dm^3/min (35 scfm) for the CX-6 type blower to 1643 dm^3/min (58 scfm) for the Apollo compressor at the required 3.24 kN/m^2 (13.0 in water). The bench-tested noise levels for the CX-6 and Apollo units were only 71 dB at 2.75 m (9 ft). The CS-6 SSP blower, as a comparison, generated 93 dB at the same distance.

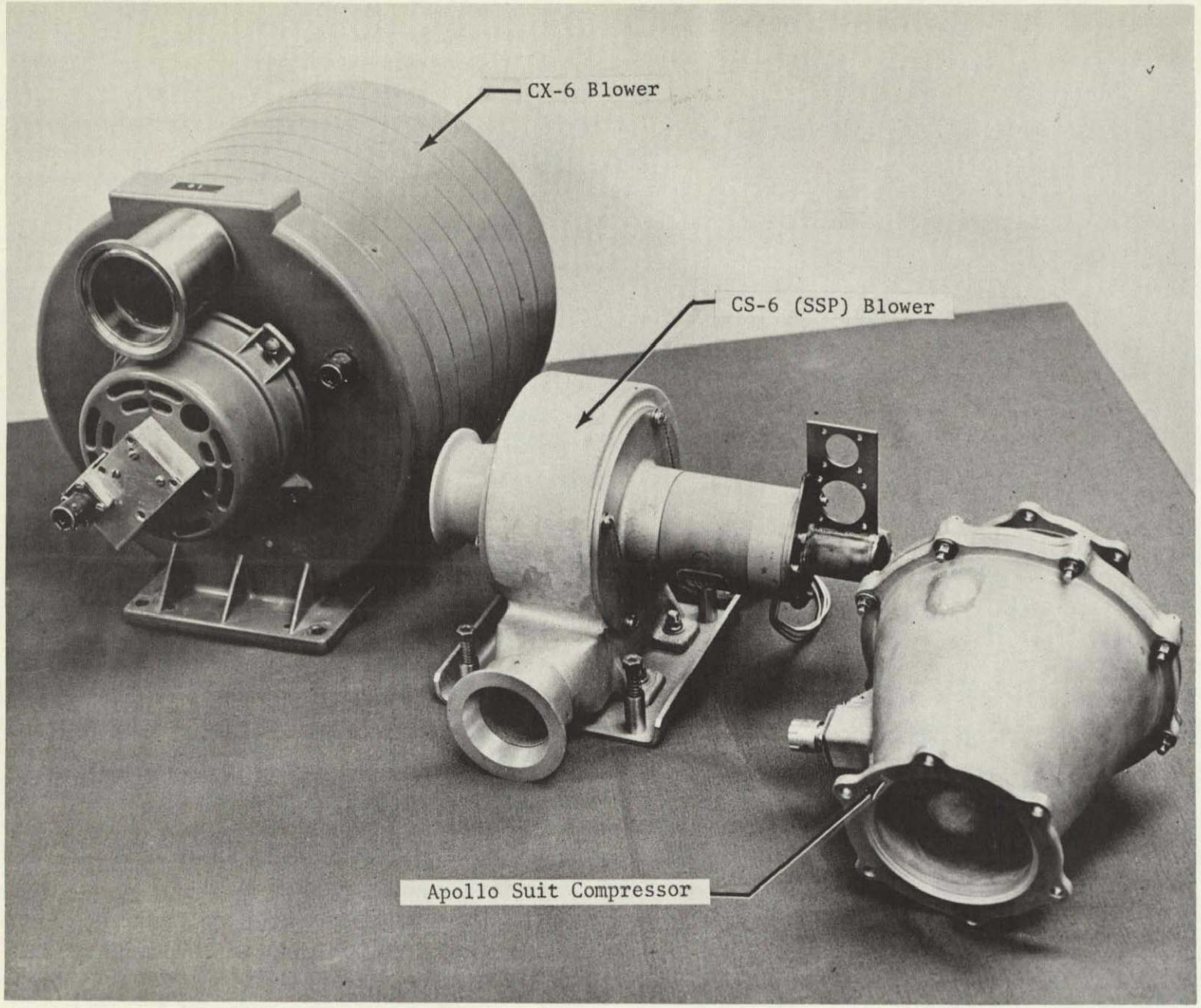

FIGURE 30 PROCESS AIR BLOWERS FOR POSSIBLE CS-6 APPLICATION

The CX-6 and Apollo units achieve their low noise levels by two different methods. The CX-6 blower limits the fan speed to less than 3600 rpm thereby causing less air turbulence and less noise. The Apollo compressor, on the other hand, operates at very high rpm (20,000) but has been constructed to minimize air turbulence. There are disadvantages to either method. The low speed CX-6 blower must compensate for its low speed by increased size (volume and weight) whereas the Apollo compressor requires difficult and expensive fabrication processes and procedures.

The power requirements of the CS-6 and Apollo blowers are identical, each needing 210W of 200 VAC, 400 Hz, three-phase power. The CX-6 blower requires 230W of 115 VAC, 60 Hz power (200 VAC, 400 Hz is available at an option). The SSP and Apollo units are both flight qualifiable, with the Apollo blower having already achieved flight certification. Table 8 summarizes, for comparison, the parameters examined.

Replacement Blower Selected

Based on the study results, the Apollo suit compressor blower was selected as a viable candidate for possible CS-6 application. Besides the reduction in noise (71 dB versus 93 dB at 2.75 m (9 ft)) only one blower would be required to satisfy the process air needs of the CS-6 for a 210W power savings and a 2.64 kg (5.81 lb) and a 4.63 dm^3 (282 in^3) weight and volume reduction. The 210W reduction would be a 21.8% reduction in total CS-6 power requirements.[6]

Lightweight CS-6 Style Module

As part of an overall effort to reduce the weight of electrochemical CO_2 removal subsystems, a lightweight CS-6 style module was designed, fabricated, assembled and checked out. The objective of the task was to physically demonstrate the capability to produce a lightweight module for the existing SSP subsystem application without committing the accepted cell and module design to changes which would require reverification of performance prior to SSP acceptance.

Weight and Volume Reduction Approach

The major effort of the activity centered around the reduction of the thickness of both the 0.127 cm (0.050 in) thick baseline anode current collector/cooling fins and the 0.152 cm (0.060 in) thick cell isolation spacers. The lightweight collector/fin thickness was to be only based on the heat removal requirement at baseline operation of 21.5 mA/cm^2 (20 ASF) rather than on an overcapacity capability of 43 mA/cm^2 (40 ASF). The intercell polysulfone isolation spacers were to be reduced in thickness since the spacers serve only as electrical isolators between the cells. Any parts of the cell relating directly to performance, such as the electrode-matrix-electrode composite, the respective process gas cavity configurations and heights, and intercell and module manifolding were to be left unchanged.

Module Design

The thickness of the new anode current collector was calculated to be 0.053 cm (0.021 in) based on an allowable thermal gradient across the active area of the cell at 21.5 mA/cm^2 (20 ASF) operation. The current collectors were to be still

TABLE 8 SIX-MAN CO_2 COLLECTION SUBSYSTEM PROCESS AIR BLOWER COMPARISON

Criteria	CS-6	CX-6	Apollo
Air Performance @ 3.25 kN/m^2 (13.0 In Water), dm^3/Min (Scfm)	0.99 (35)	1.13 (40)	1.64 (58)
Noise Level,(a) dB	93, 102	71, 77	71, 83.5
Fan Speed, Rpm	11,000	3,400	20,000
Weight, kg (Lb)	2.59 (5.7)	10.31 (22.7)	2.54 (5.6)
Volume, dm^3 (In^3)	4.27 (260)	9.60 (586)	3.92 (242)
Power Requirement, W	210	230	210
Voltage Requirement, VAC	200 @ 400 Hz	115 @ 60 Hz	200 @ 400 Hz
Phase Requirement, Phases	3	1	3
Flight Qualifiable Material	Yes	No	Yes
Flight Certified	No	No	Yes

(a) Noise level reading at 2.75 m (9 Ft) and 0.9 m (3 Ft), respectively. Ambient noise level - 62 dB.

manufactured from standard nickel sheet stock. The thickness of the intercell isolation spacers was based on manufacturing consideration, available thickness of off-the-shelf sheet stock, and sufficient ruggedness to withstand handling and standard assembly procedures. As a result, the spacer thickness was determined to be 0.025 cm (0.010 in).

Weight and Volume Reductions

The lightweight module parts were fabricated, the module assembled, pressure checked, and subjected to an eight-hour performance verification test. Figure 31 shows, for comparison, both a 16-cell CS-6 baseline module and the 16-cell lightweight module.

The actual weight achieved at the cell level was 0.65 kg (1.44 lb) per cell compared to the CS-6 baseline weight of 1.062 kg (2.337 lb) per cell. A 16-cell module comparison showed the SSP baseline module to weigh 25.4 kg (55.8 lb), while the new lightweight module weighed only 18.8 kg (41.5 lb) or a weight reduction of 26%. Also, a 21% reduction in module volume was achieved.

For the six-module CS-6 subsystem, this would result in a 40 kg (86 lb) weight savings or a 11% reduction in total subsystem weight.[16]

CS-6 Honeycomb Endplates

Significant weight reductions can also be achieved in a module by optimizing the endplate design without disturbing or altering the electrode matrix or gas compartment configurations.

Lightweight Endplate Design

Three possible endplate designs were investigated. These included the use of plain aluminum plates, a sandwich structure with stainless steel faces and a plastic core, and a sandwich structure with stainless steel faces and a metal honeycomb core. Of the three, the design with the highest strength to weight ratio was the honeycomb sandwich. Further investigation into the use of the honeycomb design indicated that aluminum would be a suitable core material. The analysis also showed that the necessary loading and construction requirements could be achieved by a 1.6 cm (0.630 in) thick honeycomb endplate (the baseline thickness of a solid stainless steel endplate was 0.86 cm (0.340 in)), resulting in a calculated weight reduction from 6.8 kg to 2.5 kg (15 to 4.75 lb) per set (two) of endplates, or a reduction of 18.3% in module weight with only an 8% increase in module volume. Figures 32 and 33 show the honeycomb insert and assembly drawings, respectively, of the final endplate design.

Fabrication of Honeycomb Sandwich

Commercially available honeycomb core stock, sliced to the required thickness, was purchased. A flat aluminum plate with an internal water manifold was fabricated for use as a core-holding fixture. Hot water was circulated through the aluminum fixture plate with the honeycomb core positioned on the plate.

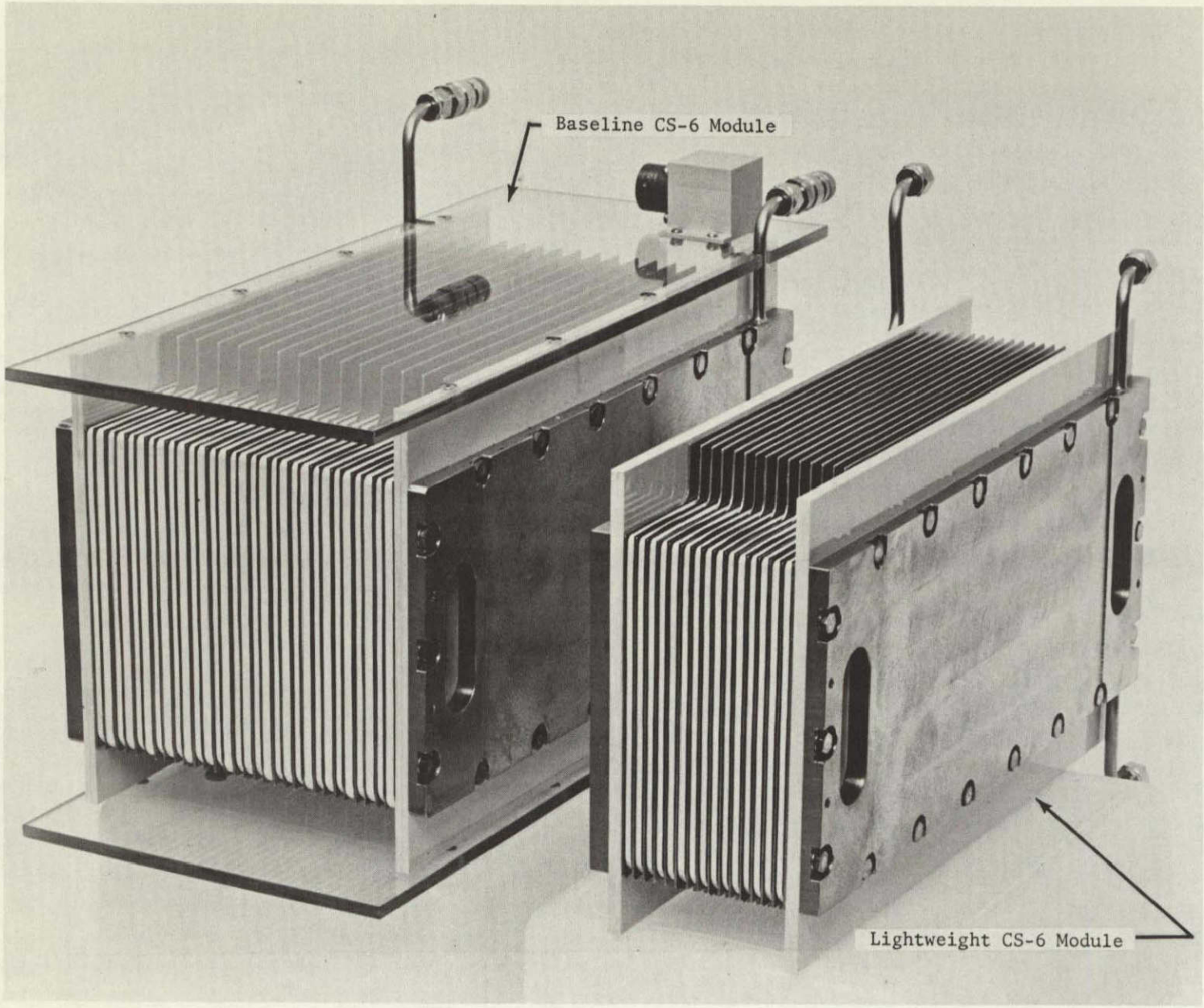

FIGURE 31 CS-6 BASELINE AND LIGHTWEIGHT MODULES

ORIGINAL PAGE IS
OF POOR QUALITY

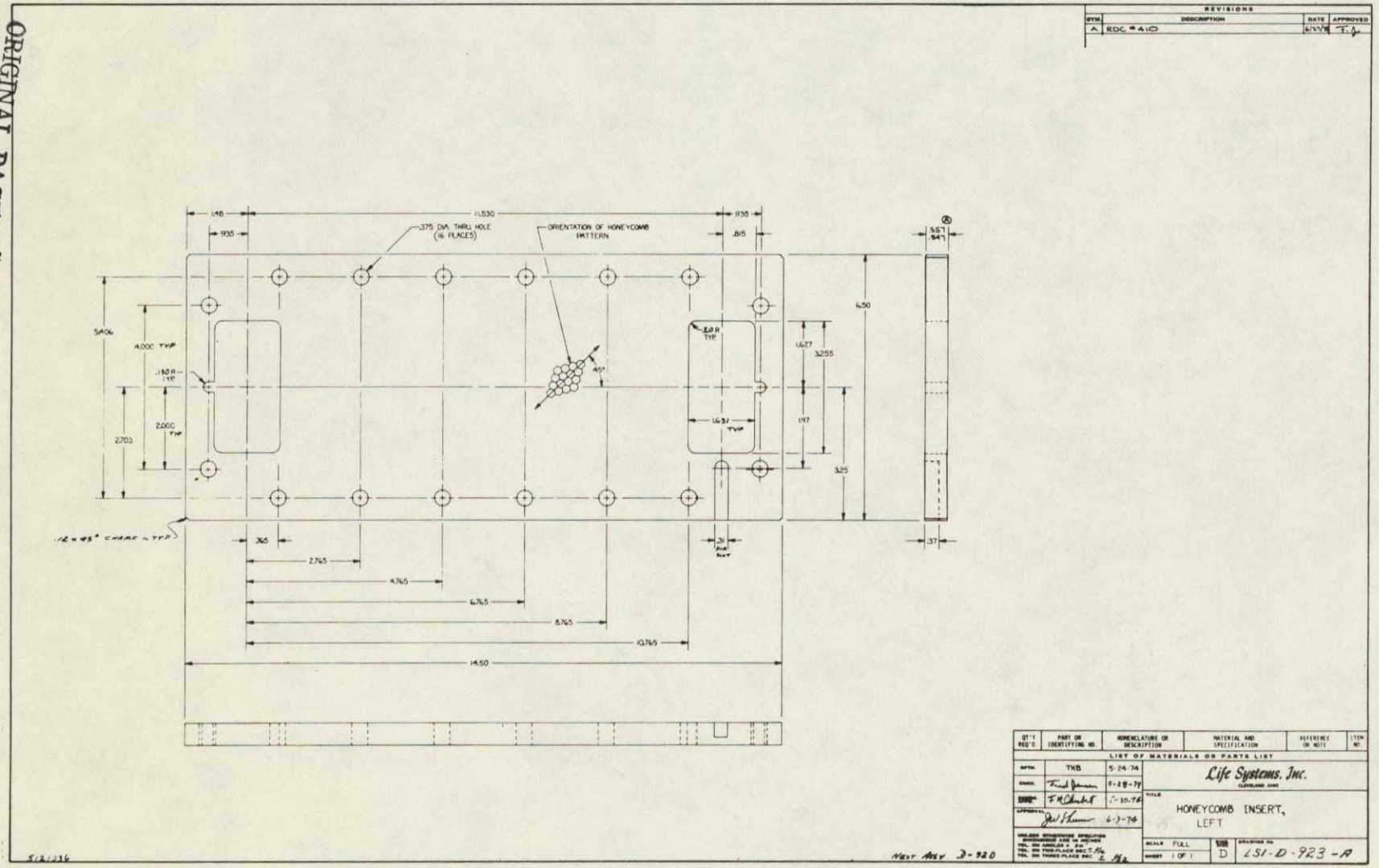

FIGURE 32 HONEYCOMB ENDPLATE INSERT

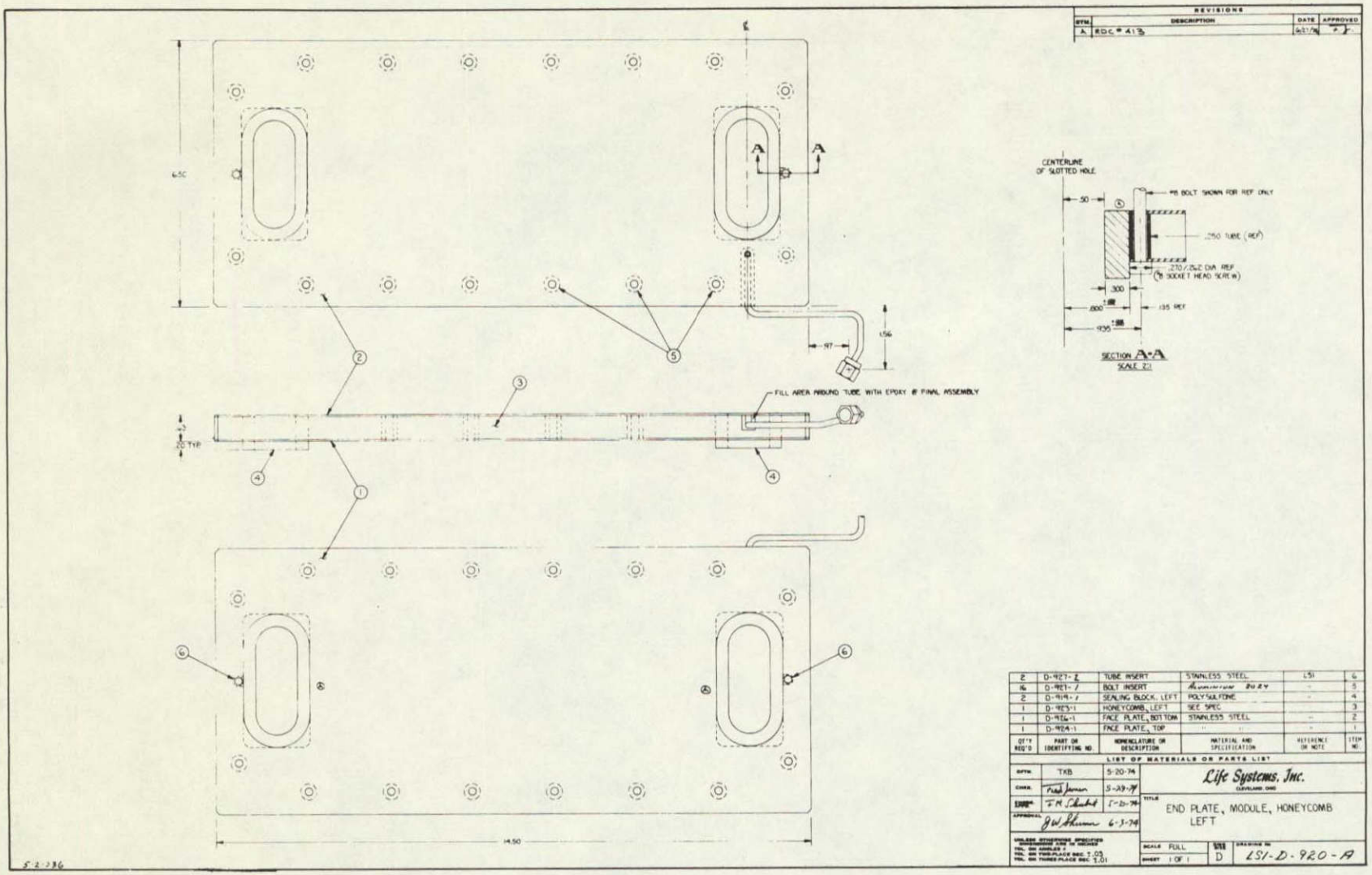

FIGURE 33 HONEYCOMB ENDPLATE ASSEMBLY

Polyethylene glycol flakes, which melt at 322 to 333K (120 to 140F), were then melted and poured over the core areas to be machined. Cold water was run through the aluminum plate, freezing the polyethylene glycol and fixing the core into position. The honeycomb metal was then machined. Following the machining, hot water was circulated through the fixture, melting the polyethylene glycol and releasing the honeycomb part. The polyethylene glycol was then totally removed by heating to ready the core for bonding.

Since the honeycomb core cannot resist high localized stresses that occur near bolt holes, aluminum inserts must be placed in the core wherever these stresses occur. Bushings were fabricated to resist the localized bolt stresses and milled stainless steel and polysulfone blocks were fabricated for the process fluid manifold and contained O-ring seals. These blocks were designed so none of the fluids passing through the sandwich structure would see a honeycomb bonding line to eliminate possible adverse effects of the electrolyte on the adhesive material. Facing plates were machined to provide the strength to the honeycomb sandwich. These facing plates were fabricated from 0.05 cm (0.020 in) thick 301 stainless steel. Figure 34 shows the aluminum bushings, facing plates, fluid manifolds, typical O-ring, and machined honeycomb core needed to fabricate a lightweight endplate.

Figure 35 shows the aluminum honeycomb core assembled and ready for the bonding process. The most important aspect of the bonding process is cleanliness. The facing plates must be clean so that the bonding material adheres to the smooth surfaces. The endplates were bonded by clamping the facing plates to the assembled core at approximately 482.6 kN/m^2 (70 psig) and then the assembly was furnace-cured at 397K (255F) for approximately four hours. A completed endplate is shown in Figure 36. The 0.318 cm (0.125 in) H_2 outlet tube was welded to the faceplate before bonding. The exposed edge surfaces of the aluminum core were covered with aluminum strips to prevent core damage (see Figure 36).

Evaluation of the Honeycomb Weight Savings

The total weight for one honeycomb endplate pair was 2.15 kg (4.75 lb). This yielded a weight savings of 68% per plate or 18.3% per one-man capacity CS-6 style module while increasing the module volume by only 8%. The completed endplates were also evaluated by assembling a full size module and compressing the cells with the lightweight endplates. Full torque values were applied to the bolts and the honeycomb endplates deflected only 0.013 cm (0.005 in). This can be compared with a 0.102 cm (0.040 in) deflection for a standard CS-6 type stainless steel endplate, yielding an 87% improvement.

On a CS-6 subsystem basis, a total weight reduction of 28.0 kg (61.5 lb) would result from the endplates for the six modules. Implementing all three weight reductions identified as part of these studies would result in 2.64 kg (5.81 lb), 43.9 kg (96.6 lb), and 28.0 kg (61.5 lb) weight reductions for the blower, lightweight modules and honeycomb endplate substitutions, respectively. The total weight savings would amount to 74.5 kg (164 lb) out of a total CS-6 weight of 368 kg (809 lb), or a 20% reduction.

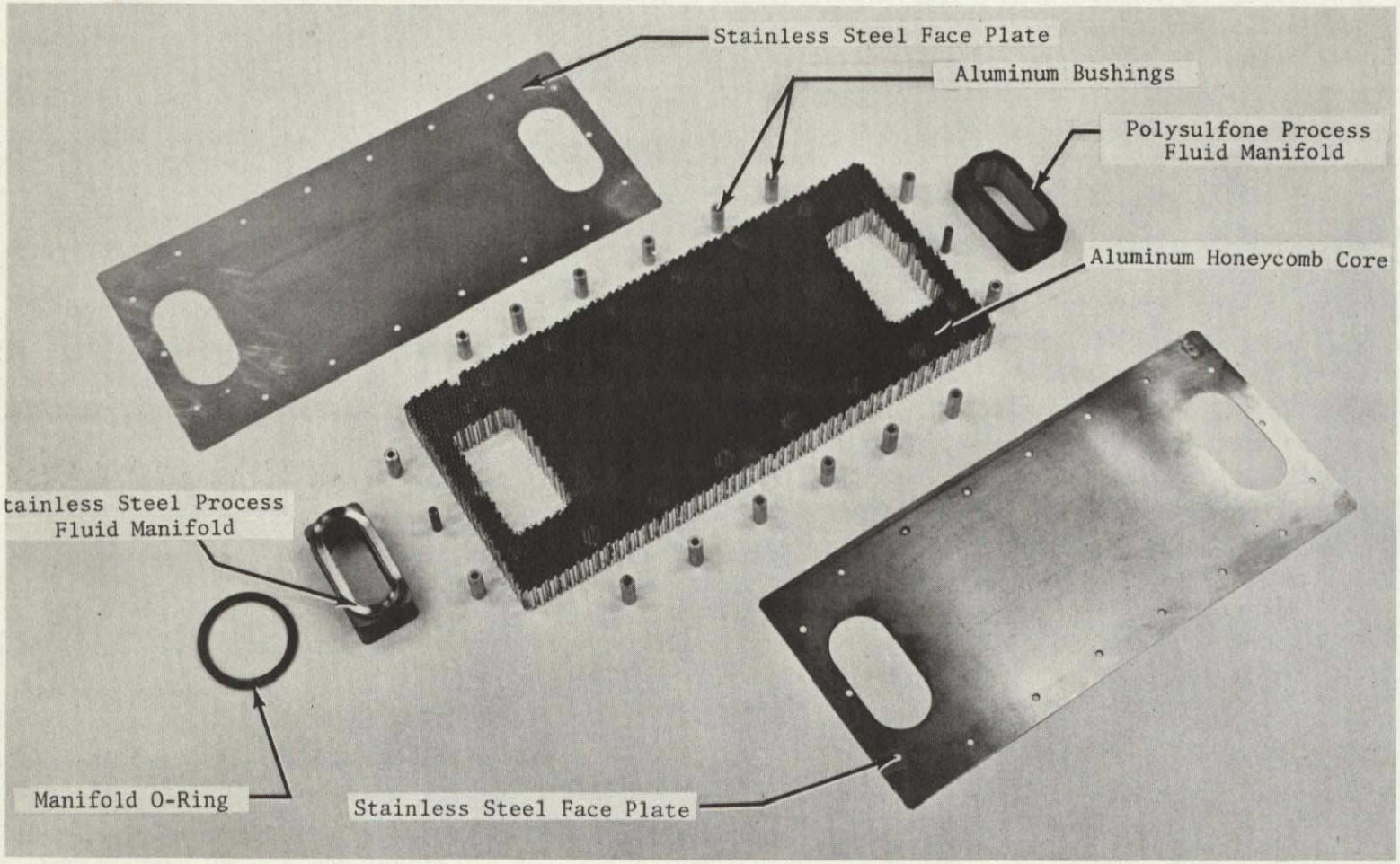

FIGURE 34 HONEYCOMB WITH INSERTS AND FACE PLATES

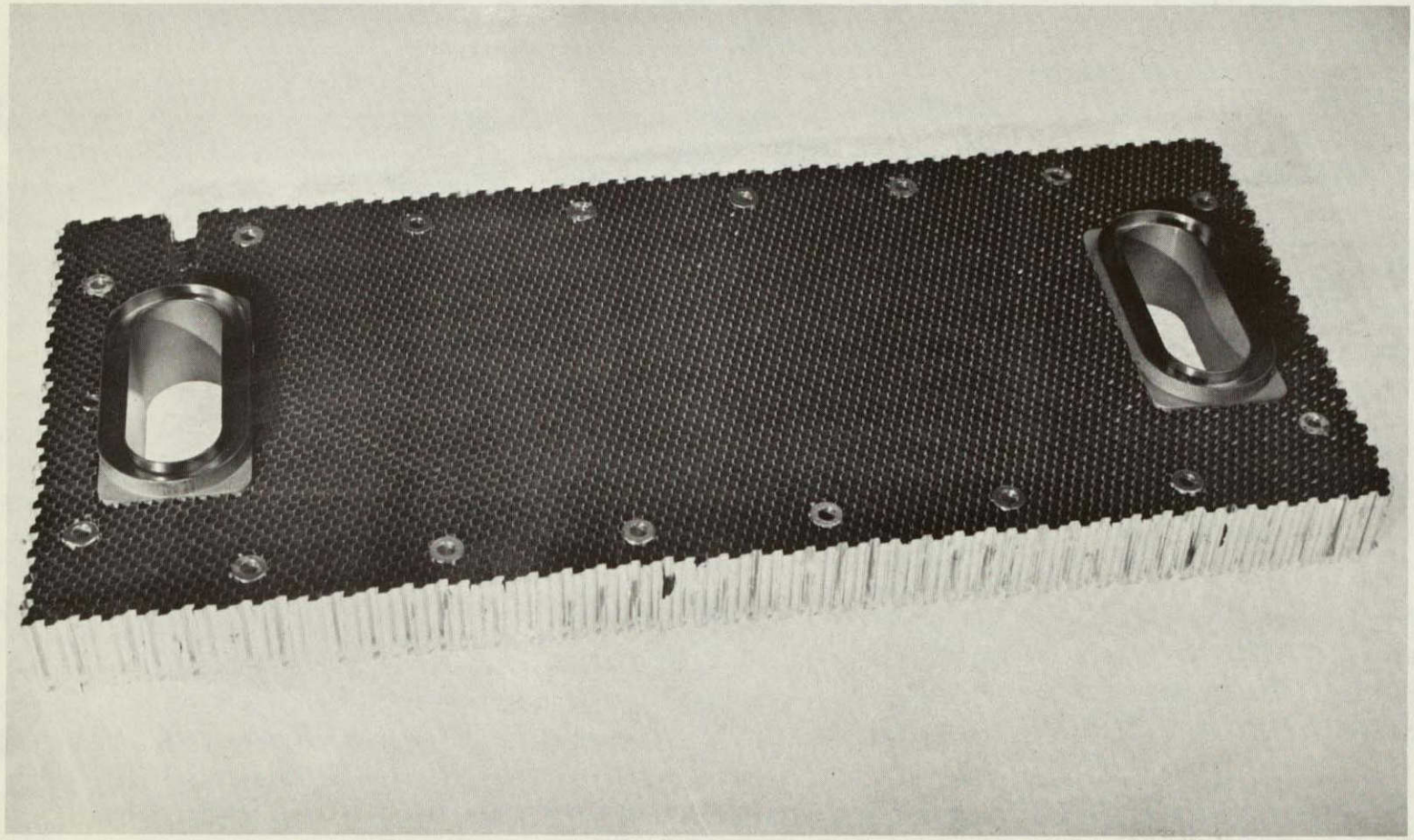

FIGURE 35 HONEYCOMB CORE ASSEMBLED AND READY FOR BONDING

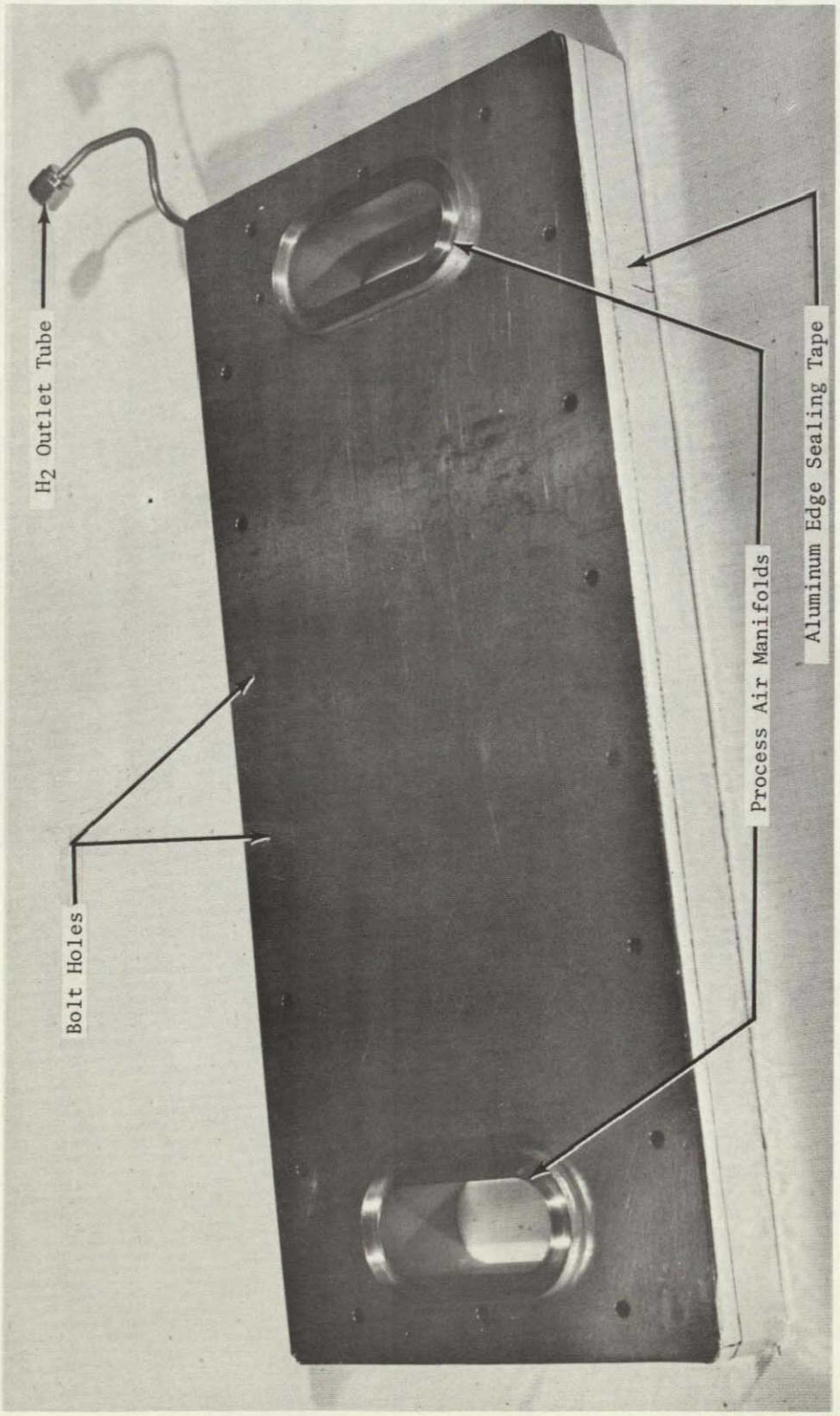

FIGURE 36 FINISHED HONEYCOMB ENDPLATE

EDC APPLICATION STUDIES

Five areas of application of the EDC as part of an overall spacecraft EC/LSS were investigated. Included were integration studies and studies relating to increased utilization of the EDC concept aboard manned spacecraft. Specifically, the five areas of investigation were:

1. Integration of the EDC with the Bosch CO_2 Reduction Subsystem (BRS) and the Solid Electrolyte Oxygen Regeneration Subsystem (SEORS)

2. Use of the EDC as an atmosphere contaminant removal subsystem

3. Use of the EDC module as a combined CO_2 and cabin humidity control component

4. Evaluation of the EDC as the CO_2 removal concept aboard the Shuttle Orbiter

5. Investigation of the feasibility of using the EDC with pre- and post-sorbers to increase CO_2 removal effectiveness at very low cabin pCO_2 levels.

EDC/BRS and EDC/SEORS Integration Studies

Under separate development efforts the EDC, BRS and SEORS are being evaluated by NASA for application to spacecraft Life Support Systems (LSS). Integration considerations must be included sufficiently early in the development of each of these subsystems to identify potential problem areas and to guide subsystem design and testing. Air revitalization within a total LSS has the primary function of O_2 generation, CO_2 removal and reclamation of O_2 from the CO_2. The EDC is a prime candidate to perform the CO_2 removal function. For O_2 recovery, both the BRS with a Water Electrolysis Subsystem (WES) and the SEORS are being considered. Study of the integration of the EDC with the BRS or the SEORS are, therefore, of interest. Mini-integration studies for the two combinations were performed as part of this program. For each of the studies the effects of the H_2/CO_2 stoichiometry, EDC anode exhaust gas characteristics and the operating modes of the CO_2 reduction subsystem on the integrated subsystems were investigated.

EDC/BRS Integration

A LSS using the EDC for CO_2 removal and the BRS for CO_2 reduction employs a WES for O_2 and H_2 generation. A block diagram showing a closed O_2 loop using these three subsystems is shown in Figure 37.

Hydrogen/Carbon Dioxide Stoichiometry. The BRS uses a closed recycle loop concept where H_2 and CO_2 combine to form water and carbon according to:

$$2H_2 + CO_2 = C + 2H_2O \qquad (7)$$

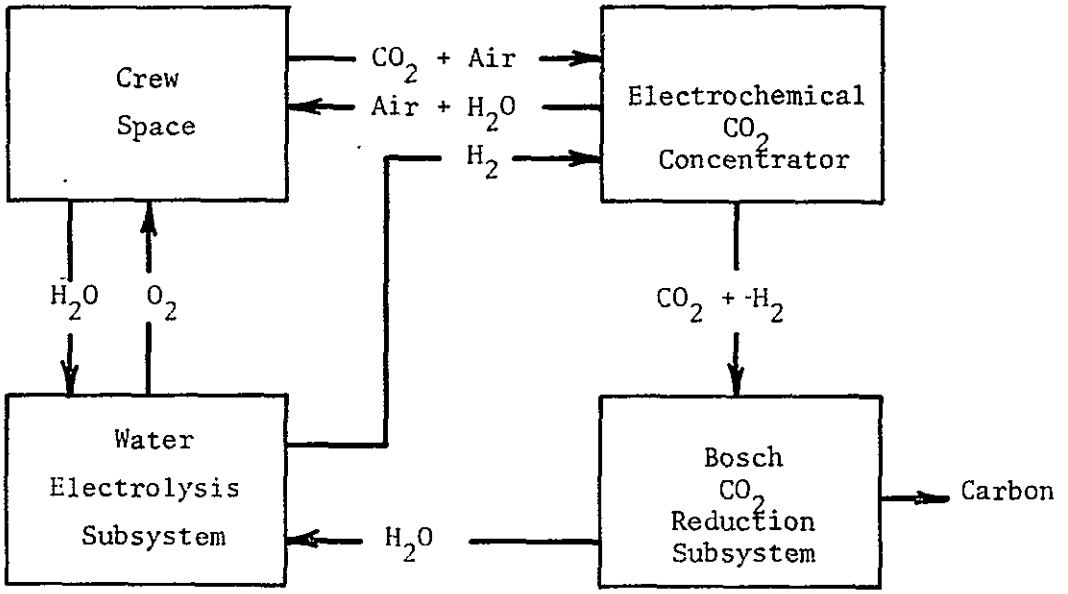

FIGURE 37 CLOSED OXYGEN LOOP WITH INTEGRATED BRS/EDC/WES

The above reaction shows that two volumes of H_2 must combine with one volume of CO_2. Any excess of either gas with respect to the other causes an undesirable pressure buildup in the closed, recycle loop of the BRS.

The volumetric ratio of H_2 to CO_2 exiting from the EDC is, therefore, of major importance. The primary operating mode of the EDC for integration with a BRS is one of constant current, hence, constant H_2 and O_2 consumption. The fluctuation in the exiting H_2 from the EDC is a direct function of the fluctuations in the O_2 and H_2 generating rates of the WES. In the LSS of the SSP, for example, a ±10% of the nominally required O_2 is used to control cabin O_2 partial pressure (pO_2). This control mode is also not necessarily repetitive on a 24-hour basis.

Based on average daily metabolic rates for man and the subsystem reactions involved, H_2 in excess of that required by the stoichiometry of the BRS reaction will always be available. In actual application, the amount of excess H_2 is even higher since additional O_2 is required to make up for cabin leakage.

While the average mass balance results in nonstoichiometric ratios of H_2 to CO_2 for the Bosch, instantaneous values for this ratio may experience even larger variations due to CO_2 removal efficiency variations and lag times in CO_2 removal rates caused by variations in cabin pCO_2 and the capacity of the cabin volume, respectively.

Resolution of this problem, i.e., the difference between the H_2/CO_2 ratio emitted by the EDC and that required stoichiometrically by the Bosch reaction is essential to insure proper EDC/BRS integration. This latter ratio (H_2/CO_2) is 2:1 by volume or 1:11 by weight, while the actual ratios experienced may vary from 2.7:1 to 4.5:1 for CO_2 removal rate variations from +10% to -20% of nominal, based on SSP performance criteria.[11]

Hydrogen/Carbon Dioxide Control Concept. Figure 38 is a flow schematic derived for an integrated system capable of maintaining the desired 2:1 H_2/CO_2 volumetric feed ratio to the BRS while enabling proper EDC and WES operation. The subsystem operates as follows: pressure regulator (PR-1) maintains a constant upstream H_2 pressure from the WES resulting in a constant H_2 flow rate to the EDC through flow restrictor (R-1). The restrictor is sized to supply a fixed flow of H_2 to the EDC sufficient to satisfy the EDC (operating at constant current) requirements, but always less than that required to cause the H_2 to CO_2 ratio of the EDC exhaust to equal 2:1. In this manner, H_2 must always be added to the BRS feed gas through FC-1, as sensed by the BRS recycle loop gas composition sensor.

Flow restrictor R-1 must be sized for a given application to insure the lower than 2:1 H_2 to CO_2 ratio for all expected CO_2 removal efficiencies of the EDC. The latter are based on cabin pCO_2 variations resulting from a fixed cabin volume, EDC characteristics and CO_2 generation profiles.[11]

Pressure regulator (PR-2) prevents the BRS recycle loop and EDC exhaust pressures from going subatmospheric by adding H_2 to the loop to throttle CO_2 and H_2 conversion efficiency at low CO_2 feed rates and/or when minimum recycle loop flow rate has been reached.

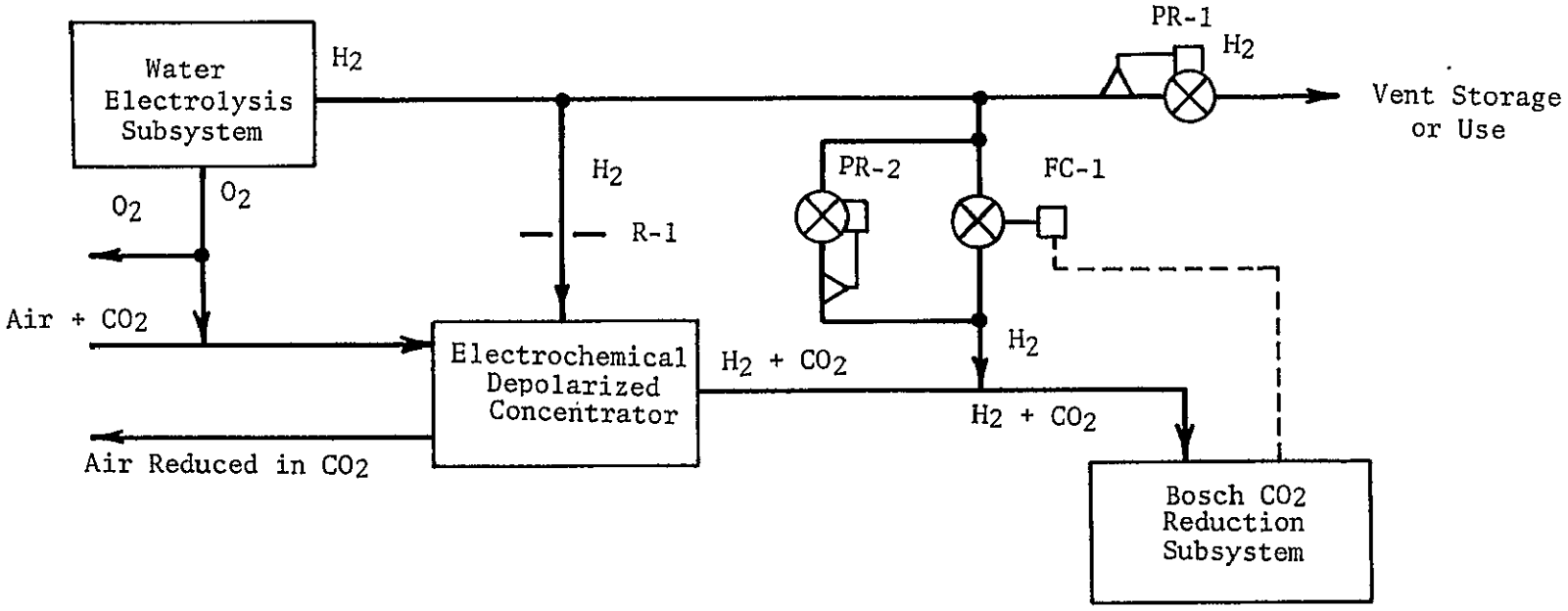

FIGURE 38 INTEGRATION SCHEMATIC FOR A WES, EDC AND BRS

Effects of Other EDC Anode Exhaust Gas Characteristics. Three other parameters associated with the EDC anode exhaust gas besides the H_2 and CO_2 content are of significance when interfacing the EDC with the BRS. They are moisture content, temperature and exhaust gas pressure.

The presence of moisture in the recycle loop decreases Bosch conversion efficiency. Therefore, by introducing the feed gas upstream of the recycle loop condenser, the moisture content of the recycle gas to the reactor will only be determined by the spacecraft liquid coolant temperatures.

Typical values for recycle gas to feed gas ratios (by weight) are 10 to 12. The effect of the EDC anode exhaust temperature, 297 ±8K (75 ±15F), when compared to the BRS operating temperature of approximately 920K (1196F) and when considering the recycle gas to feed gas ratio, is insignificant.

The preferred Bosch recycle loop pressure is 7 kN/m^2 (1 psig). Satisfactory EDC operation has been demonstrated at anode exhaust pressure levels of 0 to 35 kN/m^2 (0 to 5 psig). The EDC anode exhaust pressure is therefore compatible with integrated EDC/BRS operation.

Effects of Bosch Operating Modes on EDC Operation. Four operating modes were derived to describe BRS operation. They are (1) Normal Operating Mode, (2) Startup Mode, (3) Reactor Changeover Mode and (4) Shutdown Mode.[11] As part of this investigation, a study was conducted to analyze the impact of these modes on the operation of the EDC.

The analytical evaluations above, in conjunction with Figure 38, have established the capability of the EDC to satisfactorily interface with the Bosch when the latter is operating in its Normal Mode.

The BRS Startup Mode consists of initially evacuating both or one of the recycle loops and reactor(s) after cartridge insertion or general subsystem maintenance. The reactor(s) can then be heated to operating temperature while at a vacuum or after being filled with feed gas from the EDC. Preheating while the reactor is evacuated, followed by subsequent filling with feed gas is preferred since it prevents loss of feed gas during the heatup period due to gas expansion.

The filling of the recycle loop and reactor volume in either a cold or preheated condition is accomplished by switching the EDC anode exhaust gas flow from vacuum to the recycle loop of the BRS. The switching of the anode exhaust will not result in detrimental perturbations to the EDC since the anode exhaust of the EDC is isolated by a backpressure regulator, an integral component of the EDC subsystem itself. The EDC can be operated during preheat or during any maintenance functions on the BRS with its anode exhaust being dumped overboard or, possibly, stored. When the BRS is ready to accept feed gas flow, the anode gas output downstream of the EDC backpressure regulator is simply switched to the Bosch, bringing the unit to operating pressure. A pressure transducer signal within the BRS's recirculating loop initiates compressor operation at a convenient pressure level. Slight pressure variations in the BRS reactor will take place. These pressure fluctuations are, however, again isolated from the EDC through its own backpressure regulator.

The Reactor Changeover Mode for cartridge replacement has similar effects on the EDC as the Startup Mode. Again, switching from the spent reactor to the new reactor is very similar to conditions at startup. At the time of switchover the anode exhaust gas from the EDC is simply switched from the recycle loop of the spent reactor to the new reactor's recycle loop which is initially under a vacuum.

The effects of a scheduled or unscheduled total shutdown of the BRS on EDC operation are minimal. All that is required is a signal from the BRS to the EDC indicating that a shutdown has occurred and that the anode exhaust gases no longer will be accepted by the unit. The EDC will automatically direct the anode exhaust gas to overboard dump or storage by simply actuating a diverter valve. Diversion of anode exhaust gas, similar to that which will occur during Reactor Changeover Mode or during Shutdown Mode, from the BRS to an overboard dump has been successfully demonstrated during actual testing of the CS-6 and should provide no difficulty in interfacing the EDC with the BRS.

EDC/BRS Integration Study Results. Based on the results of the study, integrated operation of the EDC and BRS as part of a closed O_2 loop is feasible using state-of-the-art hardware. A more detailed description of EDC/BRS integration considerations are presented in literature.[11]

EDC/SEORS Integration

A LSS using the EDC for CO_2 removal and the SEORS for O_2 reclamation employs water and CO_2 electrolyzers as part of the SEORS to replenish the O_2 for metabolic and leakage requirements. A block diagram showing a closed O_2 loop using the two subsystems is shown in Figure 39.

Hydrogen/Carbon Dioxide Stoichiometry. The SEORS uses a closed recycle loop concept where the CO_2 and trace water from the EDC anode exhaust gas is electrolyzed to form H_2, O_2 and carbon monoxide (CO). The H_2 and CO are then fed first through a disproportionator where the CO forms CO_2 and solid carbon and then through a H_2 separator where H_2 is separated from the recycle loop and vented to vacuum. Since the process of electrolyzing all the metabolic CO_2 does not form all the O_2 metabolically needed, a solid electrolyte water electrolyzer is included in the SEORS to generate the remaining O_2 required (including that for cabin leakage). Under normal conditions, the SEORS reduces 1.0 kg (2.2 lb) CO_2/man-day to produce 0.73 kg (1.60 lb) O_2/man-day so that a minimum of 0.11 kg (0.24 lb) of O_2/man-day must be generated by the water electrolyzer.

In the EDC, at an average TI of 2.2, 0.45 kg (1.0 lb) O_2/man-day is required to remove the 1.0 kg (2.2 lb) CO_2 produced. To interface the EDC with the SEORS, the water electrolyzer would be required to generate the additional 0.45 kg (1.0 lb) O_2/man-day by electrolyzing 0.51 kg (1.13 lb) water/man-day to satisfy the electrochemical reactions in the EDC.

At the total water electrolyzer O_2 generation rate of 0.56 kg (1.24 lb) per man-day, 0.07 kg (0.16 lb) of H_2 are also generated. This results in 1.24 times the stoichiometric H_2 required by the EDC. Therefore, by enlarging the water electrolysis capacity to replenish the O_2 consumed by the EDC, sufficient H_2

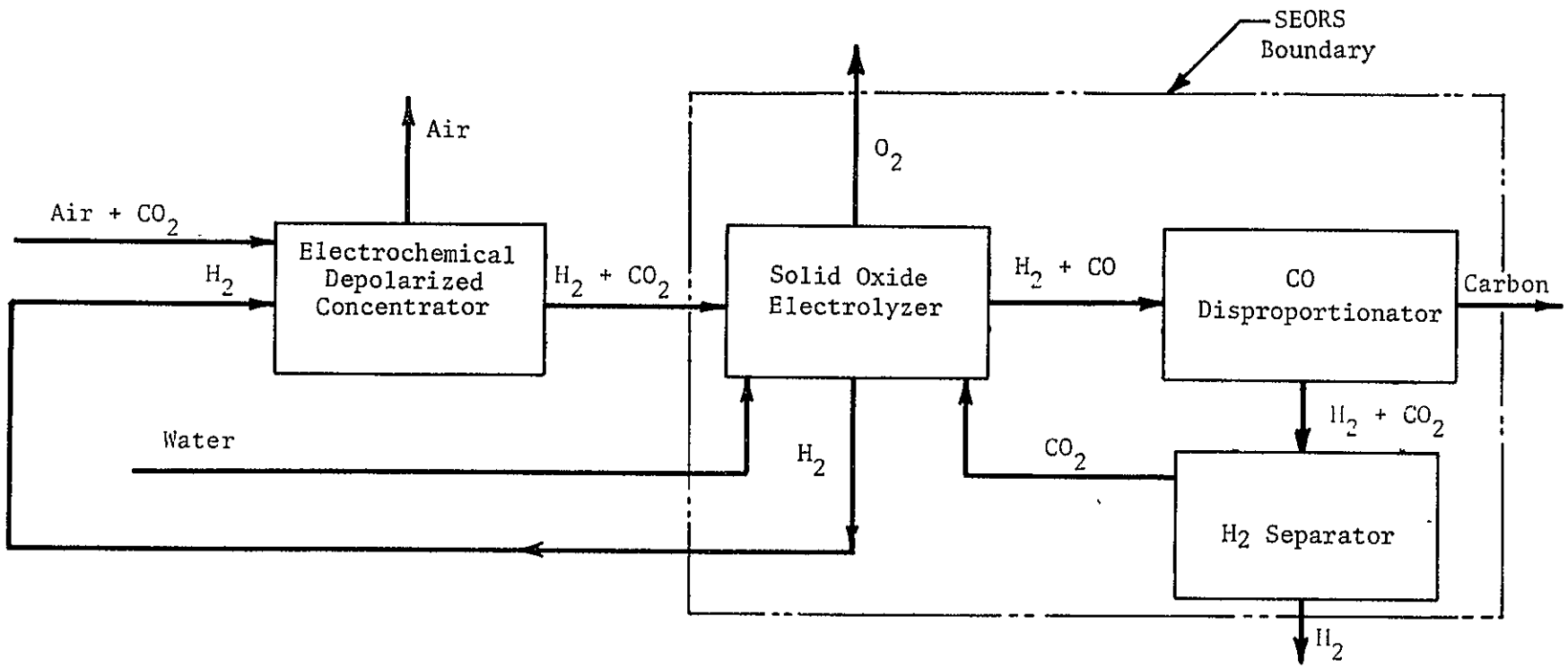

FIGURE 39 CLOSED OXYGEN LOOP WITH INTEGRATED SEORS/EDC

will always be available. Since the H_2 and O_2 consumed in the EDC combine during the reactions to form water, eventually recovered from the cabin atmosphere, no increase in stored water due to using an EDC is necessary.

Effects of Other EDC Anode Exhaust Gas Characteristics. Three other parameters associated with the EDC anode exhaust (besides the H_2 and CO_2 content) are of significance when interfacing the EDC with the SEORS. They are moisture content, temperature and exhaust gas pressure.

Any moisture in the feed gas would be electrolyzed in the CO_2 electrolyzer in the recirculation loop, with the O_2 fed back to the spacecraft atmosphere and the H_2 fed into the recirculation loop. Moisture content in the EDC exhaust poses no problem to the SEORS recycle loop.

The SEORS feed gas must be heated to 1123K (1562F) for maximum electrolyzer efficiency. The EDC anode exhaust temperature is 297 ±8K (75 ±15F). The variation in the EDC exhaust temperature, when compared to the electrolyzer temperature, is insignificant.

The preferred SEORS recycle loop pressure is 7 kN/m^2 (1 psig). Extensive operating time has been logged on EDC systems at 0 to 35 kN/m^2 (0 to 5 psig). Hence, no problem will result using a 7 kN/m^2 (1 psig) EDC anode exhaust pressure.

Effects of SEORS Operating Modes on EDC Operation. The SEORS has three steady-state operating modes and two semiautomatic modes. The three steady-state modes are Normal, Standby and Shutdown. The two semiautomatic modes are Startup and replacement of the carbon deposition cartridge. The carbon deposition cartridge can be removed and replaced while the system is in any of the steady-state modes and has no effect on the EDC.

The SEORS Startup Mode occurs whenever the unit is integrated into the total LSS. Prior to startup, the EDC will be operating with the anode exhaust vented to vacuum or stored. The SEORS reactors are then heated to operating temperature. The EDC is then directed to a Normal Mode and anode exhaust gas flows through the SEORS to vacuum. When the SEORS reaches full operating conditions, the electrolyzers are powered and the recycle loop activated. The system is then in Normal Mode.

The effects of a Standby or Shutdown Mode in the SEORS on EDC operation are minimal. All that is required is a signal from the SEORS to the EDC that the SEORS is making a mode transition from Normal Mode. The EDC will then automatically direct the anode exhaust gas overboard or to storage.

EDC/SEORS Integration Study Results. Based on the results of the study, integrated operation of the EDC and the SEORS as part of a closed O_2 loop is feasible.

Use of an EDC for Simultaneous pCO_2 and Trace Contaminant Control

A Contaminant Removal Subsystem is included in all regenerative life support systems in order to maintain contaminant concentrations in the spacecraft atmosphere below specified levels. A variety of these contaminants have been shown

to affect the electrolyte and electrodes of an EDC. A study was performed to evaluate the effects of these contaminant compounds on EDC performance, including an investigation of the feasibility of using an EDC as a simultaneous CO_2 and trace contaminant removal subsystem. Specific compounds evaluated included aldehydes, carboxylic acids, mineral acids, nitriles, and such catalyst poisons as mercaptans and sulfides.

Analytical Studies

Within the six compound groups to be studied, there are a total of 22 specific compounds which could possibly be found in a spacecraft environment. Table 9 lists these compounds, their projected production rates and maximum allowable concentrations.[12]

Based on the production rates, activities and maximum allowable concentrations, one representative compound was selected from each group. The compounds chosen were acetaldehyde, pyruvic acid, hydrogen chloride, acetonitrile, ethyl mercaptan and hydrogen sulfide. Because of the practical limitations of adding small amounts of these compounds to the process air of the EDC, three "worst case" assumptions were made:

1. The concentrations of these compounds were chosen so that the concentration of each compound was equal to the total concentration of the chemical group it represented

2. The contaminant removal subsystem does not remove any of the contaminants

3. All the contaminants could be transferred into the electrolyte retained in the cell matrix-electrode composite

EDC Performance

An electrolyte solution containing the six selected contaminants was used to charge a single cell EDC. Figures 40 and 41 show the cell's performance as a function of time and current density, respectively. During the test, no major CO_2 transfer problems occurred with the cell still exhibiting a level TI of 1.70 at 21.5 mA/cm^2 (20 ASF) after 125 hours of operation. This would indicate that even at the lower electrolyte concentration due to neutralization by the additions of acetaldehyde, pyruvic acid, hydrogen chloride and acetonitrile, practical CO_2 removal can still be accomplished effectively. Also, at start-up, the cell's TI was similar to that of baseline cells, as shown in Figures 40 and 41.

The terminal voltage, however, was well below the normal 0.35 volts, both at short-term and long-term operation. A measurement of the internal resistance (IR) voltage (see Figure 41) shows no significant change when compared to other single cells. This would indicate that some electrode catalyst poisoning had occurred.

Contaminant Control

A Contaminant Removal Subsystem aboard a spacecraft includes chemical absorbers to remove acid gases from the cabin air before and after a catalytic (toxin)

TABLE 9 TRACE CONTAMINANTS IN A SIX-MAN SPACECRAFT ENVIRONMENT[12]

Compound	Production Rate, mg/d	Maximum Allowable Concentration, mg/m^3
Acetaldehyde	125.5	36.0
Acetic Acid	12.5	2.5
Acetonitrile	12.5	7.0
Butraldehyde	12.5	70.0
Butyric Acid	12.5	14.0
Carbonyl Sulfide	12.5	25.0
Caprylic Acid	5.0	155.0
Ethyl Mercaptan	5.0	2.5
Formaldehyde	12.5	25.0
Furfural	12.5	2.0
Hydrogen Chloride	12.5	0.15
Hydrogen Fluoride	12.5	0.08
Hydrogen Sulfide	0.5	1.5
Ethyl Mercaptan	5.0	2.0
Propionaldehyde	12.5	30.0
Propionic Acid	12.5	15.0
Propyl Mercaptan	5.0	82.0
Propylene Aldehyde	12.5	10.0
Pyruvic Acid	1255.0	0.9
Sulfur Dioxide	12.5	0.8
Valeraldehyde	5.0	70.0
Valeric Acid	5.0	110.0

FIGURE 40 TRACE CONTAMINANT CELL PERFORMANCE AS A FUNCTION OF OPERATING TIME

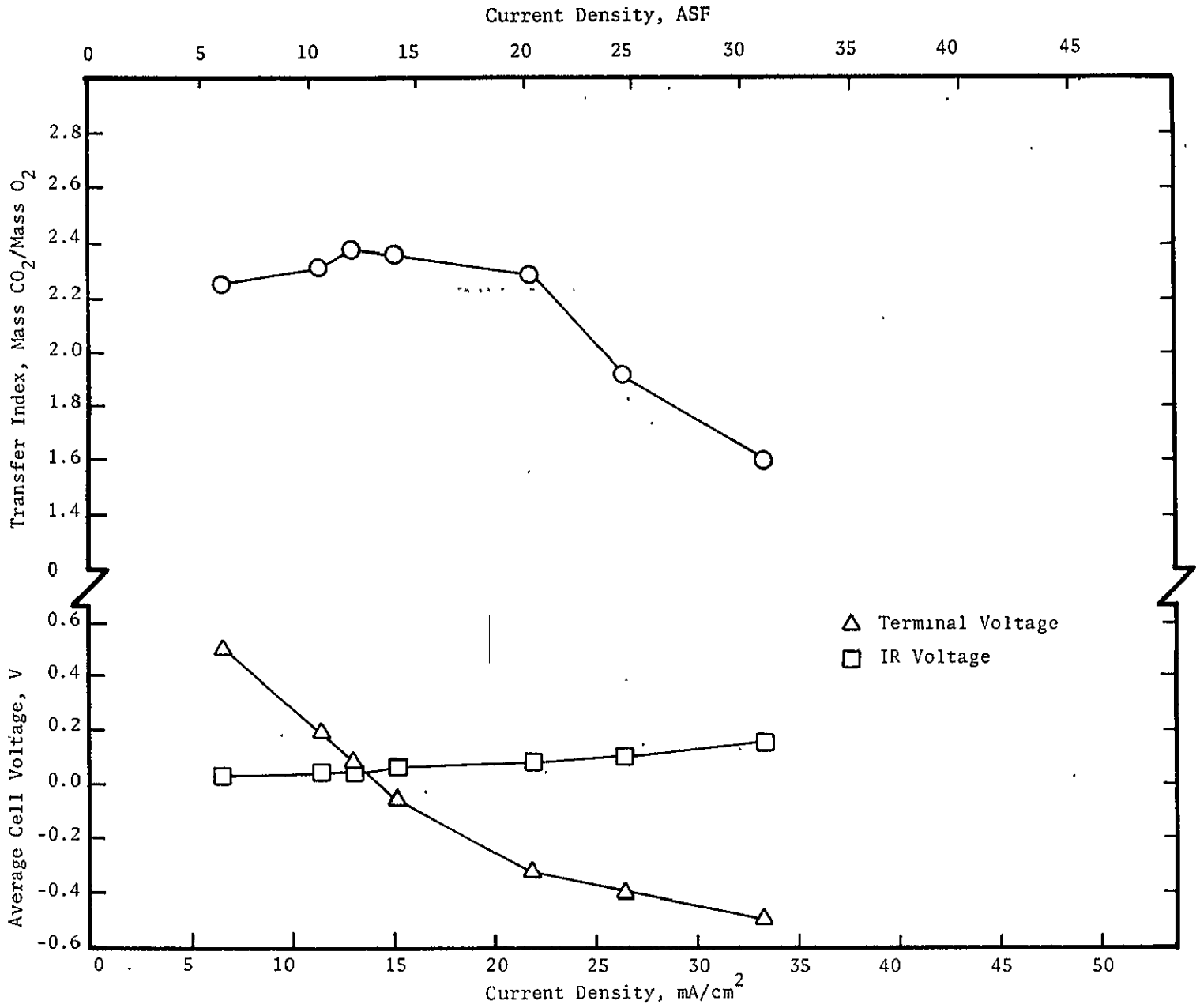

FIGURE 41 TRACE CONTAMINANT CELL PERFORMANCE AS A FUNCTION OF CURRENT DENSITY

burner. An acid gas absorber found to be effective is one that contains lithium carbonate (Li_2CO_3). The acid gas absorbers of a six-man capacity Contaminant Removal Subsystem weigh approximately 22.7 kg (50 lb), occupy 0.14 m^3 (1.5 ft^3), (12) and significantly increase the pressure drop that an air blower must overcome. The Cs_2CO_3 electrolyte retained in the cell matrices and electrodes of an EDC could serve as a sink for certain cabin air contaminants as the process air is passed through the cathode compartments as part of the CO_2 removal function.

Analysis. An analysis was performed to obtain a rough order of magnitude in elapsed time before the contaminant removal capacity of an EDC would be spent or electrolyte degradation would interfere with the primary CO_2 removal function.

Analytical predictions of electrolyte degradation based on the simultaneous effects of the multiple contaminants listed in Table 9 is difficult. The analytical approach selected was to choose a common group of contaminants and quantify the effect of the group on the electrolyte as a function of time. Should the effects of one group negate the concept of EDC trace contaminant control, further study efforts would not be required.

The most likely and predictable chemical reactions to occur between the cell electrolyte and contaminants would be those caused by the acid gases. By quantifying the amount of time required before the cell reaches its lowest permissible Cs_2CO_3 concentration due to acid gas reactions, a maximum time of contaminant control through the EDC can be established. Any additional effects of other contaminants on the cell electrolyte would only serve to lessen the available time at safe operational levels.

Acid Gas Evaluation. The following gases are those likely to be found in a spacecraft atmosphere: (12)

1. Organic Acids
    a. Acetic Acid
    b. Butyric Acid
    c. Caprylic Acid
    d. Propionic Acid
    e. Pyruvic Acid
    f. Valeric Acid
2. Mineral Acids
    a. Hydrogen Chloride
    b. Hydrogen Fluoride
    c. Hydrogen Sulfide

Based on the average generation rates, a cabin volume, and the maximum allowable contaminant concentrations, the time until maximum allowable concentration levels are reached can be calculated. The results for the acid gases selected are shown in Table 10 for a 743 m^3 (8,000 ft^3) cabin volume, a six-man crew, and assuming worst case conditions of zero contaminant removal. The results show that acid gas control must be included as part of a spacecraft LSS since, for example, the maximum allowable concentration of hydrogen fluoride is reached in only 1.44 days.

C.2

TABLE 10 TIME TO MAXIMUM ALLOWABLE ACID GAS CONCENTRATION WITHOUT CONTAMINANT CONTROL

	Generation Rate, mg/d[12]	Maximum Allowable Concentration, mg/m^3[12]	Total Time to Reach Maximum Concentration, d[a]
Acetic Acid	12.5	2.5	453.0
Butyric Acid	12.5	14.0	253.8
Caprylic Acid	12.5	155.0	2809.4
Propionic Acid	12.5	15.0	271.9
Pyruvic Acid	1255.0	0.9	0.2
Valeric Acid	5.0	110.0	4984.3
Hydrogen Chloride	12.5	0.13	2.4
Hydrogen Fluoride	12.5	0.08	1.4
Hydrogen Sulfide	0.5	1.3	654.6

(a) No. of days = (1/generation rate)(max. allowable concentration)(volume)
= days/gm x mg/m^3 x 8,000 ft^3 x 0.02832 m^3/ft^3 x 0.001 gm/mg
= (1/generation rate)(max. allowable concentration)(0.22656)

Effects of Acids on Electrolyte Concentration. Four main reactions are possible between the acid gases and the Cs_2CO_3 electrolyte. They are:

1. The carboxylic (organic) acids will react under the general formula

$$2RC(=O)-OH + Cs_2CO_3 = 2RC(=O)-OCs + H_2O + CO_2 \quad (8)$$

2. The hydrogen chloride and hydrogen fluoride will react as

$$2HX + Cs_2CO_3 = 2CsX + H_2O + CO_2 \quad (9)$$

3. Hydrogen sulfide will follow

$$2H_2S + 3O_2 = 2H_2O + 2SO_2 \quad (10)$$

perhaps

$$2H_2S + O_2 = 2H_2O + 2S \quad (11)$$

and

$$SO_2 + 2H_2S = 2H_2O + 3S \quad (12)$$

The total generation rate of acid is 21.36×10^{-3} g-M/day (see Table 11). For an electrolyte concentration change from 61.5% by weight to 57% by weight (based on operating experience), 0.147 moles/module or a total of 0.882 moles of Cs_2CO_3 would have to be converted within the CS-6 to reach the lower concentration limit.[3] The allowable decrease in the Cs_2CO_3 electrolyte concentration from 61.5% to 57% is based on past experience[12] and specific volume versus concentration data.[12] If all the available acids generated were to fully react with the Cs_2CO_3, therefore, a 57% concentration would be reached in 82.2 days.

The results of the analysis show that an EDC cannot totally satisfy acid gas removal for extended space missions. The results, however, do point out that during down time of the Trace Contaminant Subsystem, as may be required for maintenance, the EDC can provide protection for those acid gases that would build up quickly to their maximum allowable concentrations (see Table 10) without significant adverse effects on CO_2 removal.

TABLE 11 MOLES OF ACID GENERATED PER DAY

Acid	Formula	Mole Wt. g	Generation Rate mg/d	g-M/d x 10^{3}
Acetic	CH_3COOH	44	12.5	0.28
Butyric	$CH_3(CH_2)_2COOH$	72	12.5	0.17
Caprylic	$CH_3(CH_2)_6COOH$	128	5.0	0.04
Propionic	$CH_3CHCOOH$	58	12.5	0.22
Pyruvic	$CH_3COCOOH$	64	1255.0	19.61
Valeric	$CH_3(CH_2)_3COOH$	86	5.0	0.06
Hydrogen Chloride	HCl	36.5	12.5	0.34
Hydrogen Fluoride	HF	20	12.5	0.63
Hydrogen Sulfide	H_2S	34	0.5	0.01
				21.36

Combined Humidity and CO_2 Control Concept

During normal operation of an EDC, the water produced by the elctrochemical reaction is transferred into the process air stream and exhausts into the cabin atmosphere for subsequent removal by a separate humidity control subsystem. For long-term space missions the water generated by the crew and by the reactions of the CO_2 removal process must be reclaimed for use within the Water Management System of the spacecraft. For short-term missions, the recovery and use of reclaimed water and CO_2 is of less importance and both may be discarded without significant weight penalties. This suggests a concept of combining the humidity control function with the CO_2 removal function by removing both water and CO_2 from the process air stream flowing through an EDC cell. The combined concept could potentially result in overall system weight and volume savings.

An analytical and experimental feasibility study was performed to investigate a combined water-CO_2 removal concept, including the design, fabrication, assembly and testing of single-cell hardware.

General Approach

The general approach selected for the combined cabin air pH_2O and pCO_2 control concept is a baseline EDC cell with a water removal cavity located adjacent to the cathode air compartment. A functional cross section of such a cell is shown in Figure 42. The concept requires control of the total pressure level in the water removal cavity as a function of the desired process air exit dew point. Neglecting any gradients in the pH_2O resulting from mass transport requirements, the total pressure of the water cavity must be controlled to be equal to the desired pH_2O of the exiting process air. Any partial pressure gradients caused by mass transport requirements result in a decrease in the total pressure requirements of the water removal compartment. For example, to remove water vapor from cabin air having an allowable dew point range of 281 to 287K (46 to 57F) requires at least a minimum total pressure in the water compartment of 1067 to 1600 N/m^2 (8 to 12 mm Hg). Reductions in mass transport-related pressure gradients are of importance since extremely low vacuum levels in the water removal cavity are more difficult to attain since low vacuum levels require large manifold systems and may result in overall cell operational limits.

Cell Design Considerations

Primary emphasis was placed on the design of the barrier between the low pressure (near vacuum) water vapor removal compartment and the high pressure (ambient) cathode air compartment. This barrier must provide positive separation between these two compartments so that only water vapor is removed from the cathode air and not the air or any of its constituents. A porous matrix, similar to that used between the cell's electrodes, filled with cell electrolyte can perform this function. The electrolyte-containing matrix provides for positive gas separation, allows for water diffusion and has the ability to maintain equilibrium or steady-state water vapor pressures with air having RH levels encountered in spacecraft atmospheres (35 to 75%). Requirements for electrolyte volume consideration as a function of cathode air RH, therefore, also apply to the separating barrier. The barrier electrolyte must be able to tolerate the low humidity

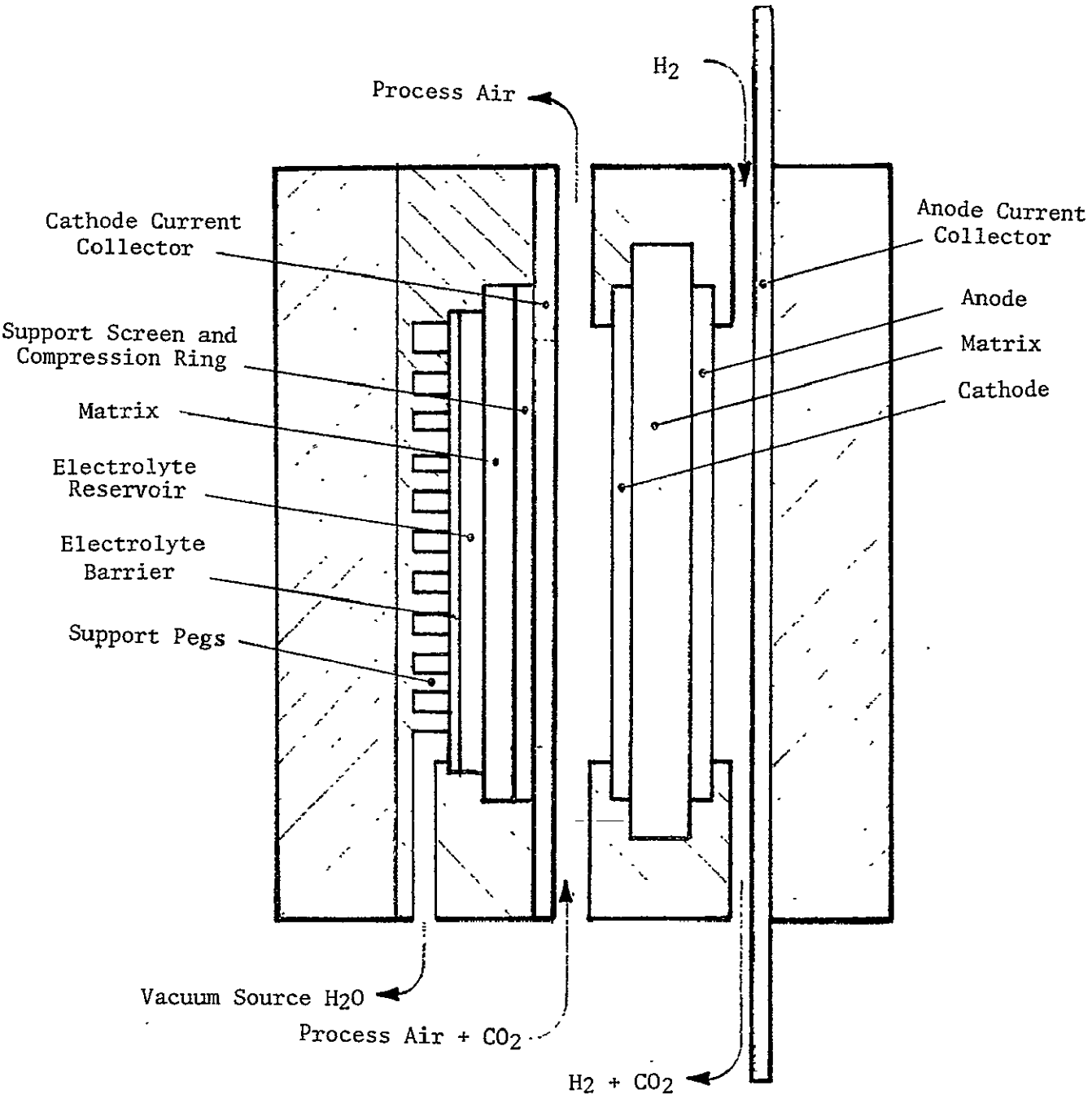

FIGURE 42 SINGLE-CELL SCHEMATIC FOR COMBINED WATER AND CARBON DIOXIDE REMOVAL

levels without precipitation while the retaining matrix must allow for changes in electrolyte volume without crossover or liquid loss corresponding to the typical ranges of cabin air humidity. These requirements suggest a two-part, porous composite, one having relatively larger pores acting as a reservoir and the second, with smaller pores, acting as the high differential pressure gas phase barrier.

Typical structural materials available to perform these functions are porous metal plaques, such as titanium or nickel, for the reservoir, and fuel cell grade asbestos for the gas separating matrix. An aqueous solution of Cs_2CO_3 cannot be used as the barrier electrolyte due to its precipitation limits. A carbonate electrolyte (LSI-B) capable of operating over the expected range of 35 to 75% RH is required.[13] Provisions to prevent liquid electrolyte loss from the composite on the water vapor compartment side, a result of a possible boiling phenomenon at the low vacuum conditions, must be included. This preventive mechanism can be provided by a hydrophobic barrier, such as a porous teflon membrane, located on the water vapor compartment side of the barrier.

As part of this study, the equations governing the mass transport of water from the cathode compartment into the water vapor compartment were derived and investigated to identify the effects of physical parameters and constants on the transport mechanisms. As mentioned above, the importance of the mass transfer relates to the resulting water vapor pressure gradient across the barrier. Should this gradient be large, the total pressure level in the water vapor removal compartment may have to be substantially lower than the lowest cabin air dew point provided, i.e., substantially lower than 1067 N/m^2 (8 mm Hg). This decrease in pressure directly affects cell design (manifolding and structural requirement) and efforts were made to minimize water transport resistance.

Carbon Dioxide and Water Removal Relationships

The relative amounts of water and CO_2 to be removed, and the conditions of the cabin air, dictate the operating parameters of the combined CO_2 and water removal cell. For purposes of this initial study, the metabolic water and CO_2 generation rates were assumed to be 1.5 kg and 1.0 kg (3.31 lb and 2.2 lb) per man-day, respectively. The cabin ambient conditions selected were a dry bulb temperature range of 291 to 297K (65 to 75F), a dew point temperature range of 281 to 287K (46 to 57F), and a maximum allowable pCO_2 of 400 N/m^2 (3 mm Hg). Besides the metabolically-generated water, the system must remove the water generated by the EDC.

Based on a TI of 2.1 at a current density of 21.5 mA/cm^2 (20 ASF) and a generation rate of 1.0 kg (2.2 lb) CO_2/man-day, 0.536 kg (1.18 lb) water/man-day are generated by the EDC. The total removal requirement, therefore, is 2.04 kg (4.49 lb) water/man-day. This total amount of water is equivalent to an EDC or fuel cell operating at an equivalent current density of 81.8 mA/cm^2 (76 ASF). A literature search investigating static water removal concepts for fuel cell systems showed that these concepts were capable of removing the water generated by fuel cells operating at ranges from 108 to 216 mA/cm^2 (100 to 200 ASF).[14]

The absolute amount of water that must be removed per unit area in a combined concept appears feasible. However, the water removal from an EDC is more difficult since the absolute pressure levels at which the water must be removed are lower than those required in fuel cells. The latter operate at 355 to 366K (180 to 200F) with similarly high dew points corresponding to water removal compartment pressures of 21 to 34 kN/m^2 (3 to 5 psia). Larger water vapor gradients can therefore be readily tolerated.

The minimum air flow rate of the combined humidity-CO_2 control cell is governed by one of three functions: (1) air flow rate based on metabolic water generation, (2) air flow rate based on metabolic CO_2 generation, or (3) air flow rate based on waste heat removal (cell cooling) requirements. For the metabolic water generation rate this minimum air flow rate was calculated to be approximately 793 dm^3/min (28 scfm) per man based on the minimum allowable outlet RH (electrolyte precipitation limit) of the process air and the minimum cabin air dew point. This compares with a similarly derived CO_2-based air flow rate requirement of only 238 dm^3/min (8.4 scfm) per man. The minimum air flow rate required to remove the waste heat generated by an electrochemical cell operating at 0.35V and 21.5 mA/cm^2 (20 ASF) is 1005 dm^3/min (35.5 scfm) per man.

These results show that the cooling air requirement is very close to the air flow requirement dictated by the water removal needs. By combining the process air and cooling air streams and flowing this total air through the cathode compartments, the cell cooling and water removal requirements can be met simultaneously. The CO_2 removal should occur at maximum efficiency for the given operating parameters due to the high average pCO_2 driving force within the cathode compartment characteristic of the higher air flow rates.

Single-Cell Design

A single water and CO_2 removal cell was designed and fabricated to perform feasibility testing. A CX-6 style cell with an internal humidifier cavity was modified by inserting a barrier between the water removal and cathode compartments. Also, the manifolding to the original humidifier cavity was enlarged to increase water vapor removal capacities at low total pressure levels. The remaining cell parts were of baseline construction.

The separation barrier was designed to consist of four basic parts: (1) a 70-mesh, 0.0254 cm (0.010 in) thick polypropylene screen, (2) a 0.0254 cm (0.010 in) thick fuel cell grade asbestos matrix, (3) a 0.127 cm (0.050 in) thick porous titanium plaque electrolyte reservoir, and (4) a 0.005 cm (0.002 in) thick Teflon electrolyte barrier. Access holes were cut into the back of the humidifier plates leading to manifold grooves machined into a plastic endplate. Direct access to the back of the water removal compartment to vacuum through the large cross sectional manifold passages allowed low absolute pressure levels to be attained during testing.

Experimental Activities

The experimental activities were divided into three parts: (1) investigation of water removal efficiency as a function of varying inlet process air dew points, (2) determination of possible CO_2 removal across the water removal barrier

solely due to diffusion through the carbonate electrolyte and (3) investigation of the effects of combined operation on overall EDC cell performance. All testing was performed while applying a continuous vacuum source to the water removal cavity resulting in a cavity total pressure level of approximately 0.133 kN/m^2 (1 mm Hg). The process air flow rate throughout all testing was held constant at 22.7 dm^3/min (0.8 scfm).

Water Removal Efficiency Investigation. During the first phase of testing the water removal capacity of the selected cell configuration was determined as a function of process air inlet dew point. For this testing the inlet air dew point was varied from 282 to 290K (48 to 63F) which corresponds to a pH_2O variation of 1.06 to 2.00 kN/m^2 (8 to 15 mm Hg). The pCO_2 of the process air was maintained at ambient levels and the cell current was set at zero to eliminate effects of internal cell water generation, possible CO_2 diffusion, or bicarbonate formation on water removal capacities.

The results of the first phase of testing are shown in Figure 43. The results demonstrate a near linear increase in water removal rate as a function of increasing process air inlet dew point over the range of dew points investigated. The data is shown as the amount of water removed per hour per unit area of barrier surface. The data show that at the maximum allowable cabin dew point of 287K (57F), 0.182 $kg/hr\text{-}m^2$ (0.0373 $lb/hr\text{-}ft^2$) of water were removed.

Based on the average metabolic generation rate of 1.50 kg (3.31 lb) of water/man-day and a water generation rate due to the EDC of 0.536 kg (1.18 lb) per man-day, a total water removal of 2.04 kg (4.49 lb) per man-day is required. Based on this requirement and on the data generated, a total surface area of approximately 0.465 m^2 (5.0 ft^2) per man is needed at a process air inlet dew point of 287K (57F). Comparing the surface area required for water removal (based on average metabolic generation rates) with that required for CO_2 removal, using baseline CS-6 type cells of 0.0227 m^2 (0.244 ft^2) per cell, shows that a total of 21 instead of 15 cells are required per man. These results indicate that the water removal function would govern the sizing of a combined-concept module.

Maximum, instantaneous water generation rates then can be experienced aboard a spacecraft and would further increase the number of cells needed to maintain cabin dew point levels within allowable limits. The exact cell number would be a function of cabin volume and the water generation profile.

Carbon Dioxide Diffusion Investigation. The second phase of testing was performed to determine the amount of CO_2 that would diffuse through the barrier separating the water compartment from the cathode compartment. This diffusion would be caused by the concentration gradient in the barrier electrolyte resulting from the different pCO_2 levels in the two compartments.

The testing was performed at zero cell current and with a 0.133 kN/m^2 (1 mm Hg) total pressure level on the water removal cavity side. The process air inlet pCO_2 was raised to 0.333 kN/m^2 (2.5 mm Hg), an approximate average value for cathode side pCO_2 levels during normal EDC cell operation. The cell was allowed to reach steady-state conditions. At this point the inlet and outlet pCO_2 of the process air were determined. Based on these values, the amount of CO_2

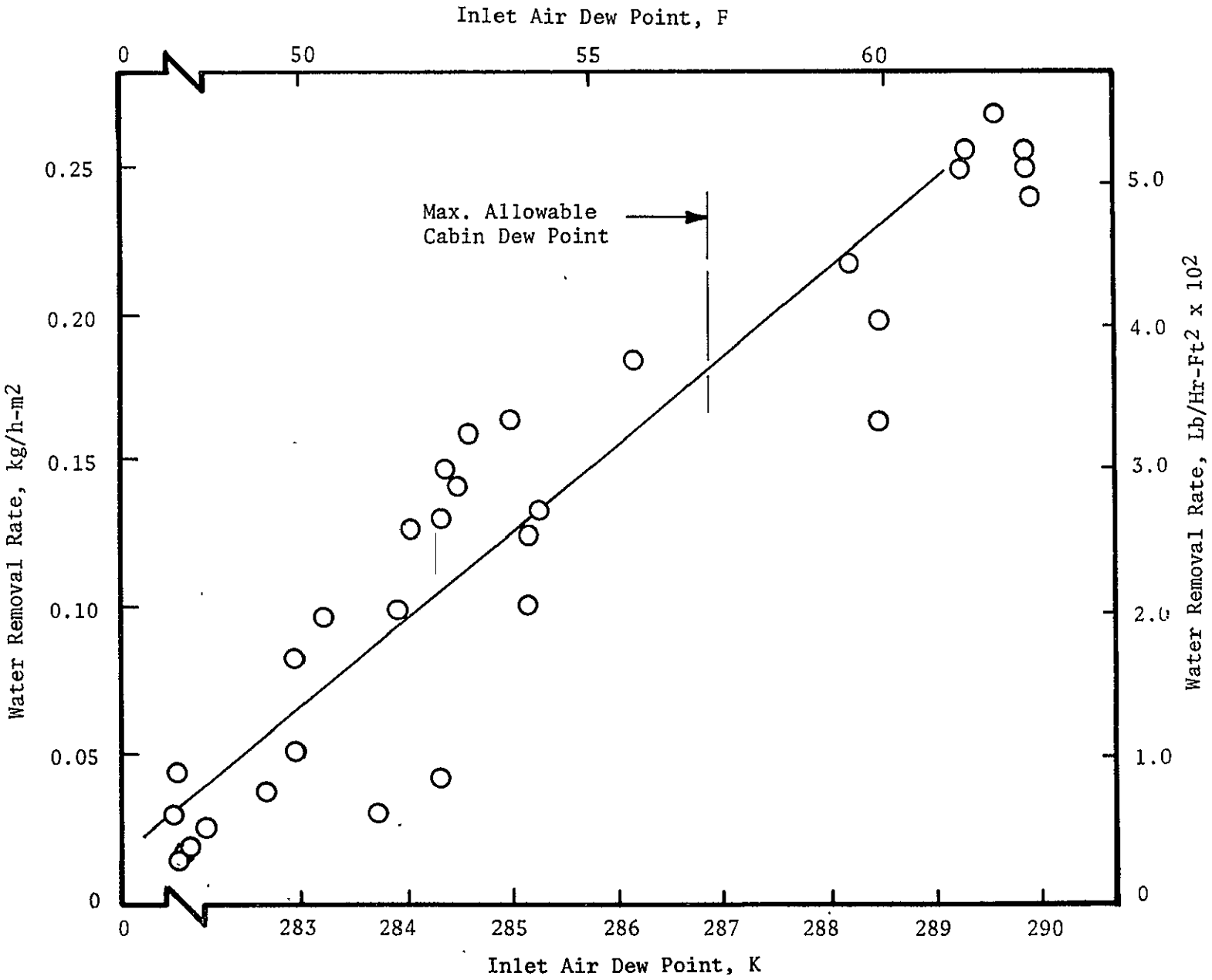

FIGURE 43 PERFORMANCE AS A FUNCTION OF INLET DEW POINT TEMPERATURE.

removed by diffusion through the water removal cavity was calculated. The results showed that only about 3.4% of the CO_2 entering the cathode compartment was removed. When compared to the normal 40 to 60% removal of CO_2 from the cathode air by the electrochemical reaction, the amount of CO_2 removed by the diffusion process, although beneficial, was considered negligible.

Combined Water and Carbon Dioxide Removal Testing. The effects of the combined operation on CO_2 and water removal were investigated during the final phase of testing. A combined-concept cell was operated for 100 hours to establish baseline CO_2 removal capacity. During this time vacuum was not applied to the water removal cavity and the cell was operated strictly as a CO_2 removal cell. Following the 100 hours of operation, during which the CO_2 removal efficiency and cell voltage were comparable to typical baseline operation, a vacuum was drawn on the water removal cavity. The vacuum level was maintained between greater than 0 and 0.133 kN/m^2 (0 and 1 mm Hg). The cell was then operated at this condition for an additional 50 hours. During this time slight variations in the process inlet air dew point were made to detect resulting changes in water removal. The data obtained during this test time indicated that the water removal capacity was independent of the CO_2 removal function and that the data followed the results of the first phase of the testing, as represented in Figure 43. Also, the water removal function did not appear to interfere with the CO_2 removal process.

Based on the results of the testing, a combined water and CO_2 removal concept module is feasible. Trade studies should be performed to compare the tested concept with combined water and CO_2 removal systems such as are presently envisioned for Shuttle Orbiter application.[15,16]

EDC for Shuttle Application

For short-term space missions, i.e., Gemini or Apollo, nonregenerative CO_2 removal methods using chemicals such as lithium hydroxide (LiOH) absorbents, proved to be simple and lightweight. However, as mission length increases, both the volume and weight of the expendable LiOH increases quickly until a regenerative CO_2 removal method with its lower expendable weight penalties becomes competitive. As a regenerative CO_2 removal method, the EDC offers high reliability, no scheduled maintenance, and minimal expendables. As part of this program, a preliminary mini-design of an EDC for Shuttle application was performed.

Subsystem Design

The design specifications used for the Shuttle-oriented EDC subsystem are presented in Table 12. A simplified schematic of the proposed subsystem is shown in Figure 44. The design approach follows the Shuttle philosophy of requiring no scheduled and only minimal unscheduled crew maintenance by utilizing component redundancy wherever feasible. The unit contains two process air blowers, two air filters, eight electrically operated valves, two thermal regulating valves, two gas pressure regulators, four check valves, seven electronic sensors, a liquid-to-air heat exchanger, one electronic control package and a 15-cell electrochemical module (projected second generation AEDCM).

TABLE 12 SHUTTLE DESIGN REQUIREMENTS[15]

Crew Size, Men	4
Mission Duration, Day	7, +2 contingency
CO_2 Production Rate, kg/hr (Lb/hr)	0.17 (0.37)
Cabin Pressure, kN/m^2 (Psia)	101.3 (14.7)
Cabin Volume, m^3 (Ft^3)	28.3 (1000)
CO_2 Partial Pressure, N/m^2 (mm Hg)	
Nominal	666.6 (5.0)
Maximum	1013.2 (7.6)
Cabin Temperature, K (F)	289.5 to 298 (65 to 80)
Cabin Dew Point, K (F)	275 to 288 (39 to 63)
Coolant	Water
Heat Rejection Penalty, kg/kW (Lb/kW)	179.6 (396)
Power Penalty	
Fixed Weight, kg/kW (Lb/kW)	72.6 (160)
Expendables, kg/kW-h (Lb/kW-Hr)	0.603 (1.333)

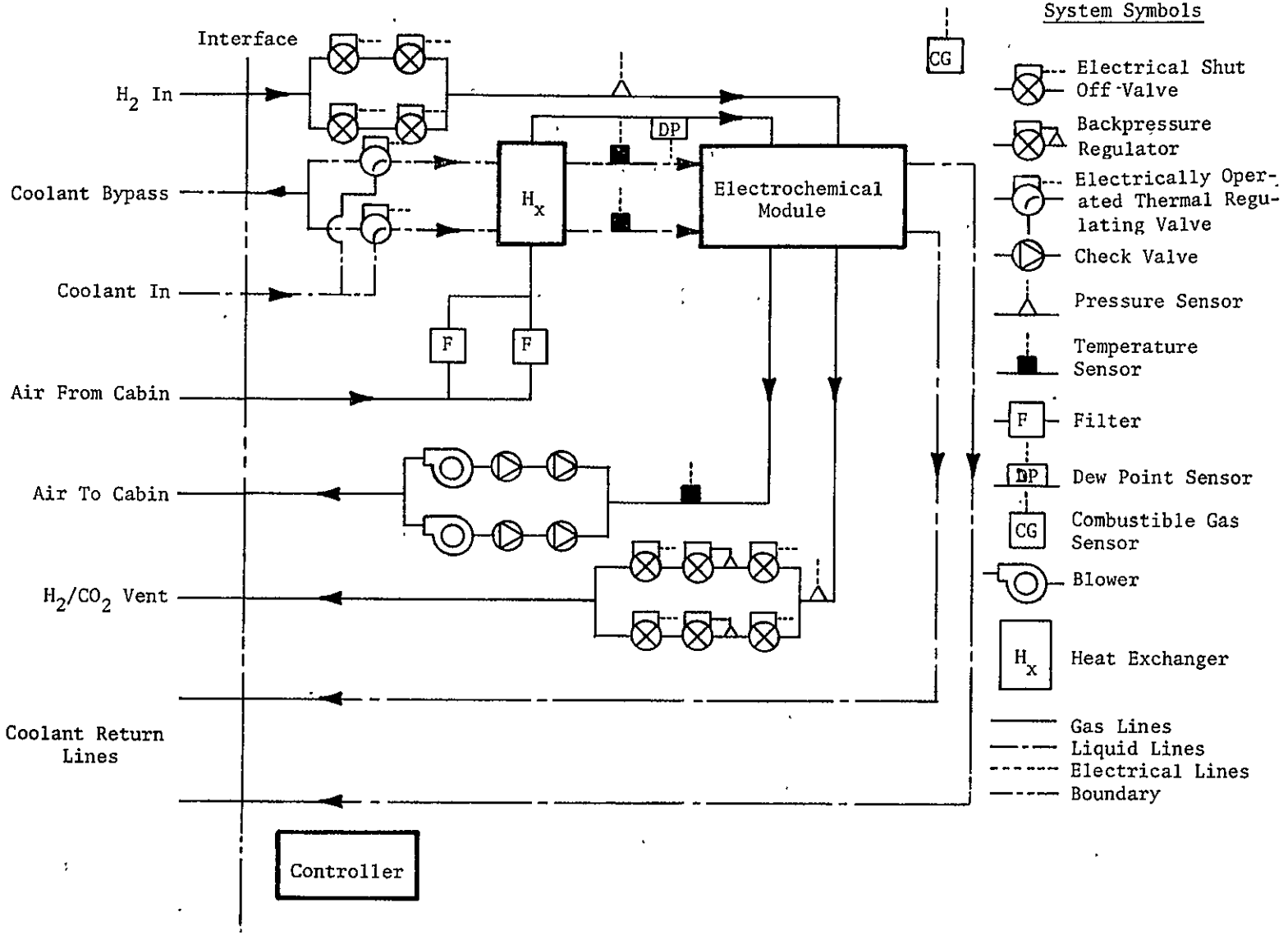

FIGURE 44 SCHEMATIC FOR SPACE SHUTTLE ORIENTED CO_2 COLLECTION SUBSYSTEM

In an effort to minimize subsystem weight, the electrochemical module used for the preliminary design was a projected second generation AEDCM design containing 15 cells. Each cell has an active electrode area of 453 cm^2 (0.488 ft^2). The Shuttle-designed module would use cell housings, cathode current collector cooling fins and insulation plates thinner than those used for the AEDCM and would use lightweight honeycomb structural endplates similar to those developed for the CS-6 style EDC modules. By reducing the cell housing thickness the individual cell weight can be reduced to 0.78 kg (1.71 lb) without directly affecti any of the cell's CO_2 removal components. Furthermore, fabricating honeycomb structural endplates and using insulation plates only as thick as the cathode cooling compartment requires results in a total projected module weight of 18.06 kg (39.82 lb). Table 13 is a summary of the module design characteristics.

The module is projected to operate at 32.3 mA/cm^2 (30 ASF) with a TI of 2.5 (92%) at an average pCO_2 of 666.5 N/m^2 (5 mm Hg). The average projected cell voltage is 0.35V/cell, producing a total 76.9W of unregulated DC power. The module is designed to operate over a current density range from 0 to 1.3 times of the design current density to allow for variable CO_2 removal rates (based on CO_2 generation) should this mode of operation be desirable.

The control instrumentation includes circuitry to monitor and control all important operating parameters and interfaces with the Shuttle data management computer for fault detection and isolation analysis. The controller utilizes circuitry similar to that developed for the SSP CO_2 Collection Subsystem to control the Shuttle pCO_2 levels.[5]

A list of the Shuttle EDC Subsystem components is presented in Table 14. Included in the table are weight, volume and power requirements of each component and of the total subsystem. The projected subsystem weighs 46.5 kg (102 lb), occupies 0.13 m^3 (4.74 ft^3) and requires 109W of power assuming module power utilization, or 186W if the module power is not used.

Total Equivalent Weight

The total equivalent weight of a subsystem must include the fixed hardware weight, a heat rejection weight penalty, a power weight penalty, and an expendable weight penalty. Table 15 contains the heat rejection and power penalties for the EDC subsystem and Table 16 summarizes the subsystem total equivalent weight. For a 28 man-day mission, the total equivalent weight for a four-man EDC is 154.3 kg (339.6 lb) if full credit is given to the EDC generated power. If this power is not used the weight equals 167.5 kg (369.2 lb).

EDC/LiOH Comparison

Presently, a LiOH CO_2 removal concept is planned for the Shuttle Orbiter. Because LiOH is not regenerative, the advantage of the relatively lightweight concept decreases rapidly due to the required expendables as mission length and/or crew size increases, a LiOH subsystem also requires scheduled maintenance in order to replace the expended adsorption beds with fresh LiOH.

TABLE 13 SHUTTLE DESIGNED EDC MODULE CHARACTERISTICS

Cell Weight, kg (Lb)	0.78 (1.71)
Cell Frame	0.26 (0.57)
Anode Current Collector	0.56 (0.12)
Cathode Current Collector	0.25 (0.55)
Misc. Cell Parts	0.21 (0.47)
Endplate Weight (2), kg (Lb)	6.43 (14.17)
Number of Cells	15
Module Weight, kg (Lb)	18.06 (39.82)
Operating Current, A	14.64
Active Electrode Area, cm^2 (Ft^2)	452.9 (0.488)
Current Density, mA/cm^2 (ASF)	32.3 (30)
Transfer Index, Mass CO_2/Mass O_2	2.5
Average Cell Voltage, V	0.35

TABLE 14 SHUTTLE EDC SUBSYSTEM COMPONENT SIZES

Component Description	Component				Subsystem		
	Weight, kg (Lb)	Volume, dm^3 (Ft^3)	Power, Watt	No. Reqd	Weight, kg (Lb)	Volume, dm^3 (Ft^3)	Power, Watt
Module	18.1 (39.8)	19.8 (0.70)	-76.9	1	18.1 (39.8)	19.8 (0.70)	-76.9
Valve, Check, Air	0.3 (0.6)	1.4 (0.05)	0	4	1.2 (2.4)	5.7 (0.20)	0
Blower	2.5 (5.6)	5.7 (0.20)	150	2	5.1 (11.2)	11.3 (0.40)	150(a)
Filter, Air	0.5 (1.0)	2.8 (0.10)	0	2	1.0 (2.0)	5.7 (0.20)	0
Heat Exchanger	1.4 (3.0)	1.7 (0.06)	0	1	1.4 (3.0)	1.7 (0.06)	0
Valve, Thermal, Regulating	0.3 (0.6)	1.4 (0.05)	8	2	0.5 (1.2)	2.8 (0.10)	8(a)
Valve, Electrical, H_2 and H_2+CO_2	0.2 (0.5)	0.3 (0.01)	8	8	1.8 (4.0)	2.3 (0.08)	8(b)
Regulator, H_2+CO_2	0.3 (0.6)	1.4 (0.05)	0	2	0.5 (1.2)	2.8 (0.10)	0
Sensor, Temperature	0.1 (0.1)	0.6 (0.02)	0(c)	3	0.2 (0.3)	1.7 (0.06)	0(c)
Sensor, Dew Point	0.1 (0.1)	1.4 (0.05)	0(c)	1	0.1 (0.1)	1.4 (0.05)	0(c)
Sensor, Combustible Gas	0.5 (1.0)	2.8 (0.10)	0(c)	1	0.5 (1.0)	2.8 (0.10)	0(c)
Sensor, H_2 Pressure	0.1 (0.1)	0.6 (0.02)	0(c)	2	0.1 (0.2)	0.6 (0.02)	0(c)
Controller	5.4 (12.0)	8.5 (0.30)	20	1	5.4 (12.0)	8.5 (0.30)	20
	Component Subtotal:				35.8 (78.4)	67.1 (2.37)	109.1
	Packaging at 30% for Wt. and 100% for Vol.				10.7 (23.5)	67.1 (2.37)	- -
	System Total:				46.5 (101.9)	134.2 (4.74)	109.1

(a) Only one unit powered at a time
(b) Power needed only during valve operation (assumed to average 1W per valve)
(c) Power for fault isolation contained in Shuttle information subsystem

TABLE 15 EDC WEIGHT PENALTIES

Heat Generated, W			
Module (Sensible)[a]	193.3		
Module (Latent)[b]	46.3		
Electrical Valves	8.0		
Blower	150.0		
Instrumentation	20.0		
Total	417.6		
Heat Rejection Penalty, kg (Lb)[c]		75.0	(165.4)
Power Consumed, W	186.0		
Power Generated, W[d]	-76.9		
Total	109.1		
Power Penalty, kg (Lb)[e]			
Fixed		7.9	(17.5)
Expendable		11.1	(24.4)
Total Penalty Weight, kg (Lb)		94.0	(207.3)
Total Penalty Weight[f], kg (Lb)		107.3	(236.9)

(a) 15 cells x (1.23V -0.35V x 14.64A)
(b) 15 cells x 14.64A x 7.4 x 10^{-4} Lb Water/Cell-A-Hr x 284.8W-Hr/Lb Water
(c) 179.6 kg/kW (396 Lb/kW)
(d) Unregulated DC power produced by the EDC, 15 cells x 14.64A x 0.35V
(e) 72.6 kg/kW + 0.603 kg/kW-h (160 Lb/kW + 1.333 Lb/kW/Hr)
(f) Not utilizing EDC generated power

TABLE 16 EDC TOTAL EQUIVALENT WEIGHT[a]

Basic Subsystem Weight, kg (Lb)	46.5	(101.9)
Heat Rejection Penalty, kg (Lb)	75.0	(165.4)
Fixed Power Penalty[b], kg (Lb)	7.9	(17.5)
Total Fixed Weight, kg (Lb)	129.4	(284.8)
Expendable Oxygen Penalty[c], kg (Lb)	12.3	(27.0)
Expendable Hydrogen Penalty[c], kg (Lb)	1.5	(3.4)
Expendable Power Penalty[b], kg (Lb)	11.1	(24.4)
Total Expendable Weight, kg (Lb)	24.9	(54.8)
Total EDC Equivalent Weight, kg (Lb)	154.3	(339.6)
Total EDC Equivalent Weight[d], kg (Lb)	167.5	(369.2)

(a) For 28 man-day mission, unspared
(b) Utilizing EDC power
(c) Includes 10% tankage penalty
(d) Not utilizing EDC power

Figure 45 is a simplified schematic of a Shuttle applicable system and Table 17 lists the weights, volumes and power requirements of the components found in a LiOH based subsystem. Although fixed weight and heat rejection penalties are less for the LiOH method, both the power penalties (due to the lack of generated power) and expendables are less for the EDC. Table 18 lists the heat rejection and power penalties for the LiOH unit and Table 19 lists the system's total equivalent weight.

Figure 46 compares total equivalent weights of the EDC and the LiOH subsystems. The LiOH unit exhibits an initially lower total equivalent weight which increases slowly as power and expendables are required. The EDC weight starts higher but increases at a slower rate until it is equal to the LiOH system after 22 man-days with EDC power use and 31 man-days without EDC power use. At the end of a 120 man-day mission, the EDC is lower in equivalent weight by 163.0 kg (358.5 lb).

COMPOSITE CARBON DIOXIDE REMOVAL PROCESS

Present physiological considerations project possible requirements of operating space cabin atmospheres at lower than 400 N/m^2 (3 mm Hg) pCO_2 levels. As the pCO_2 in the atmosphere decreases, EDC CO_2 removal efficiency also decreases, resulting in increased hardware and power requirements. One possible method by which a CO_2 removal process could yield higher removal efficiencies at low pCO_2 levels is by combining a chemical pre- and post-sorber with the EDC and cyclically alternating the flow direction of the process air. The feasibility of such a scheme was evaluated as part of this program.

Concept Description

The composite CO_2 removal method derived and analyzed is shown in Figure 47. The concept allows process air, partially depleted of CO_2, to exit the EDC and enter a post-sorber. Here the remaining CO_2, or a large portion of it, is adsorbed. When the sorbing chemical reaches its maximum capacity, the flow is reversed with the process air now entering the initial post-sorber. By changing the operating conditions of the now pre-sorber, i.e., increasing the temperature, the CO_2 collected on the chemical is driven off and enters the EDC. This increases the inlet pCO_2 above the cabin level, increasing the EDC efficiency. As the air flows through the EDC a portion of the CO_2 is removed with the remaining CO_2 removed by the post-sorber , or former pre-sorber. The air exiting from the composite system is at a very low (or zero) pCO_2 level while the system still can take advantage of the EDC's higher efficiency at higher pCO_2 levels.

Concept Evaluation

The composite concept was evaluated on an equivalent weight basis. Comparisons were not made at a total system level, but only between the total equivalent, unspared weight of the EDC module sized to operate directly with the cabin air pCO_2 versus an EDC module sized to operate with pre- and post-sorbers, but at an inlet pCO_2 higher than that of the cabin. Peripheral system components such as valves and blowers were assumed to vary equally with cabin pCO_2 for either approach; a safe assumption considering the preliminary nature of the evaluation. A decision was made to use state-of-the-art hardware to allow the comparison to be made at equal levels of development.

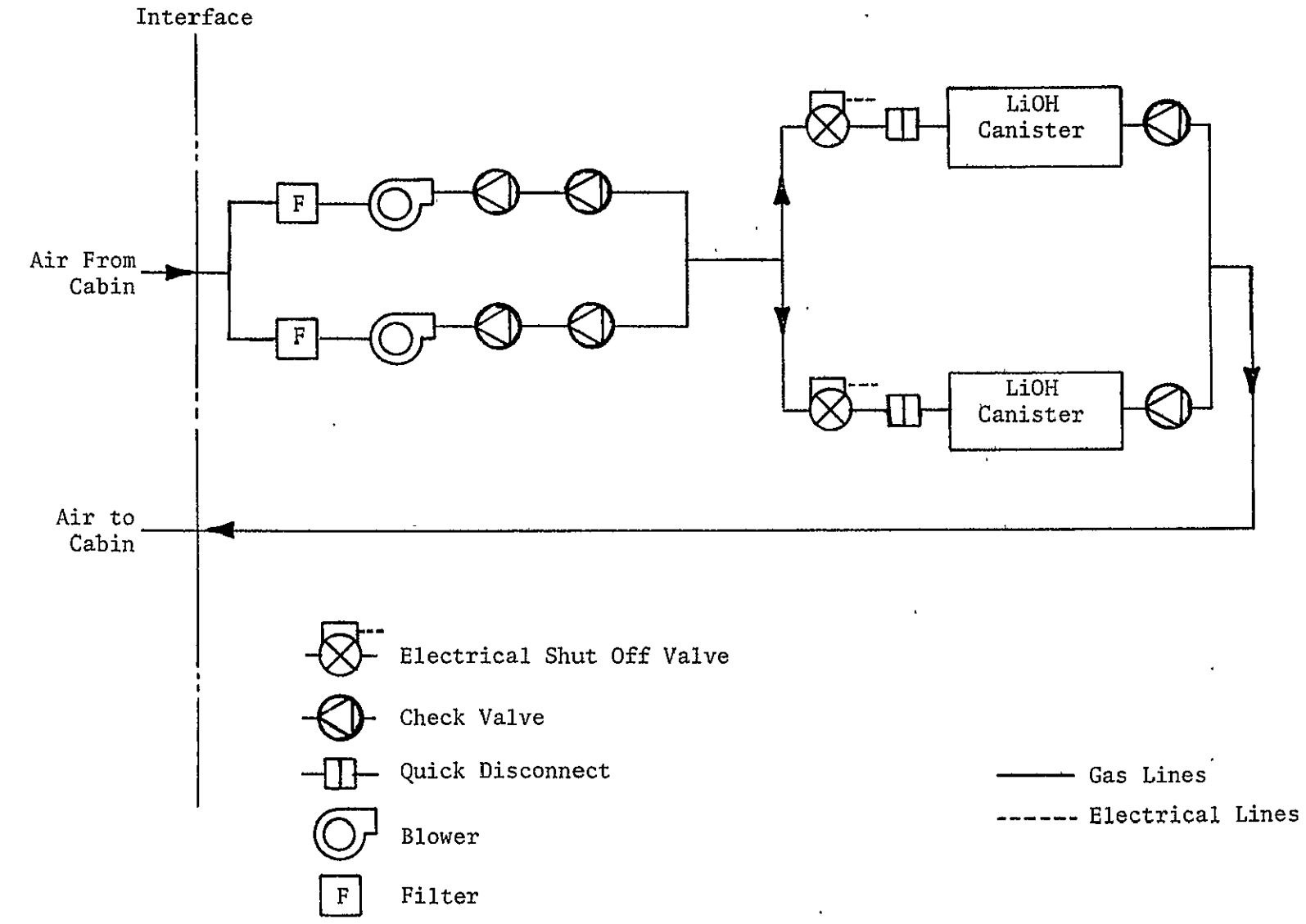

FIGURE 45 SCHEMATIC SPACE SHUTTLE LiOH SUBSYSTEM

TABLE 17 LiOH SUBSYSTEM COMPONENT SIZE

Component Description	Component				Subsystem		
	Weight, kg (Lb)	Volume, dm^3 (Ft^3)	Power, Watt	No. Reqd	Weight, kg (Lb)	Volume, dm^3 (Ft^3)	Power, Watt
LiOH Canister	7.9 (17.5)	14.2 (0.50)	--	2	15.9 (35.0)	28.3 (1.0)	--
Blower	2.5 (5.6)	5.7 (0.20)	150	2	5.1 (11.2)	11.3 (0.4)	150 (a)
Valve, Check, Air	0.3 (0.6)	1.4 (0.05)	--	6	1.6 (3.6)	8.5 (0.3)	--
Filter	0.5 (1.0)	2.8 (0.10)	--	2	0.9 (2.0)	5.7 (0.2)	--
Valve, Electrical, Air	0.5 (1.0)	0.8 (0.03)	12	2	0.9 (2.0)	1.7 (0.06)	2 (b)
	Component Subtotal:				24.4 (53.8)	55.5 (1.96)	152
	Packaging at 30% for Wt. and 100% for Vol.				7.3 (16.1)	55.5 (1.96)	--
	System Total:				31.7 (69.9)	111.0 (3.92)	152

(a) Only one blower powered at a time
(b) Power needed only during valve operation (assumed 2W per valve)

TABLE 18 LiOH WEIGHT PENALTIES

Heat Generated, W			
LiOH Canister (Sensible)[15]	90.3		
LiOH Canister (Latent)[15]	45.1		
Solenoid	2.0		
Blower	150.0		
Total	287.4		
Heat Rejection Penalty[a], kg (Lb)		51.6	(113.8)
Power Consumed, W	152.0		
Power Penalty[a], kg (Lb)			
Fixed		11.0	(24.3)
Expendable		15.4	(34.0)
Total Penalty Weight, kg (Lb)		78.0	(172.1)

(a) See Table 15

TABLE 19 LiOH TOTAL EQUIVALENT WEIGHT[a]

Basic Subsystem Weight, kg (Lb)	31.7	(69.9)
Heat Rejection Penalty, kg (Lb)	51.6	(113.8)
Fixed Power Penalty, kg (Lb)	11.0	(24.3)
Total Fixed Weight, kg (Lb)	94.3	(208.0)
Expendable LiOH[b], kg (Lb)	55.6	(122.5)
Expendable Power Penalty, kg (Lb)	15.4	(34.0)
Total Expendable Weight, kg (Lb)	71.0	(156.5)
Total LiOH Equivalent Weight, kg (Lb)	165.3	(364.5)

(a) For 28 man-day mission, unspared
(b) Based on one 7.9 kg (17.5 Lb) LiOH cartridge per four man per day[15]

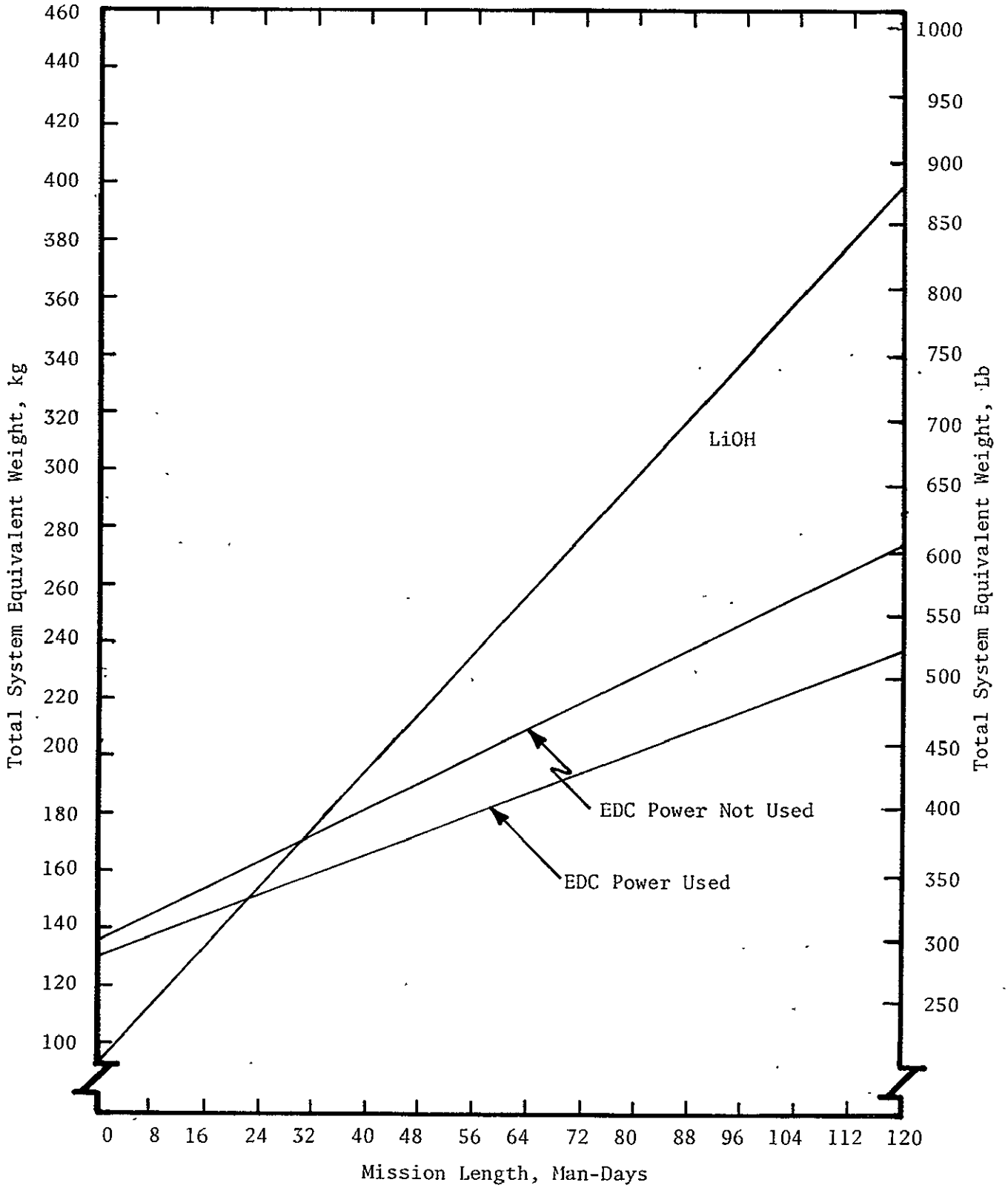

FIGURE 46 EDC/LiOH TOTAL EQUIVALENT WEIGHT COMPARISON

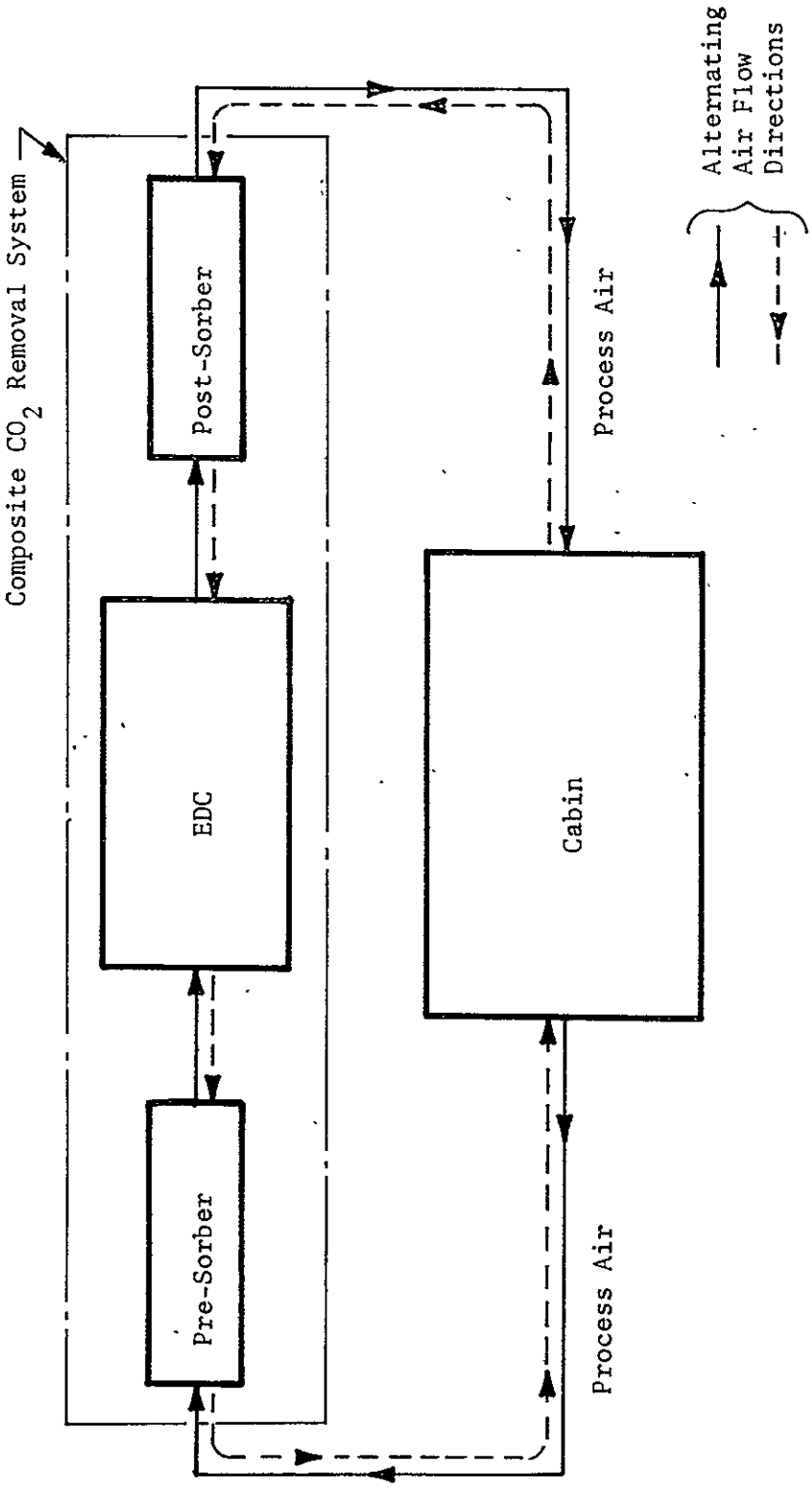

FIGURE 47 COMPOSITE CO_2 REMOVAL DIAGRAM

During the initial portion of the study various sorbent materials were evaluated, including solid amines, regenerative alkali metal carbonates, metal hydroxides, and molecular sieves. A molecular sieve (type 5A)[17] CO_2 sorbent was selected. Table 20 lists the major design specifications used for the comparison. Figure 48 is referenced in Table 20 and presents the EDC CO_2 removal performance used. Figure 49 is a functional schematic of the concept evaluated. Since molecular sieves have an affinity for water, each sorbent bed requires two predriers, one for each flow direction. Again, a molecular sieve material (type 13X)[18] was selected to perform the drying function.

Concept Operation

The selected concept operates as follows (see Figure 49). Cabin air is drawn through Drier No. 1 where moisture is removed from the air. The air then passes through a regenerative heat exchanger where it is pre-warmed prior to entering Molecular Sieve A. The latter is being heated, driving off previously adsorbed CO_2 which is added to that of the cabin, raising the pCO_2 to the EDC. Drier No. 2 is also heated, driving off the water adsorbed previously from the EDC exhaust air. Prior to entering the EDC, the air enriched in CO_2 and near a cabin humidity level is cooled in the regenerative heat exchanger.

Air leaving the EDC contains water and CO_2. The first is adsorbed in Drier No. 3, while the CO_2 is adsorbed in Molecular Sieve B. Both Drier No. 3 and Molecular Sieve B have been cooled to room temperature. Drier No. 4 is being heated to remove the moisture previously adsorbed. When Molecular Sieve A and Drier No. 2 are desorbed, the air flow direction is switched and the process reverses. All adsorbers are sized to provide for zero breakthrough of either CO_2 or water within a selected cycle time.

Equivalent Weight Calculations

Expressions were derived for the equivalent weights of the AEDCM as a function of air inlet pCO_2 and of the composite system as a function of cabin pCO_2 and pH_2O, and cycle and heatup times.

AEDCM Equivalent Weight

The total equivalent weight of the AEDCM (W_{EDCM}) consists of fixed hardware weight (W_H), sensible heat load penalty (W_{SH}), latent heat load penalty (W_{LH}), and O_2 consumption penalty (W_{O_2}).

Based on the hardware weight of the present AEDCM of 1.02 kg (2.25 lb) per cell, an endplate weight of 6.4 kg (14.2 lb) per set, and the weight penalties of Table 20 an expression for equivalent weight of the module (W_{AEDCM}) as a function of TI was derived, or

$$W_{AEDCM} = \left(\frac{655.8}{TI} + 6.4\right) \text{ kg} \qquad (13)$$

Using the TI versus inlet pCO_2 relationship of Figure 48, the equivalent weight of the AEDCM as a function of pCO_2 was calculated and is shown in Figure 50.

TABLE 20 COMPOSITE CO_2 REMOVAL SYSTEM DESIGN SPECIFICATIONS

Capacity, Number of Men	6
CO_2 Removal Requirement, kg/d (Lb/Day)	6.0 (13.2)
Cabin Pressure, kN/m^2 (Psia)	101.2 (14.7)
Cabin Temperature, K (F)	291 to 297 (65 to 75)
Cabin Dew Point, K (F)	281 to 287 (46 to 57)
Cabin pO_2, kN/m^2 (Psia)	22.0 (3.2)
Cabin Diluent	N_2
EDC Module Hardware Level	AEDCM
EDC Current Density, mA/cm^2 (ASF)	21.5 (20)
EDC Cell Voltage, V	0.35
CO_2 Removal Performance	Figure 48
Minimum Air Flow per Cell, dm^3/m (Scfm)	22.7 (0.80)
Maximum Number of Cells per EDC Module	30
Pre- and Post- CO_2 Sorbent	Molecular Sieve (Type 5A)
Water Vapor Sorbent	Molecular Sieve (Type 13X)
Molecular Sieve Desorption Temperature, K (F)	533 (500)
Composite System Cycle Time	Variable
Power Penalty (raw DC),[6] kg/kW (Lb/kW)	122.7 (270)
Heat Load Penalty[6] (to Ambient), kg/kW (Lb/Btu/Hr)	199 (128)
Water Vapor Rejection to Ambient,[6] kg/kg H_2O/h (Lb/Lb H_2O/Hr)	134 (134)
O_2 Consumption,[6] kg/kg O_2/h (Lb/Lb O_2/Hr)	1536 (1536)

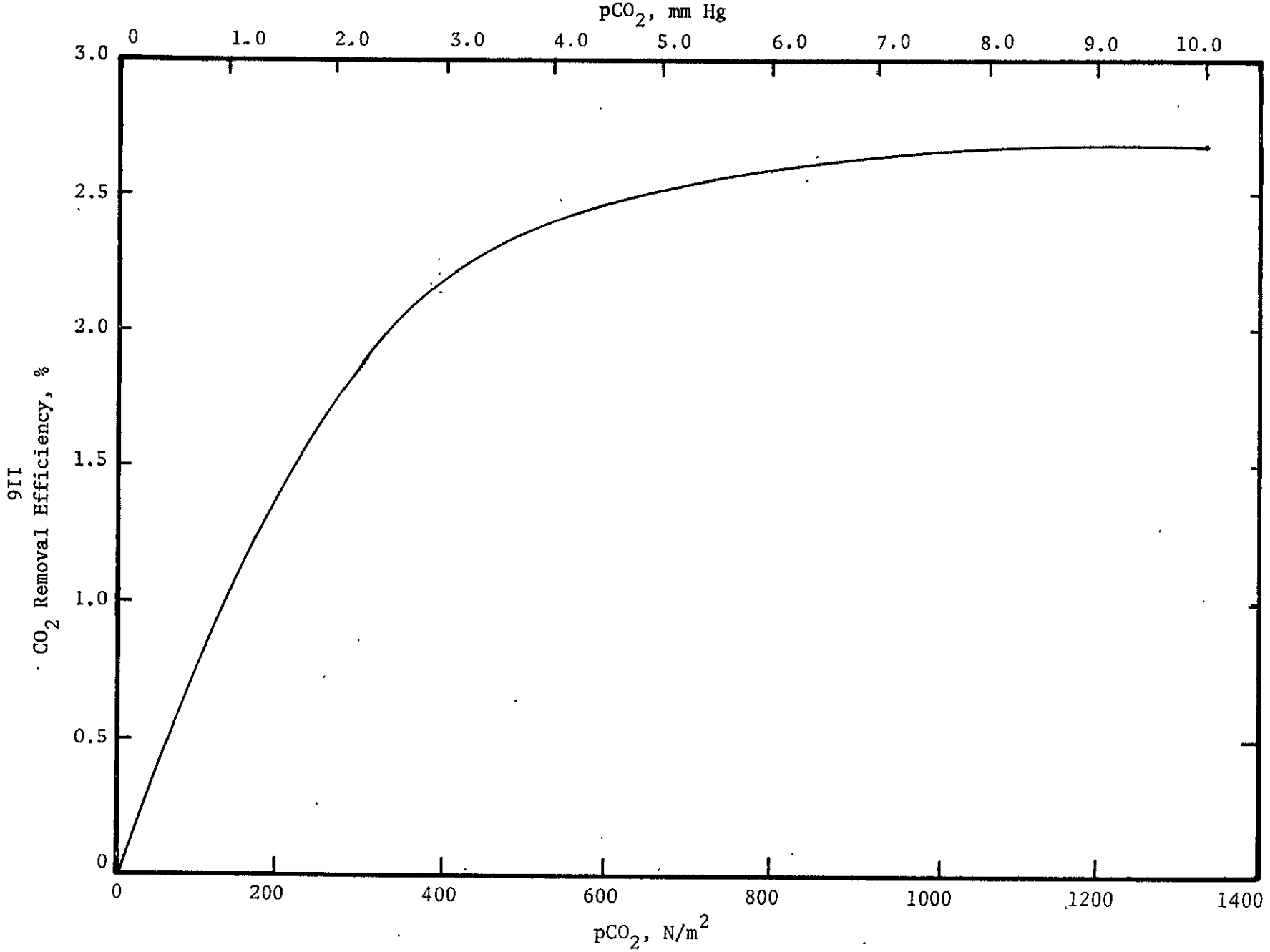

FIGURE 48 EDC CO_2 REMOVAL EFFICIENCY AS A FUNCTION OF CABIN pCO_2

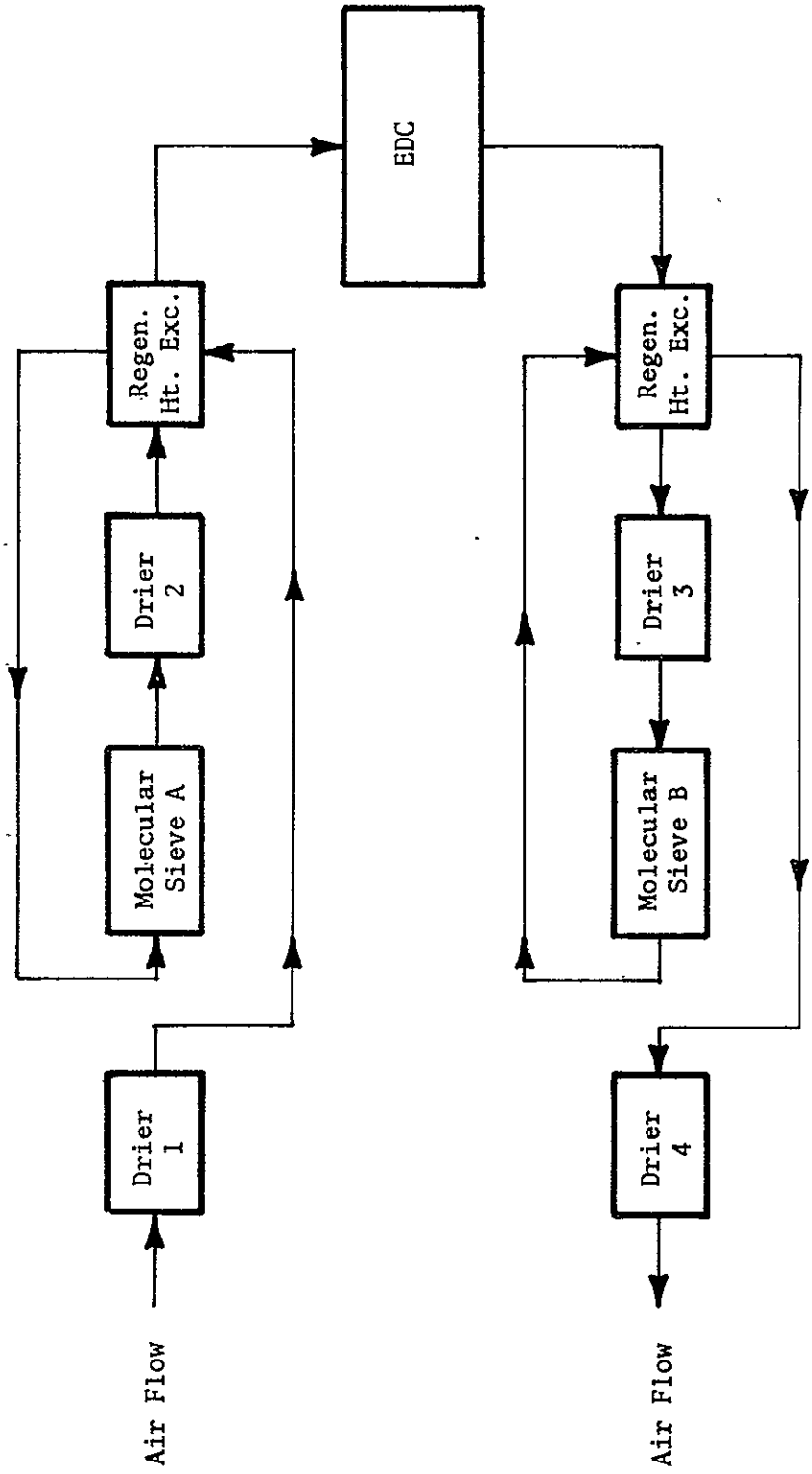

FIGURE 49 COMPOSITE CO_2 REMOVAL SYSTEM FUNCTIONAL SCHEMATIC

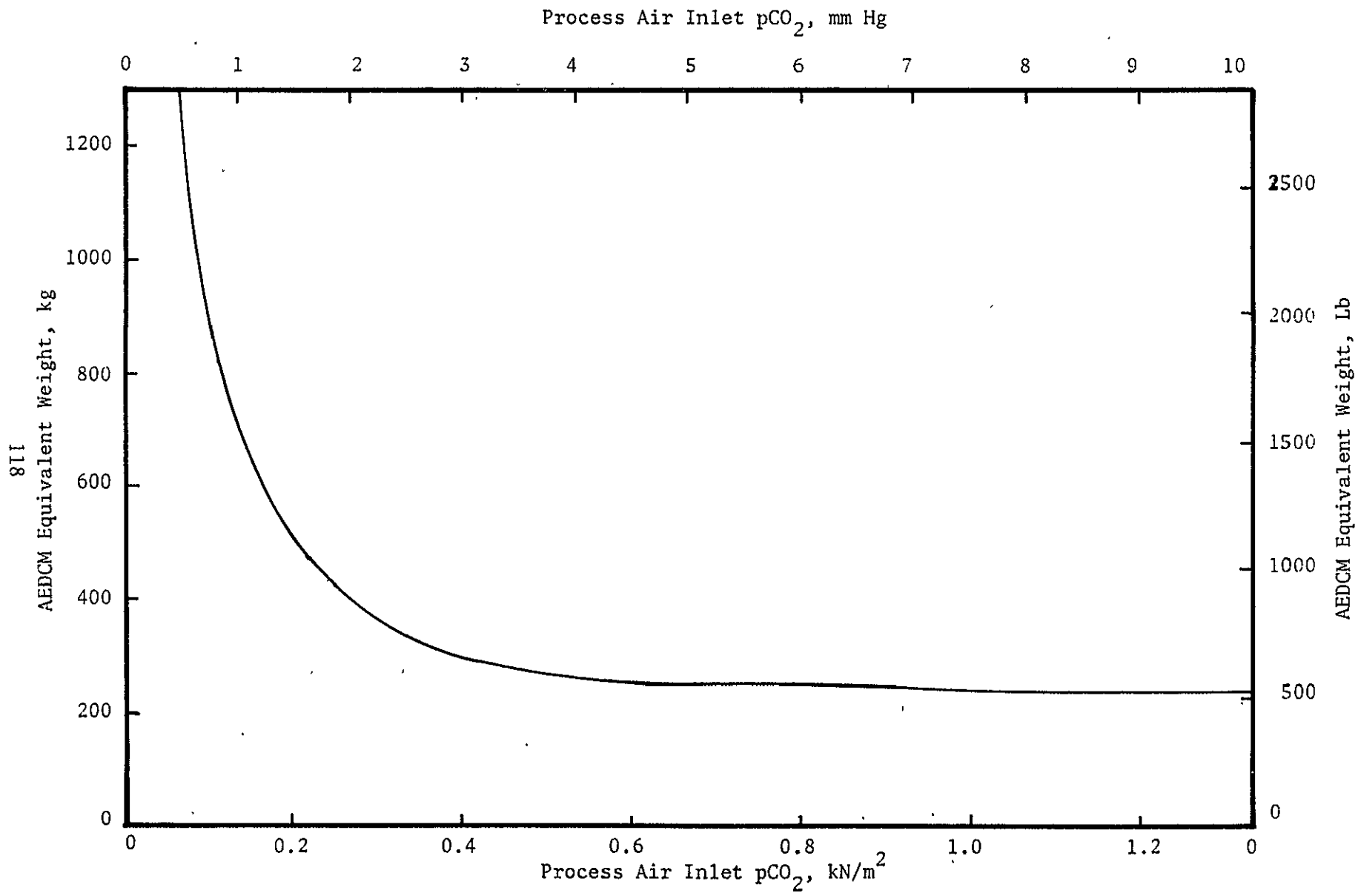

FIGURE 50 AEDCM EQUIVALENT WEIGHT VERSUS INLET AIR pCO_2

Composite System Equivalent Weight

The total equivalent weight of the components of the composite system (W_{COMS}) used for the comparison consists of the hardware weights of an AEDCM, two CO_2-adsorbing molecular sieves and four water vapor adsorbing molecular sieves. The weights of the regenerative heat exchangers (having an assumed effectiveness of 85%) were assumed negligible compared to other components. In addition to the hardware weights, the penalty weights for the power to heat one CO_2 adsorbing molecular sieve and two water vapor adsorbing molecular sieves per cycle as well as the heat load penalties for heating the air (considering the 85% effective regenerative heat exchanger) were included.

The net expression for W_{COMS} was expressed in terms of cabin pCO_2, cabin pH_2O, pCO_2 at the EDC inlet, TI of the EDC, cycle time and heatup time. The performance characteristics used for the two molecular sieve types are shown in Figures 51 and 52 for the CO_2 sorber and water sorber, respectively. The solution of the equivalent weight equation was computerized and solved for various values of the six variables.

Figure 53 shows the equivalent weight for the composite system components as a function of cabin air pCO_2 for typical values of cabin pH_2O, EDC inlet pCO_2 and cycle and heat-up/cool-down times as listed in Figure 53. Also shown in Figure 53 for comparison is the total equivalent weight of the AEDCM (same as Figure 50).

Concept Comparison

The results as shown in Figure 53 indicate that at no cabin air pCO_2 level is the composite concept competitive. The slopes of the curves also show that they do not intersect at practical pCO_2 levels. The results obtained for different values in system parameters compared to those used to obtain Figure 53 (EDC inlet pCO_2, process air inlet pH_2O, etc.) resulted in a similar conclusion.

The least load and power penalties associated with the CO_2 and water sorbers more than offset the hardware weight savings that result using the composite concept. An EDC directly interfacing with air at the cabin pCO_2 level still appears to be the most economical approach for the application considered.

CONCLUSIONS

The following conclusions are a direct result of the program studies.

1. The process air pressure drop through EDC cells using expanded metal (Exmet) cavity spacers can be analytically predicted using geometric constants of Exmet configurations. Also, Exmet process air cavity spacers increase mass transport of CO_2 to the electrolyte-air interface by increasing air turbulence. Resulting increases in process air pressure drop are more than offset by gains in CO_2 removal efficiency since at equal blower power cells using Exmet showed an 87% increase in CO_2 removal efficiency compared to cells using simple slotted process air cavity spacers.

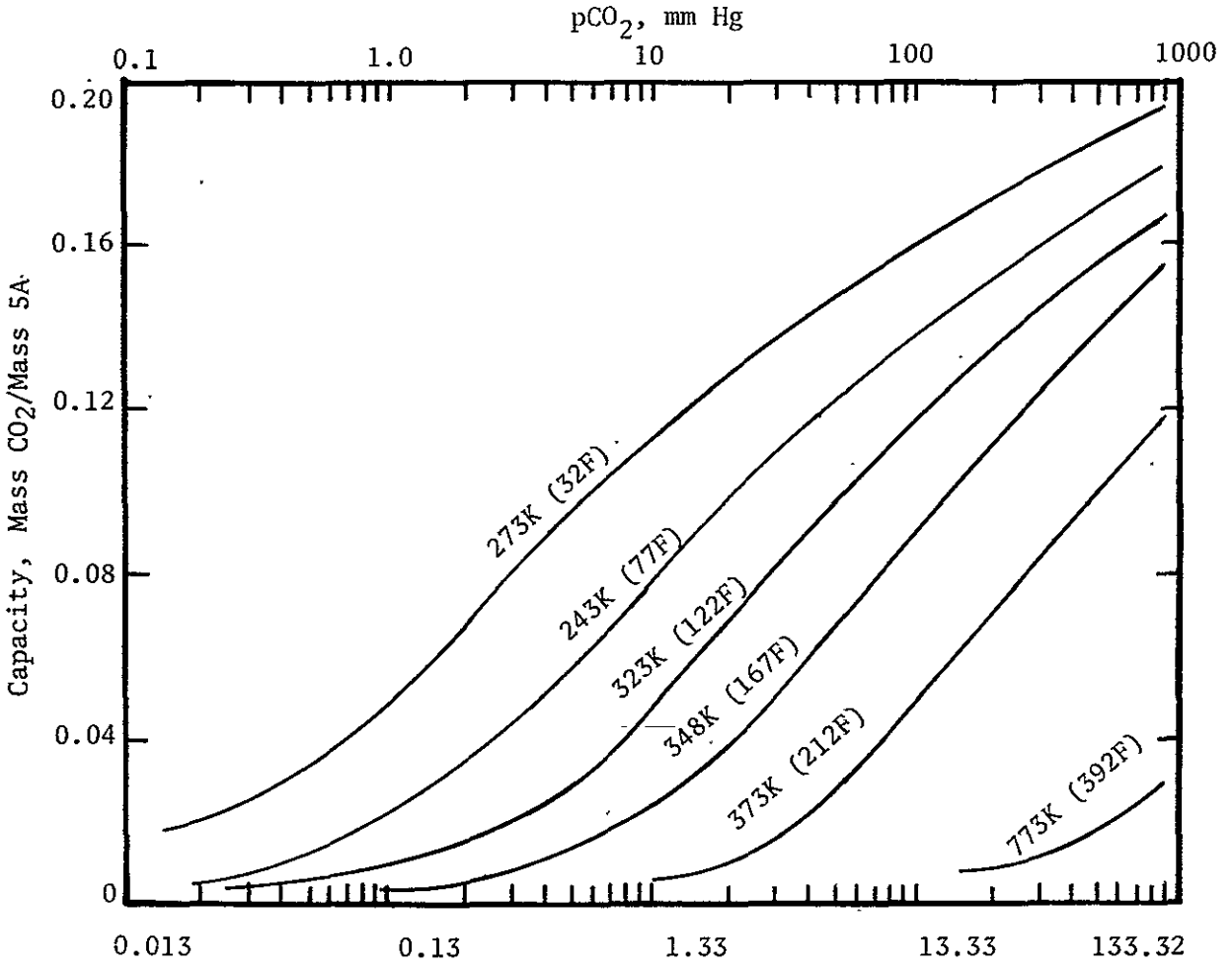

FIGURE 51 MOLECULAR SIEVE CO_2 CAPACITY[17]

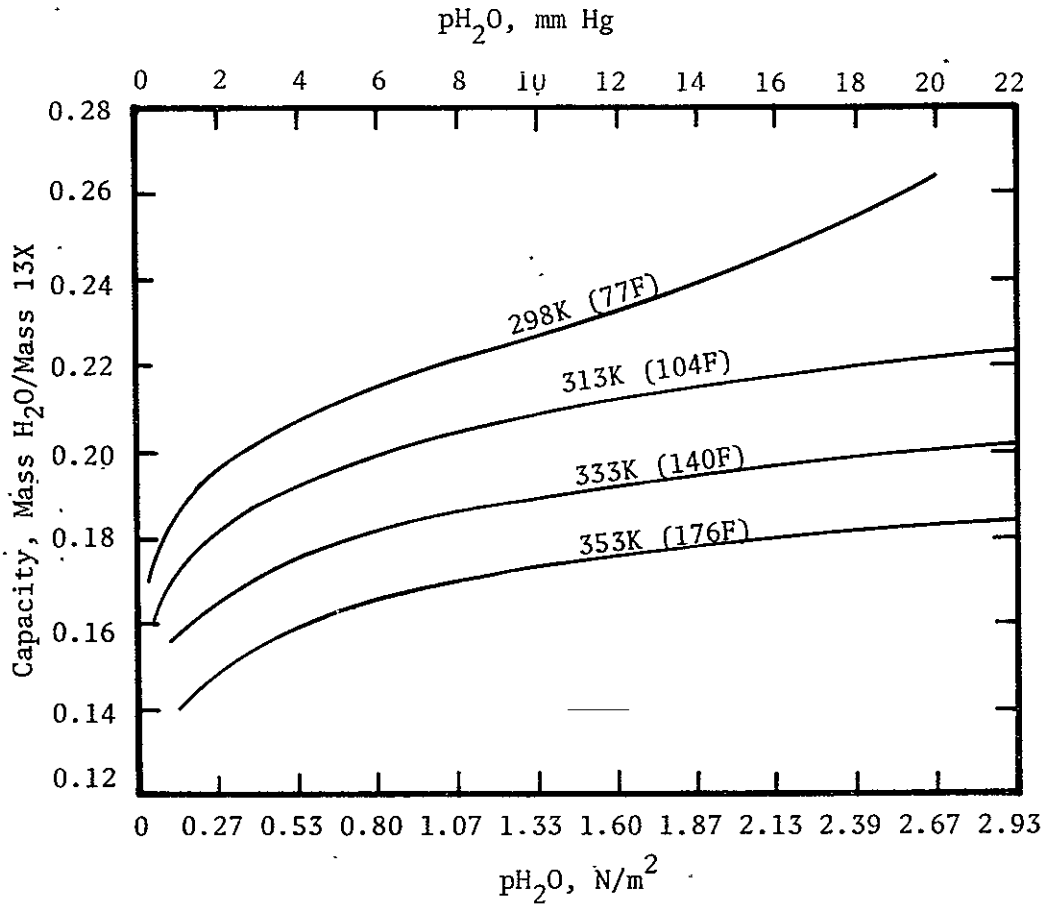

FIGURE 52 MOLECULAR SIEVE WATER REMOVAL CAPACITY[18]

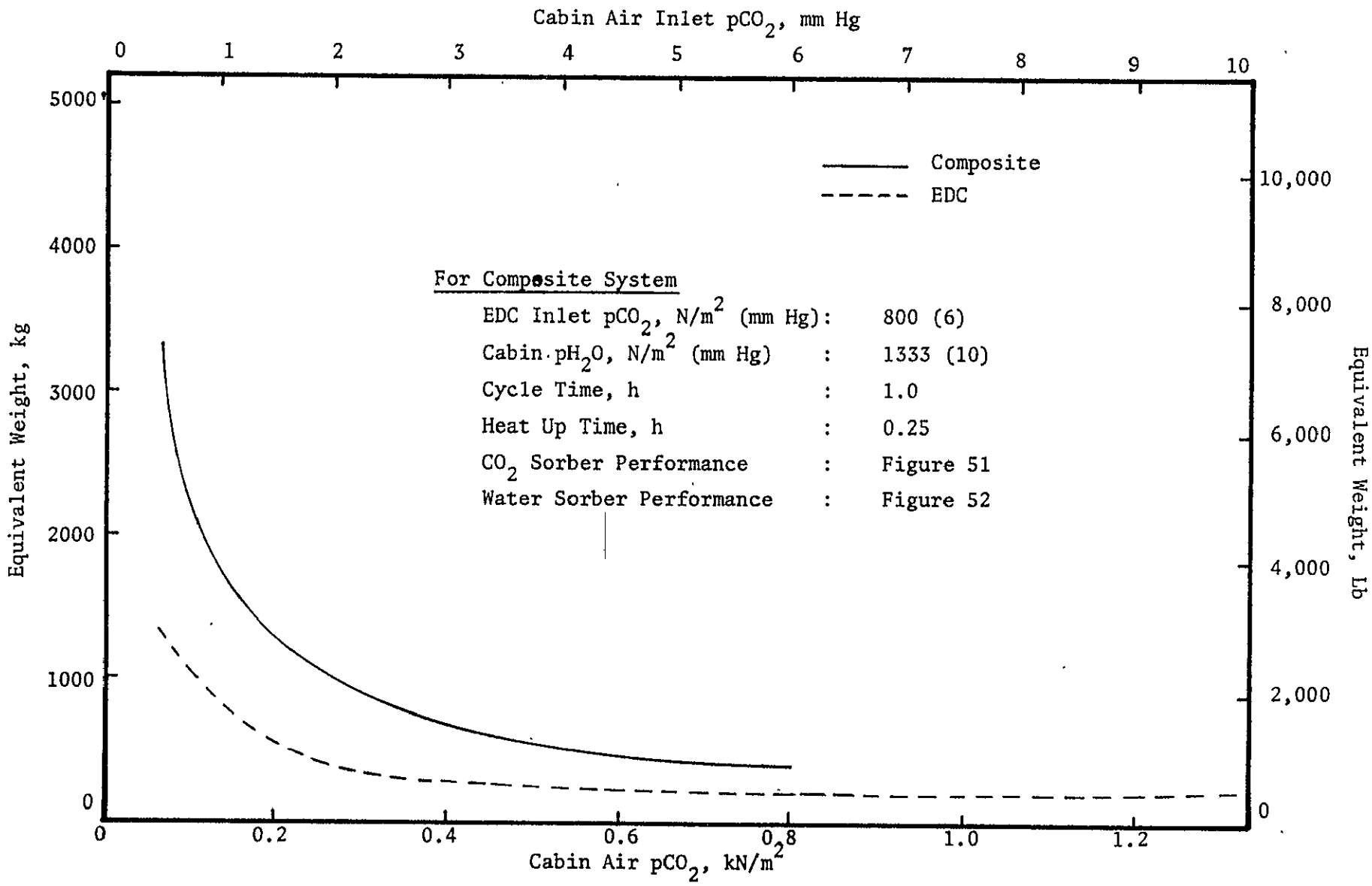

FIGURE 53 COMPOSITE CO_2 REMOVAL SYSTEM EQUIVALENT WEIGHT VERSUS CABIN pCO_2

2. Multiple access port endplates can be successfully used to determine gradients in process air, static pressure, pCO_2, dry bulb temperature and dew point over a cell's active electrode area. The use of such endplates in single cell mapping tests showed that no maldistribution in process air flow exists, but that for externally air-cooled EDC cells extreme RH variations outside allowable limits can occur although both inlet and outlet RH process air values are within allowable limits for specific electrolytes.

3. Standard mass transport equations can be used to describe the transport of the water generated within an EDC from the anode side of a cell into the process air stream. Experimental and analytical investigations showed that a maximum and minimum electrolyte volume of 64% and 50%, respectively, based on the total volume of electrode and cell matrix, is required to insure efficient operation with a CS-6 style baseline cell.

4. Internal liquid-cooling of EDC cells minimizes electrolyte concentration and volume gradients and allows for operation over wide ranges of process air RH with increased CO_2 removal efficiencies. A 25% and 38% improvement in TI (mass of CO_2 removed per mass of O_2 consumed) was observed at 333 kN/m^2 (2.5 mm^2Hg) for 21.5 and 43.0 mA/cm^2 (20 and 40 ASF), respectively.

5. Spectrographic analyses of EDC exhaust gases show that the EDC is not a source of cabin or CO_2 reduction subsystem catalyst contamination.

6. The contractor's baseline electrode-matrix-electrode composite is capable of operating with an anode gas (H_2 + CO_2) backpressure of 34.5 kN/m^2 (5 psig) above the process air pressure level for a range in module-temperature-to-process-air-inlet-dew point differential from 8.8 to 13.0K (14 to 24F). Operation over this range in temperature is possible while maintaining the CO_2 removal and electrical efficiencies above design level.

7. Development of a four-man capacity Advanced EDC Module (AEDCM) resulted in the following conclusions:

    a. Substantial weight and volume savings can be achieved at the cell hardware level by (1) selecting internal air- or liquid-cooling versus externally-cooled fins, (2) directly plating the anode current collector onto the injection molded polysulfone cell frame, and (3) providing for external process air manifolding. A 52% weight savings and a 26% volume savings was demonstrated.

    b. The active electrode area for a single cell can be increased by a factor of two and the number of cells per module increased from 16 to 20 without sacrificing the electrical or CO_2 removal performance.

c. A four-man CO_2 removal capacity can be packaged into a single module using advanced cell frames resulting in a 64% weight and 57% volume savings compared to CS-6 style module construction.

d. Process air pressure drop through the cathode air compartment (using Exmet) can be substantially reduced (90%) by proper cathode compartment-height-to-air-flow selection without sacrificing CO_2 removal or electrical efficiency.

8. A flight-tested Apollo suit compressor offers comparable performance to the SSP commonality blowers used for the CS-6 process air. This alternate blower produced only 1/64 of the noise while saving 210W of electrical power.

9. A module weight and volume savings of 26% and 21%, respectively, is possible by sizing a CS-6 style cell specifically for SSP baseline operation. This would represent a total weight reduction of 40 kg (86 lb) for the CO_2 Collection Subsystem of the SSP (CS-6), or a total weight savings of 11% based on the total subsystem weight.

10. The use of honeycomb endplates can substantially reduce module weight with a minimal increase in module volume while maintaining required endplate stiffness. The total weight of one pair of honeycomb endplates for a CS-6 style module was 2.15 kg (4.75 lb) compared to the baseline stainless steel endplate weight of 6.8 kg (15 lb). The resulting weight reduction amounts to 68% per plate, or 18.3% based on a one-man capacity CS-6 style module while increasing the module volume by only 8%. In addition, an improvement in deflection (endplate stiffness) of 87% was achieved.

11. The fixed hardware weight of the CS-6 for the SSP can be reduced by 74.5 kg (164 lb) for a total reduction of 20% by implementing the low-noise single blower, and using six sets of honeycomb endplates and the lightweight modules.

12. The electrochemical CO_2 removal concept can be readily integrated with a Bosch CO_2 Reduction Subsystem (BRS) or a Solid Electrolyte Oxygen Regeneration Subsystem (SEORS) with only a minimum number of interface components and using state-of-the-art hardware.

13. Projected nominal trace contaminant levels in a spacecraft cabin atmosphere do not affect the operation of an EDC. Even at "worst case conditions" (all trace contaminants present at maximum allowable concentrations with a non-operating trace contaminant removal system) the EDC can still perform its CO_2 removal function but suffers in electrical power output.

14. An EDC can achieve partial, short-term trace contaminant control of a spacecraft environment by absorption of the contaminants into the cell electrolyte, but cannot totally replace the function of a trace

contaminant removal subsystem. For example, acid gases that build up quickly to their maximum allowable concentration (less than several hours) during downtime of the spacecraft trace contaminant control subsystem could be successfully controlled.

15. A concept to combine cabin atmosphere humidity control as well as CO_2 control within the cathode compartment of EDC cells is possible. For the sizing of the module this combined concept is governed by the water removal function with 40% additional cell area required at nominal water generation rates compared to the CO_2 removal function only.

16. The EDC is a viable alternate to the lithium hydroxide (LiOH) based CO_2 Collection Subsystem planned for use in the EC/LSS of the Shuttle Orbiter. The EDC represents a lower total equivalent weight for any Shuttle flight period over 24 man-days. A reduction of 163 kg (358.5 lb) in total equivalent weight is possible at the end of a 120 man-day mission using the EDC instead of the LiOH concept.

17. A composite CO_2 removal concept utilizing both an EDC and molecular sieve pre- and post-sorbers is feasible for operation at low cabin pCO_2 levels. However, the increase in total equivalent weight associated with using the additional components is greater than a comparable EDC-only system.

RECOMMENDATIONS

The following recommendations are a direct result of the program's conclusions.

1. The lightweight, four-man capacity AEDCM has been developed but its performance has only been characterized at the module level. The module, together with other subsystem components, should be packaged into an integrated, self-contained, four-man capacity subsystem consistent with requirements of the advanced module's process fluid routing techniques. Following assembly of the integrated four-man capacity subsystem, the unit should undergo extensive parametric and endurance testing. The associated Ground Support Accessories (GSA) needed to perform the recommended test functions should also be developed.

2. The high performance liquid-cooled concentrator concept should be scaled-up from the demonstrated single- and three-cell level to the one-man capacity module using the advanced cell design. Testing at the one-man capacity level shall be both parametric and endurance in nature.

3. A comparison study should be performed to evaluate the internal CO_2 and water removal concept demonstrated at the single cell level against presently used or envisioned concepts performing a similar function.

4. Additional technology studies, both analytical and experimental, are required. Areas of interest include electrolyte studies, electrode kinetic studies and cell matrix advancement.

REFERENCES

1. Quattrone, P. D., Babinsky, A. D. and Wynveen, R. A., "Carbon Dioxide Control and Oxygen Generation," Paper No. 70-AV/SpT-8, presented at the ASME Conference, Los Angeles, CA, June 21-24, 1970.

2. Wynveen, R. A. and Quattrone, P. D., "Electrochemical Carbon Dioxide Concentrating System," Paper No. 71-AV-21, presented at the SAE/ASME/AIAA Conference, San Francisco, CA, July 12-14, 1971.

3. Marshall, R. D., Schubert, F. H. and Carlson, J. N., "Electrochemical Carbon Dioxide Concentrator: Math Model," Final Report, Contract NAS2-6478, CR-114639, Life Systems, Inc., Cleveland, OH, August, 1973.

4. Powell, J. D., Schubert, F. H., Marshall, R. D. and Shumar, J. W., "Six-Man, Self-Contained Carbon Dioxide Concentrator Subsystem," Final Report, Contract NAS2-6478, CR-114743, Life Systems, Inc., Cleveland, OH, June, 1974.

5. Kostel, G. D., Schubert, F. H., Shumar, J. W., Hallick, T. M. and Jensen, F. C., "Six-Man, Self-Contained Carbon Dioxide Concentrator Subsystem for Space Station Prototype (SSP) Application," Final Report, Contract NAS2-6478, CR-114742, Life Systems, Inc. Cleveland, OH, May, 1974.

6. Marshall, R. C., Carlson, J. N. and Schubert, F. H., "Electrochemical Carbon Dioxide Concentrator Subsystem Math Model," Final Report, Contract NAS2-6478, CR-137565, Life Systems, Inc., Cleveland, OH, September, 1974.

7. Shumar, J. W. and Powell, J. D., "Hydrogen Detection Study," Final Report, Contract NAS2-6478, CR-137563, Life Systems, Inc., Cleveland, OH, September, 1974.

8. Lin, C. H. and Winnick, J., "An Electrochemical Device for Carbon Dioxide Concentration, II Steady-State Analysis CO_2 Transfer," I & EC Process Design and Development, Volume 13, p. 63, January, 1974.

9. Wynveen, R. A., Schubert, F. H. and Powell, J. D., "One-Man, Self-Contained CO_2 Concentrator System," Final Report, Contract NAS2-6118, CR-114426, Life Systems, Inc., Cleveland, OH, March, 1972.

10. Schubert, F. H. and Quattrone, P. D., "Development of a Six-Man, Self-Contained Carbon Dioxide Collection Subsystem for Spacecraft Application," Paper No. 74-ENAs-16, Intersociety Conference on Environmental Systems, Seattle, WA, July 29-August 1, 1974.

11. Schubert, F. H., "Study of the Integration of the Electrochemical Depolarized CO_2 Concentrator with the Bosch CO_2 Reduction Subsystem," Final Report, Contract NAS8-29623, Life Systems, Inc., Cleveland, OH, ER-185-4, June, 1974.

12. Olcott, T. M., "Design of a Spacecraft Contaminant Control System," SAE/ASME/AIAA Life Support and Environmental Control Conference, July 12-14, 1971.

13. Woods, R. R., Schubert, F. H. and Hallick, T. M., "Electrochemical Air Revitalization System Optimization Investigation," Final Report, Contract NAS9-14301, Life Systems, Inc., Cleveland, OH, ER-247-3, October, 1975.

14. Handley, L. M., Meyer, A. P. and Bell, W. F., "Development of Advanced Fuel Cell System (Phase II)," Contract NAS3-15339, CR-134721, Pratt & Whitney Aircraft, South Windsor, CT.

15. Hamilton Standard, "Space Shuttle Environmental Control/Life Support Systems," NAS CR-1981, Windsor Locks, CT, 1972.

16. Lovell, J., "HS-C - A Regenerable CO_2/H_2O Sorbent for a Shuttle Type Spacecraft," Paper No. 74-ENAs-57, presented at the Intersociety Conference on Environmental Systems, Seattle, WA, July 29-August 1, 1974.

17. Grace & Company, W. R., Davison Chemical Division, "Davison 5A Molecular Sieves," Bulletin PC/ADS-103-172, Baltimore, MD.

18. Grace & Company, W. R., Davison Chemical Division, "Davison 13X Molecular Sieves," Bulletin ADS-96-D-272, Baltimore, MD.